Ingenieurfakultät Bau Geo Umwelt

Lehrstuhl für Hydrologie und Flussgebietsmanagement

Dynamic flood inundation forecasting in real-time including associated uncertainties for operational flood risk management

Punit Kumar Bhola

Vollständiger Abdruck der von der Ingenieurfakultät für Bau Geo Umwelt der Technischen Universität München zur Erlangung des akademischen Grades eines

Doktor-Ingenieurs (Dr.-Ing.)

genehmigten Dissertation.

Vorsitzender: Prof. Dr.-Ing. Michael Manhart

Prüfer der Dissertation:

      1. Prof. Dr.-Ing. Markus Disse

      2. Prof. Dr.-Ing. Bruno Merz

      3. Prof. Dr. Robert Jüpner

Die Dissertation wurde am 02.05.2019 bei der Technischen Universität München eingereicht und durch die Ingenieurfakultät Bau Geo Umwelt am 17.07.2019 angenommen

Abstract

Floods are one of the most destructive natural hazards and have severe social and economic impacts. Therefore, improvements are urgently required in the operational flood risk management, in particular, the qualitative assessment of existing flood forecasting and early warning systems. With the objective of improving flood forecasting, I have divided this dissertation into four research topics; (i) inundation forecast validation, (ii) real-time flood inundation forecasting, (iii) uncertainty quantification of forecasting models, and (iv) communication of uncertainties.

In operational flood forecasting, hydrological models are used to forecast only discharges at specific gauges. However, to determine the distributed predictions of flood hazards, hydrodynamic models should be used to generate high-resolution spatial-temporal flood inundation maps. These maps depict inundated areas for floods above certain exceedance levels, which improves flood risk assessment by enhancing civil security and urban development. Despite the importance of flood inundation maps, flood management agencies do not generate them in real-time since unsteady hydrodynamic models are data-rich and computationally too expensive to run. To tackle this issue, I have developed a framework for real-time flood forecasting based on a pre-recorded scenario database. The framework overcomes the high computational time required by hydrodynamic models to provide dynamic inundation maps. It consists of 180 scenarios and uses real-time discharge forecasts as an input to generate inundation maps for a lead-time of 12 hours.

To evaluate the accuracy and predictive capabilities of the inundation forecasts, their validation is essential, and it is important to build trust by reducing false alarms with the help of validation data. However, spatial and temporal flood validation data is scarce in urban areas. Fortunately, recent technological developments have led to new genres of data sources, such as images and videos from smartphones and CCTV cameras. I have presented a new methodology that employs this validation data in a flood forecasting framework in order to improve the forecasting and to establish a communication from crowd-source back to the inundation forecasts. The results show that with the use of validation data, the number of false alarms, as well as the equifinality in the model parameters, can be reduced significantly.

Furthermore, incorporating uncertainties into flood risk assessment has received increasing attention over the last two decades. However, the uncertainties are often not

reported due to the lack of best practices and too wide uncertainty bounds. In this dissertation, I have reviewed and quantified major sources of uncertainty with a focus on flood inundation forecasting. I developed a method to constrain the hydrodynamic model roughness based on measured water levels and to reduce the uncertainty bounds of a two-dimensional hydrodynamic model. The results show that the uncertainties in the flood forecasting models are significant and can have a major impact on the prediction of the extent of inundation. This information is vital for decision-makers in order to optimise early warning and evacuation planning.

In addition, the effective communication of the quantified uncertainties to decision-makers is a challenging issue. In operational flood risk management, the impact of flooding is assessed using a single best-model, which might misrepresent uncertainties in the modelling process. I have developed a novel methodology, which assesses the impact of flooding using a multi-model combination by incorporating buildings to develop hazard maps based on exceedance probability scenarios. These maps take into account underlying uncertainties and are ready-to-use for decision-makers for a variety of purposes, such as flood impact assessment, spatial planning, early warning and emergency planning.

This dissertation presents a prototype framework for flood inundation forecasting by combining the four research topics. The framework incorporates underlying uncertainties and communicates them to the decision-makers in the field of flood risk management. The major advantage of the framework is that it is independent from the choice of forecasting models, thus, making it suitable for use in other study areas, regardless of their size.

Keywords: flood forecast; flood inundation map; flood risk assessment; hydrodynamic model; hydrological model; scenario database; uncertainty quantification; uncertainty communication; forecast validation

Zusammenfassung

Hochwässer sind eine der zerstörerischsten Naturgefahren und führen zu gravierenden sozialen und wirtschaftlichen Auswirkungen. Daher sind Verbesserungen im operationellen Hochwasserrisikomanagement dringend erforderlich, insbesondere die qualitative Bewertung vorhandener Hochwasservorhersagen und Frühwarnsysteme. Mit dem Ziel, die Hochwasservorhersage zu verbessern, wurde diese Dissertation in vier Forschungsthemen unterteilt; (i) Validierung der Hochwasservorhersage, (ii) Vorhersage von Überschwemmungsflächen in Echtzeit, (iii) Quantifizierung der Unsicherheit von Vorhersagemodellen und (iv) Kommunikation von Unsicherheiten.

Bei der operationellen Hochwasservorhersage werden hydrologische Modelle verrwendet, um Durchflüsse an bestimmten Pegeln vorherzusagen. Um jedoch eine räumlich verteilte Vorhersage über Hochwassergefahren erstellen zu können, sollten hydrodynamische Modelle zur Erstellung von Gefahrenkarten genutzt werden. Diese Gefahrenkarten zeigen überschwemmte Gebiete oberhalb bestimmter Überschreitungsniveaus. Mit Hilfe dieser Information können sowowhl Katastrophenschutz als auch Städtbauliche Planung optimiert werden, was insgesamt zu einer Verbesserung des Hochwasserrisikos führt. Trotz des großen Potenzials erstellen die zuständigen Behörden bislang keine Überschwemmungskarten in Echtzeit, da die instationären hydrodynamischen Modelle für diese Zielsetzung zu daten- und rechenintensiv sind. Um dieses Problem zu lösen, wurde ein Framework für die Echtzeit-Hochwasservorhersage basierend auf einer vorab aufgezeichneten Szenariodatenbank entwickelt. Das Framework, welches die hohen Rechenzeiten der hydrodynamischen Modelle zur Erstellung von dynamischen Überschwemmungskarten überwindet, besteht aus 180 Szenarien und verwendet Echtzeit-Durchflussvorhersagen, um Überschwemmungskarten mit einer Vorlaufzeit von 12 Stunden zu generieren.

Um die Genauigkeit und die Prognosefähigkeiten der generierten Vorhersagen zu bewerten, ist ihre Validierung ebenso wie die Reduzierung von Fehlalarmen mit Hilfe von beobachteten Daten von Bedeutung, um Vertrauen in das Framework aufzubauen. Daten zur räumlichen und zeitlichen Validierung von Hochwassern in städtischen Gebieten werden jedoch nur unzureichend erhoben. Moderne Technologien haben jedoch zu neuen Datenquellen geführt, wie Bilder und Videos von Smartphones und Überwachungskameras. In dieser Dissertation wird eine neue Methodik vorgestellt, die diese neuen Datenquellen in einem Framework zur Hochwasservorhersage verwendet,

um Vorhersagen zu verbessern und eine Kommunikationsschnittstelle von den Erstellern der crowdgesourcte Daten für die Überschwemmungsvorhersage herzustellen. Die Ergebnisse zeigen, dass die Anzahl der Fehlalarme sowie die Äquifinalität der Modellparameter durch die Verwendung der Validierungsdaten signifikant reduziert werden konnten.

Darüber hinaus hat die Berücksichtigung von Unsicherheiten bei der Bewertung des Hochwasserrisikos in der Wissenschaft in den letzten zwei Jahrzehnten zunehmend Beachtung gefunden. Aus Mangel an etablierten Verfahren und großer Unsicherheitsgrenzen wird die Bewertung jedoch oft nicht publiziert. In dieser Dissertation wurden wichtige Unsicherheitsquellen überprüft und quantifiziert, wobei der Schwerpunkt auf der Überschwemmungsvorhersage liegt. Es wurde eine Methode zur Beschränkung der hydrodynamischen Modellrauheit entwicklt, die auf gemessenen Wasserständen basiert und die Unsicherheitsgrenzen eines zweidimensionalen hydrodynamischen Modells reduziert. Die Ergebnisse zeigen, dass Unsicherheiten in den Hochwasservorhersagemodellen ein wichtiger Faktor sind und die Vorhersage der Ausdehnung von Überschwemmungsflächen erheblich beeinflussen können. Diese Informationen sind zur Optimierung von Alarmierungs- und Evakuierungsplänen für Entscheidungsträger sehr wichtig.

Die effektive Übermittlung der quantifizierten Unsicherheiten an Entscheidungsträger stellt ebenso eine Herausforderung dar. Im operationellen Hochwasserrisikomanagement wird meist ein Best-Pratice Modell verwendet um die Auswirkungen von Überschwemmungen zu bewerten. Bei der Erstellung des Modells können jedoch Unsicherheiten nicht oder falsch dargestellt werden. In dieser Dissertation wurde eine neue Methode entwickelt, um den Einfluss von Überschwemmungen mit Hilfe einer Kombination aus mehreren Modellen zu bewerten. Die entwickelte Methode identifiziert betroffene Gebäude für verschiedene Überschreitungswahrscheinlichkeitsszenarien und erstellt hieraus eine gebäudeabhängige Gefahrenkarte. Diese Karten berücksichtigen die zugrundeliegenden Unsicherheiten und können von Entscheidungsträgern für eine Vielzahl von Zwecken verwendet werden, wie z. B. für die Bewertung des Hochwasserrisikos, der Raumplanung, der Frühwarnung und der Notfallplanung.

In dieser Dissertation wird ein Prototyp-Framework für die Überschwemmungsvorhersage vorgestellt, indem vier Forschungsthemen kombiniert werden. Das Framework enthält grundlegende Unsicherheiten, die den

Entscheidungsträgern im Bereich des Hochwasserrisikomanagements mitgeteilt werden. Der größte Vorteil des Frameworks ist, dass es unabhängig vom Vorhersagemodell ist und sich dadurch für die Verwendung in anderen Untersuchungsgebieten, unabhängig von deren Größe, eignet.

Schlüsselwörter: Überschwemmungsvorhersage; Überschwemmungskarten; Hochwasserrisikobewertung; Hydrodynamische Modelle; Hydrologische Modelle; Szenariendatenbank; Unsicherheitsquantifizierung; Vorhersagevalidierung.

Affidavit

I hereby affirm that I wrote this doctoral thesis independently and on my own without illegal assistance of third parties. To the best of my knowledge, all sources that I used to prepare this dissertation are labelled as such. This dissertation has not been received by any examination board, neither in this nor in a similar form.

Munich, 02.05.2019

_____
Punit Kumar Bhola

Acknowledgements

Meyer, who was always there for me. Thank you for your patience, motivation and moral support.

Contents

List of figures

List of tables

List of abbreviation

1D	One Dimensional
2D	Two Dimensional
3D	Three Dimensional
BMBF	Federal Ministry of Education and Research
CCTV	Closed-circuit Television
COSMO	Consortium for Small-scale Modeling
CPU	Central Processing Unit
DWD	German Meteorological Services
e	Absolute Error
EFAS	European Flood Alert System
EPS	Ensemble Prediction System
ESPADA	Evaluation Et Suivi Des Pluies En Agglomération Pour Devancer L'alerte
F	Fit Statistic
FIMAN	Flood Inundation Mapping and Alert Network
GKD	Bavarian Hydrological Services
GPU	Graphics Processing Unit
GUI	Graphical User Interface
HD	Hydrodynamic
HPC	High Performance Computing
HQ	Return Period
KOSTRA	Koordinierte Starkniederschlags-regionalisierungs-auswertungen
k_{st}	Strickler Value
LARSIM	Large Area Runoff Simulation Model
LfU	Bavarian Environment Agency
LIDAR	Light Detection and Ranging
MCS	Monte Carlo Simulations
MNQ	Lowest Value of a Year
MQ	Arithmetic Mean
NOAA	National Oceanic and Atmospheric Administration
NSE	Nash Sutcliffe Efficiency
PEN	Praxisrelevante Extremwerte Des Niederschlags
R^2	Coefficient of Determination
$RMSE$	Root Mean Square Error
RP	Return Period
SD	Standard Deviation
TBM	Turning Bands Method
THW	Federal Agency for Technical Relief
TUM	Technical University of Munich
wr^2	Weighted Coefficient of Determination
WWA	Water Management Authority

List of publications

Peer-reviewed

1. **Bhola, P. K.**, Nair, B. B., Leandro, J., Rao, S. N., and Disse, M.: Flood inundation forecasts using validation data generated with the assistance of computer vision, J. Hydroinform., 21, 240-256, https://doi.org/10.2166/hydro.2018.044, 2018b.

2. **Bhola, P. K.**, Leandro, J., and Disse, M.: Framework for offline flood inundation forecasts for two-dimensional hydrodynamic models, Geosciences, 8, 346, https://doi.org/10.3390/geosciences8090346, 2018a.

3. **Bhola, P. K.**, Leandro, J., and Disse, M.: Reducing uncertainties in flood inundation outputs of a two-dimensional hydrodynamic model by constraining roughness, Nat. Hazards Earth Syst. Sci., 19, 1445-1457, https://doi.org/10.5194/nhess-19-1445-2019, 2019

4. Disse, M., Konnerth, I., **Bhola, P. K.**, and Leandro, J.: Unsicherheitsabschätzung für die Berechnung von dynamischen Überschwemmungskarten – Fallstudie Kulmbach, in: Vorsorgender und nachsorgender Hochwasserschutz: Ausgewählte Beiträge aus der Fachzeitschrift WasserWirtschaft Band 2, edited by: Heimerl, S., Springer Fachmedien Wiesbaden, Wiesbaden, 350-357, 2018.

5. **Bhola, P. K.**, Leandro, J., and Disse, M.: Hazard maps with differentiated exceedance probability for flood impact assessment, Nat. Hazards Earth Syst. Sci. Discuss., https://doi.org/10.5194/nhess-2019-158, in review, 2019.

6. Beg, M. N. A., Leandro, J., **Bhola, P. K.**, Konnerth, I., Willems, W., Carvalho, R. F., and Disse, M.: Discharge interval method for uncertain flood forecasts using a flood model chain: city of Kulmbach, J. Hydroinform., https://doi.org/10.2166/hydro.2019.131, 2019.

7. Leandro, J., Gander, A., Beg, M. N. A., **Bhola, P. K.**, Konnerth, I., Willems, W., Carvalho, R. F., and Disse, M.: Forecasting upper and lower uncertainty bands of river flood discharges with high predictive skill, J. Hydrol., https://doi.org/10.1016/j.jhydrol.2019.06.052, 2019.

Conference paper

- Bhola, P. K., Disse, M., Kammereck, B., and Haas, S.: Uncertainty quantification in the flood inundation modelling, applying the GLUE methodology, 12th International Conference on Hydroinformatics (HIC 2016): Smart Water for the Future, Incheon, South Korea, 21-26 August 2016, 2016.

- Bhola, P. K., Ginting, B. M., Leandro, J., Mundani, R.-P., and Disse, M.: Model parameter uncertainty of a 2D hydrodynamic model for the assessment of disaster resilience, EnviroInfo, Garching, Garching, Germany, 5-7 September 2018, 2018c.

- Bhola, P. K., Leandro, J., Konnerth, I., Amin, K., and Disse, M.: Dynamic flood inundation forecast for the city of Kulmbach using offline two-dimensional

hydrodynamic models, 13th International Conference on Hydroinformatics (HIC 2018), Palermo, Italy, 1-5 July 2018, 2018d.

- Bhola, P. K., Leandro, J., Videkhina, I., and Disse, M.: Dynamic risk mapping in fluvial flood application using a two-dimensional hydrodynamic model incorporating the model parameter uncertainties, International Conference on "Natural Hazards and Risks in a Changing World", Potsdam. Germany, 2018e.

- Ginting, B. M., Bhola, P. K., Ertl, C., Mundani, R.-P., Disse, M., and Rank, E.: Hybrid-parallel simulations and visualisations of real flood and tsunami events using unstructured meshes on high-performance cluster systems, SimHydro 2019, Sophia Antipolis, France, 12-14 June 2019, 2019, *Submitted*.

- Leandro, J., Konnerth, I., Bhola, P. K., Amin, K., Köck, F., and Disse, M.: FloodEvac Interface zur Hochwassersimulation mit integrierten Unsicherheitsabschätzungen, FloodEvac interface for flood simulation with integrated uncertainty assessments, Tag der Hydrologie, Trier, 23-24 March 2017, 2017.

- Beg, M. N. A., Leandro, J., Bhola, P. K., Konnerth, I., Amin, K., Koeck, F., Carvalho, R. F., and Disse, M.: Flood forecasting with uncertainty using a fully automated flood model chain: A case study for the city of Kulmbach, 13th International Conference on Hydroinformatics (HIC 2018), Palermo, Italy, 1-5 July 2018, 2018.

Author contributions

Chapter 3 to 7 in this work have been submitted or published in a similar form in the following peer-reviewed journals

Chapter 3

Bhola, P. K., Nair, B. B., Leandro, J., Rao, S. N., and Disse, M.: Flood inundation forecasts using validation data generated with the assistance of computer vision, J. Hydroinform., 21, 240-256, https://doi.org/10.2166/hydro.2018.044, 2018b.

Punit K. Bhola drafted the manuscript, designed, and set up the framework and models as well as carried out the data collections. Bhavna B. Nair and Sethuraman N. Rao carried out the image processing and drafted computer vision method section. Markus Disse reviewed the manuscript. Jorge Leandro helped to review the manuscript. All authors read and approved the final manuscript.

Chapter 4

Bhola, P. K., Leandro, J., and Disse, M.: Framework for offline flood inundation forecasts for two-dimensional hydrodynamic models, Geosciences, 8, 346, https://doi.org/10.3390/geosciences8090346, 2018a.

Punit K. Bhola drafted the manuscript, designed, and set up the framework and models as well as carried out the primary data collections. Jorge Leandro helped with the conceptualisation and review the manuscript. Markus Disse reviewed the manuscript. All authors read and approved the final manuscript.

Chapter 5

Bhola, P. K., Leandro, J., and Disse, M.: Reducing uncertainties in flood inundation outputs of a two-dimensional hydrodynamic model by constraining roughness, Nat. Hazards Earth Syst. Sci., 19, 1445-1457, https://doi.org/10.5194/nhess-19-1445-2019, 2019a.

Punit K. Bhola drafted the manuscript, designed, and set up the framework and models as well as carried out the primary data collections. Markus Disse helped with the conceptualisation and review the manuscript. Jorge Leandro reviewed the manuscript. All authors read and approved the final manuscript.

Chapter 6

Disse, M., Konnerth, I., Bhola, P. K., and Leandro, J.: Unsicherheitsabschätzung für die Berechnung von dynamischen Überschwemmungskarten – Fallstudie Kulmbach, in: Vorsorgender und nachsorgender Hochwasserschutz: Ausgewählte Beiträge aus der Fachzeitschrift WasserWirtschaft Band 2, edited by: Heimerl, S., Springer Fachmedien Wiesbaden, Wiesbaden, 350-357, 2018.

Punit K. Bhola drafted the manuscript together with Iris Konnerth and Jorge Leandro. Punit K. Bhola performed the formal analysis of the hydrodynamic model section and results. Iris Konnerth performed the hydrological model section and results. Markus Disse conceptualises the study and review the manuscript. Jorge Leandro conceptualises the FloodEvac tool and reviewed the manuscript. All authors read and approved the final manuscript.

Chapter 7

Bhola, P. K., Leandro, J., and Disse, M.: Hazard maps with differentiated exceedance probability for flood impact assessment, Nat. Hazards Earth Syst. Sci. Discuss., https://doi.org/10.5194/nhess-2019-158, in review, 2019b.

Punit K. Bhola drafted the manuscript, designed, and set up the framework and models as well as carried out the primary data collections. Jorge Leandro helped with the conceptualisation and review the manuscript. Markus Disse reviewed the manuscript. All authors read and approved the final manuscript.

Chapter

1. Introduction and research questions

1.1. Motivation

Floods are one of the most destructive natural hazards and lead to severe social and economic impacts (European Union, 2007; Alfieri et al., 2016). Recent extreme precipitation events in central Europe, for example, have highlighted the vulnerability of settlements and infrastructures to flooding. The number of people exposed to recent flooding that occurred in many Central European countries stresses the importance of assessing flood hazards. For example, during the extensive June 2013 floods in Germany, more than 80,000 people in eight federal states had to be evacuated (Thieken et al., 2016). Furthermore, the extensive 2016 summer floods that hit Southern Germany and its neighbouring countries led to monetary losses of more than 2.6 billion euros (Munich Re, 2017). Figure 1-1 shows the vulnerability of people and infrastructures in the case of two recent floods in the cities Passau and Simbach in Germany.

(a) **Passau on June 4, 2013**   (b) **Simbach on June 2, 2016**

Figure 1-1. Recent Floods in Bavaria in the cities Passau and Simbach.

The magnitude and frequency of extreme flooding events are likely to rise due to global warming (Sayers et al., 2013). Given the worldwide significance of floods, early warning systems and flood forecasting need to be as robust as possible and should be able to cope with a changing climate. This motivates the need to improve the current operational flood risk frameworks, in particular, flood forecasting and early warning, in order to reduce the impact of floods on people and assets. In Germany, flood risk management plans rely on flood forecasting models to determine the impact of flooding on areas of potential risk (Thieken et al., 2016). Furthermore, a challenging issue in natural hazards is the quantification of uncertainties in flood forecasting models and the effective communication of uncertainties to decision-makers (Pappenberger and Beven, 2006; Doyle et al., 2019). Therefore, with the aim to improve deterministic flood forecasting, I present my dissertation on flood inundation forecasting in real-time including associated uncertainties for operational flood risk management.

1.2. Main objectives

The main objective of my doctoral research is to develop a framework for real-time flood inundation forecasting that is hydrodynamic (HD) based and includes uncertainties in the modelling process. The framework should be operationally applicable to meso-scale catchments and should be easy to implement. Furthermore, scientific and economic connectivity of the framework should be achieved by taking into consideration the following objectives:

- Increase of civil security during major floods by improving flood forecasting
- Efficient operations and cost savings using the framework
- Ensure early warning for flood forecasting
- A coordinated response by decision-makers through model uncertainties
- Easy application of the framework and methodologies to study areas
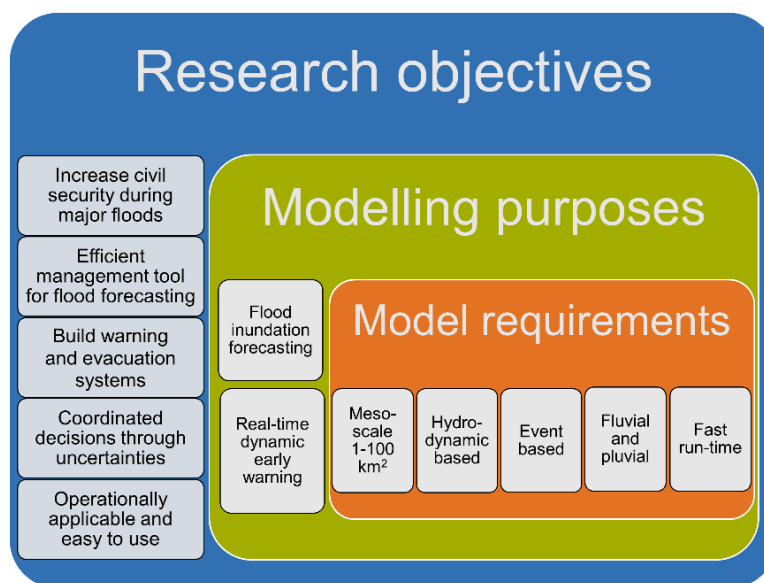
Figure 1-2. Overview of the research objectives along with modelling purposes and model requirements

An overview of the research objectives along with modelling purposes and model requirements is presented in Figure 1-2. The framework is data-driven and depends on the predictions of deterministic flood forecasting models. These models need to be selected based on the modelling purposes and require a framework that is able to provide dynamic flood inundation maps in real-time to end-users. For my dissertation, the users consist of a group of decision-makers, such as the Bavarian Water Authorities (LfU) and disaster relief organizations in Germany, the Federal Agency for Technical Relief (THW) or the German Red Cross (DRK). Furthermore, the inundation maps should be simulated using an HD model and a fast run-time for the models is required to apply

the framework in meso-scale catchments. In addition, the models should be able to simulate both fluvial and pluvial flooding.

1.3. Research questions and hypothesis

The main objective of the dissertation is to enhance flood inundation forecasting frameworks applied in the field of flood risk management. To reach this objective, four main research topics (Figure 1-3) are conceptualized in this dissertation – (i) inundation forecasts validation, (ii) real-time flood inundation forecasting, (iii) uncertainty quantification, and (iv) communication of uncertainties.

• Bhola et al., 2018, Framework for offline flood inundation forecasts, *Geosciences*

• Bhola et al., 2018, Flood inundation forecasts using computer vision, *J Hydroinrm.*

• Disse et al., 2018, Unsicherheitsabschätzung von dynamischen Überschwemmungskarten, *Springer*
• Bhola et a., 2019, Reducing uncertainty bounds by constraining model roughness, *Nat. Hazards Earth Syst. Sci.*

• Bhola et al, 2019, Hazard maps with differentiated exceedance probability, *Nat. Hazards Earth Syst. Sci*
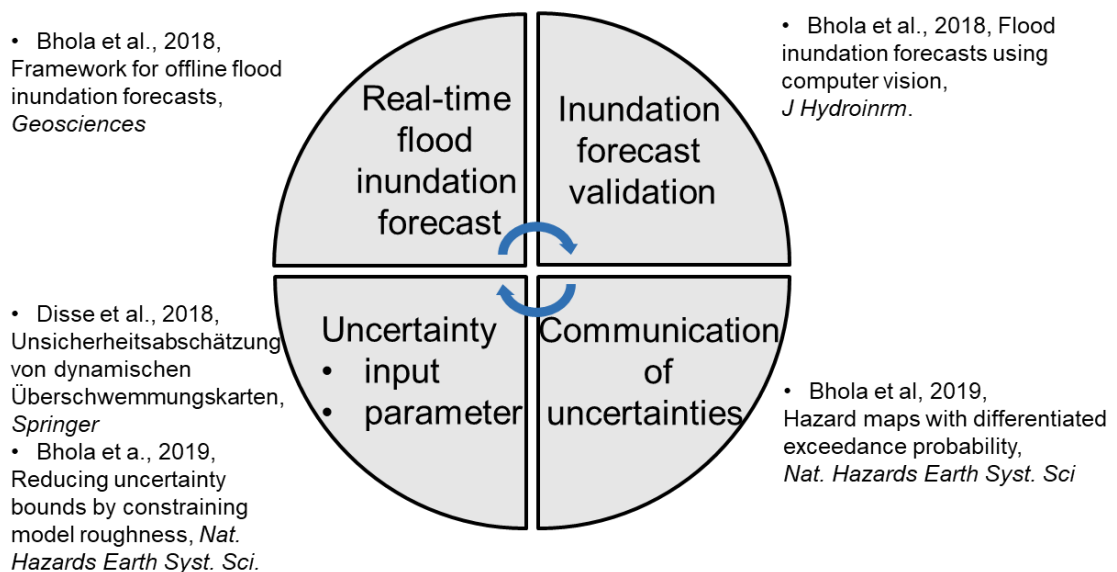
Figure 1-3. Conceptualisation of the four research topics in this dissertation.

To address the research topics, the corresponding research questions are presented in the following:

(i) Inundation forecasts validation
Research question #1:   Can new technologies in computer vision, such as edge detection and image segmentation be applied to generate additional validation data for flood inundation forecasting?
Research question #2:   How can the additional data be used in a flood forecast framework?

(ii) Real-time flood inundation forecasting

Research question #3:   Can a database of flood map scenarios be used to provide dynamic flood maps in real-time?
Research question #4:   How accurate are the selected maps from the database?

(iii) Uncertainty quantification

Research question #5:   What are the major sources of uncertainties in flood forecasting?

Research question #6:   How can we deal with high uncertainties in flood forecasting?

(iv) Communication of uncertainties

Research question #7:   How can the uncertainties be represented and visualized?

Research question #8:   How can the uncertainties be communicated to decision-makers?

An overview of the four research topics including specific research questions and associated hypothesis is presented in Table 1-1. The research questions will be addressed by testing the hypotheses in a series of publications (Chapters 3-7).

Table 1-1. Overview of the research questions and hypotheses.

	Research questions	Hypotheses	Chapter	References
	Real-time inundation forecast using validation data – State of the art and new possibilities			
1)	Can the new technologies in computer vision, such as edge detection and image segmentation be applied to generate additional validation data?	• New technologies in computer vision can assist to improve the accuracy of flood inundation forecasting	3	Bhola et al., 2018b
2)	How the additional data can be used in a flood forecast framework?	• Equifinal model parameters can be used in combination with the validation data to provide optimal forecasts		
	Hydrodynamic-based dynamic flood inundation forecast in real-time using scenario database			
3)	Can a database of flood map scenarios be used to provide dynamic flood maps in real-time?	• Pre-recorded database of flood maps can be used to provide accurate inundation maps to decision-makers in real-time	4	Bhola et al., 2018a
4)	How accurate are the selected maps from the database?			
	Sources of uncertainties in flood forecasting models – Model input and model parameter			
5)	What are the major sources of uncertainties in flood forecasting?	• Measured water levels can be used to reduce uncertainty bounds	5, 6	Bhola et al., 2019a; Disse et al., 2018
6)	How can we deal with high uncertainties in flood forecasting?	• Uncertainties in model input have a significant impact on the flooding extent		
	Communication of uncertainties			
7)	How can the uncertainties be represented and visualized?	• A multi-model combination of 2D HD models approach can communicate uncertainties to decision-makers	7	Bhola et al., 2019b
8)	How can the uncertainties be communicated to decision-makers?	• The multi-model based approach outperforms the *best-model* approach in flood inundation forecasting		

1.4. Outline of the dissertation

This dissertation comprises of five self-contained research articles with relevant literature reviews. To summarise, this chapter outlined the objectives and gives an overview of the conducted research. A short overview of the study area, forecasting models used and methods is given in Chapter 2. The four research topics and hypotheses are tested in Chapters 3-7. For each chapter, the background, methodology, results, discussion and conclusions are given. At last, in chapter 8 major findings are discussed and concluded as well as a prototype framework flood forecasting is presented based on the findings.

In Chapter 3, I have used the hypothesis that *new technologies can assist to improve flood inundation forecasting* with the use of crowd-sourced data. In order to use new technologies in a framework, I have presented a methodology that integrates additional validation data, which is extracted from an image with the assistance of a computer vision algorithm. The hypothesis that *the accuracy of inundation forecasting can be improved by additional validation data* is tested by using water levels obtained from images.

In Chapter 4, the research questions 3 and 4 are addressed using the hypothesis that *a pre-recorded database of flood maps can be used to provide accurate inundation maps to decision-makers in real-time*. I have developed an efficient framework for offline flood inundation forecast that selects inundation maps in real-time from the database for fluvial flood forecasts. The performance of the framework was assessed by comparing offline and online inundation maps for a lead time of 12 hours and updating the map selection at every three-hour interval.

Chapters 5 and 6 address the research questions 5 and 6 and the hypothesis that *measured water levels can be used to reduce uncertainty bounds of HD model outputs*. I have selected extreme ranges of model roughness in literature and gradually narrowed them by reducing the uncertainty bounds based on the measured data. Chapter 6 originally was published in German but for consistency, it has been translated to English in this dissertation. The chapter presents the propagation of uncertainties from hydrological model parameters to HD model outputs.

In Chapter 7, a novel methodology based on a multi-model approach is presented to address the research questions 7 and 8. I have focused on developing building hazards maps that visualise underlying uncertainties in forecasting models. Thus, the hypotheses that *a multi-model combination of 2D HD models approach can communicate*

uncertainties to decision-makers and *the multi-model based approach outperforms a single best-model approach in flood inundation forecasting* are addressed in this chapter.

In Chapter 8, the major findings of the dissertation are presented and an assessment of the results regarding recent literature is discussed. In addition, the advantages and limitations of the methodologies developed are discussed. Combining all the methodologies developed in previous chapters, a prototype framework for flood inundation forecasting is presented that incorporates underlying uncertainties and communicates them to the decision-makers in the field of flood risk management.

Chapter

2. Study area, models and methods

2.1. Study area

2.1.1. Upper Main

In this dissertation, the river catchment of the Upper Main is investigated, which is located in the North-East of Bavaria, Germany. It refers to a rather dry region of Bavaria. It covers an area of about 4244 km^2 and stretches approximately from latitude 49.8 N to 50.5 N and longitude 10.5 E to 11.8 E, with a mean North-South extension of approximately 70 km, and a mean West-East extension of about 90 km (Figure 2-1a).

In the catchment, the water contributing to a flood event originates mainly from upstream headwater streams. River peak flow is mainly produced by heavy rainfall or winter snowmelt. Extreme floods that caused damages within the Upper Main catchment are consistently recorded (Yörük 2009; Pakosch 2011). In the Upper Main, the development of settlements in floodplains has led to a loss of retention areas (Yörük 2009). In order to secure houses and properties, inhabitants and authorities have developed hydro-technical flood control infrastructure (HOPLA Main 2012). Despite the high-financial expenditure on technical flood protection measures, flood events have still caused considerable damages in recent decades. Alternative options to technical flood control, such as nature-based solutions to mitigate the negative effect of floods have not received much consideration in this region (Früh-Müller and Wegmann, 2015). Nevertheless, the catchment is data-rich and contains a vast network of high-quality precipitation and discharge gauging stations (Roth, 2008). There are 77 rain gauges along with 104 gauging stations in operation in which water levels and discharges are measured and on eight stations flood warning is published (HND, 2019). Historical time-series of rainfall is available at each rain gauge from 2005 to present with an hourly temporal resolution of 1-hour. The discharge data is also available at hourly temporal resolution and can be assessed by the Bavarian Hydrological Services (GKD, 2019).

2.1.2. Kulmbach

The methodologies presented in my dissertation have all been validated in the city of Kulmbach. Three rivers contribute to the city: Schorgast, White Main and Red Main. Sub-catchments for the three rivers are shown in Figure 2-1b namely Ködnitz, Kauerndorf and Unterzettlitz. The city has around 26,000 inhabitants. With a population density of 280 inhabitants per km^2 in an area of 92.8 km², it is categorized as a great district city. Traditionally, it has been a manufacturing base for the food and beverage industry.

(a) Upper Main

(b) Focus area
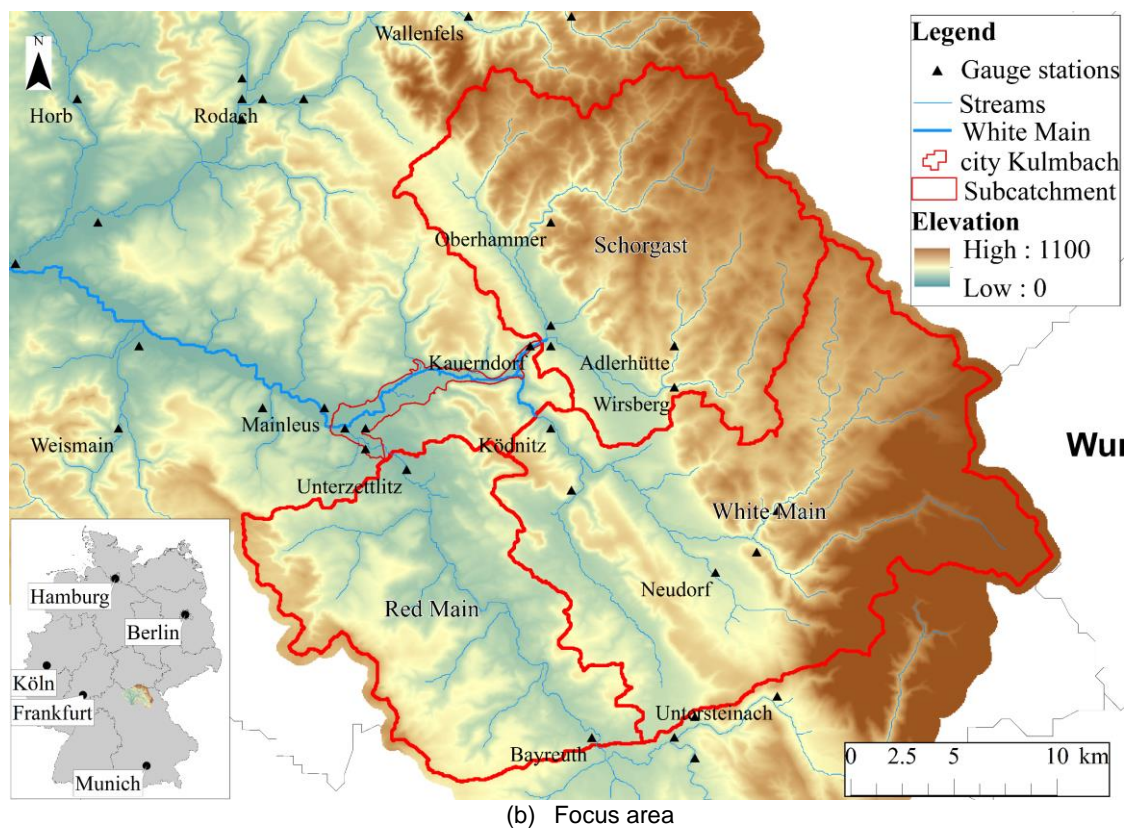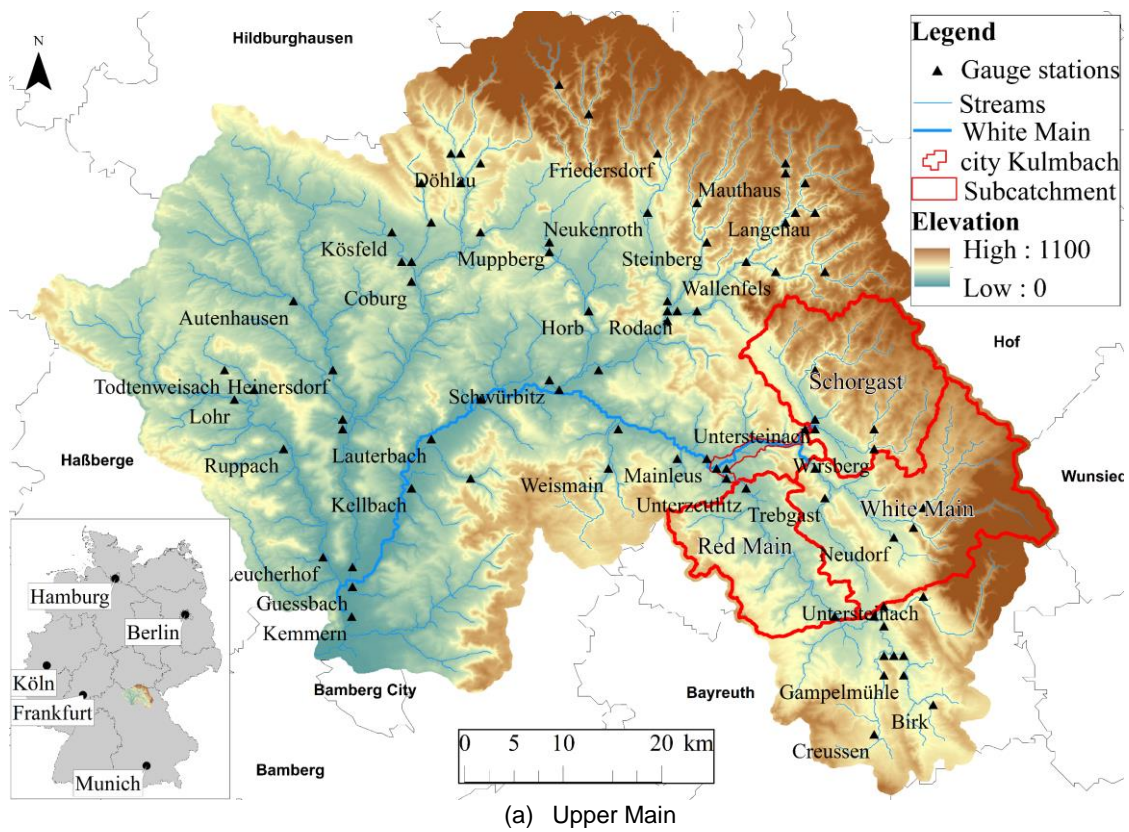
Figure 2-1. The entire Upper Main catchment and focus of upstream sub-catchments of the city of Kulmbach.

The city is crossed by the river White Main and a diversion canal for flood protection, the Mühl canal. Schorgast is one of the main tributaries that meets the White Main upstream of the city. In the north, a small tributary Dobrach meets the White Main and from the south side, two stormwater canals meet the Mühl canal. Although these three tributaries are comparatively small, they still contribute to the flooding in the city. The river Red Main merges with the White Main near Kulmbach from the South to form the river Main, the longest tributary of the Rhine. The latter joins downstream of the city centre; hence it is not important in assessing the impact of flooding in the city centre. Main gauging stations upstream of the city are Ködnitz at White Main and Kauerndorf located at the river Schorgast.

Flood mitigation measures were started in the 1930s and a flood channel was built north of the city centre. Two weirs were built to control the flow in the river and discharge of up to 5m^3/s could flow through the original path of Mühl canal, which is passing through the city centre of Kulmbach. On 28th May 2006, intense rainfall of up to 80 mm occurred and within a few hours all the streams and rivers were filled (TVO, 2015). The incident prompted decision-makers to revisit the flood protection measures for the city. Planning of a new flood protection strategy was started in 2009 with an estimated cost of around 11.5 Mio. Euro (WWA, 2018a). In 2014, the original path of the White Main was renovated. In March 2017, construction works for the flood channel were started again for flood retention purposes.

Figure 2-2 present time-series of measured discharges for a duration of 40 years (1978-2017) for the gauging stations upstream of the city. The figure also identifies major flood events as well as various return period (RP) discharges of the gauges. Floods in the order of a 100-year return period were frequently recorded in the last decades, mainly May 2006, January 2011, May 2013 and February 2005 (in the order of magnitude). These events are further used for hindcasting and validating proposed methodologies.

(a) Ködnitz
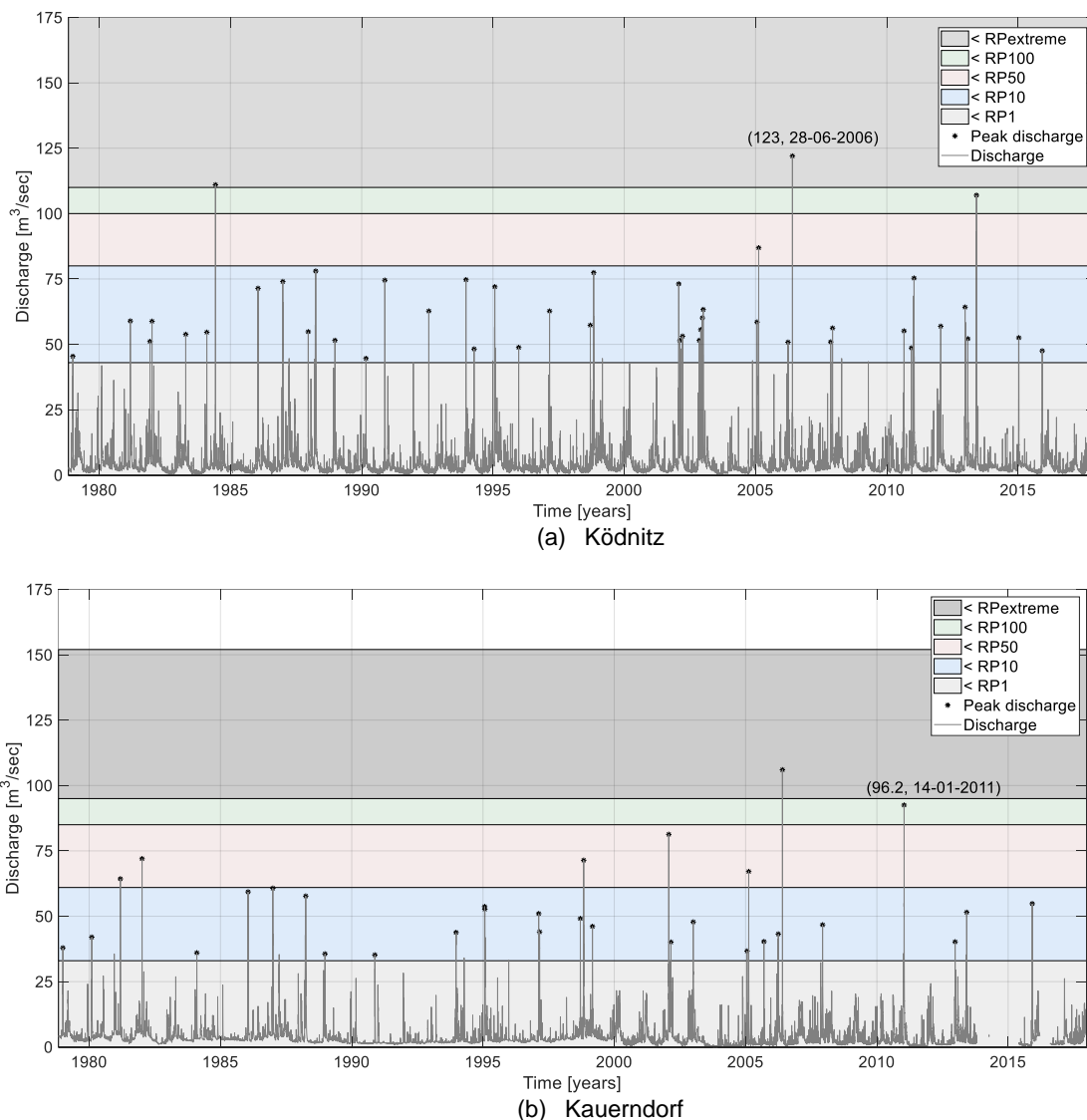
(b) Kauerndorf

Figure 2-2. Measured discharge at upstream gauges Ködnitz and Kauerndorf for a duration of 40 years (1978 – 2017). RP denotes return period. Data source: Bavarian Hydrological Service, www.gkd.bayern.de.

2.2. Flood forecasting models

2.2.1. Hydrological model

LARSIM (Large Area Runoff Simulation Model) is a conceptual hydrological model used in this thesis to study the hydrology of the Upper Main catchment and to generate the inflow boundary conditions to hydrodynamic (HD) models.

The hydrological processes are simulated in a series of subarea elements connected by flood routing elements in a pre-determined sequence. The model simulates the hydrologic processes for one element for a defined period and passes the resulting output hydrographs information to the next element (Figure 2-3). The model structure

can be both grid-based or based on hydrologic sub-catchments. The model uses a soil module with storage capacities in considering infiltration, evapotranspiration and runoff generation. The discharge generation consists of three components: runoff generation, runoff concentration and river component.
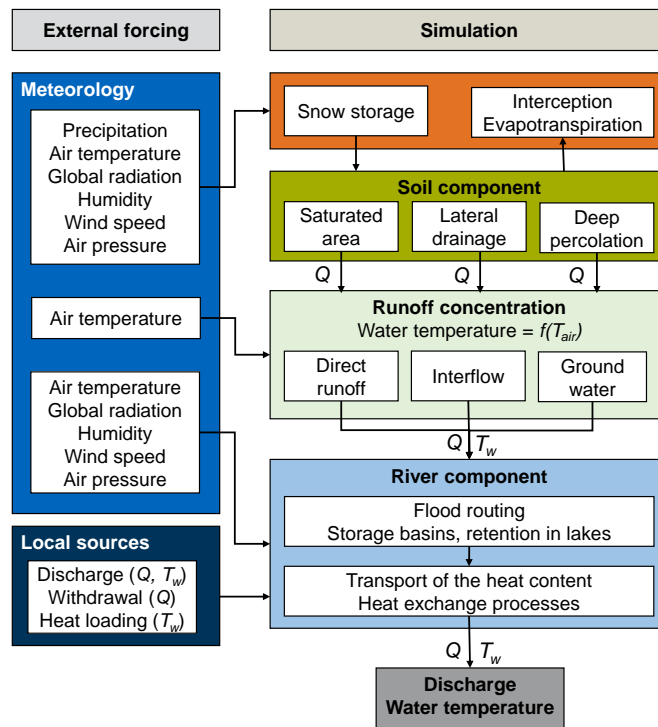
Figure 2-3. LARSIM water balance model. Source based on Ludwig and Bremicker (2006)

The model includes 34 parameters that allow modelling of different processes such as direct discharge, interflow and groundwater flow. The important parameters used in this dissertation and eight most sensitive parameters are presented in Table 2-1. Soil storage represents the most sensitive model component in the calibration of LARSIM. An extensive overview of the parameters and description can be found in Haag et al., (2016) and Ludwig and Bremicker (2006).

In addition to simulating hydrological processes, LARSIM is most suitable in operational flood forecasting. It deals with the gaps in hydrometeorological input data and allows for the correction/manipulation of numeric weather forecasts (e.g. external forcing parameters). Furthermore, the automated processes for the assimilation of hydrological data and for tracking models are crucial in flood forecasting (Luce et al., 2006; Haag and Bremicker, 2013).

Table 2-1. Parameters of the LARSIM water balance model including initially calibrated ranges (Data source: Based on Haag et al., 2016). Eight parameters (in bold) were identified as the most sensitive in this dissertation.

Parameter	Unit	Description	Ranges (L-U)
External forcing			
KG	[-]	Correction factor for the areal precipitation	0.9 – 1.1
KWD	[-]	Correction factor for the available amount of water including snowmelt	0.9 – 1.1
Nkor	[-]	Correction factor for rainfall measurements error	0.9 – 1.1
Snow storage			
T_Gr	[°C]	Mean temperature of the transition zone from snowfall to rain	-3 – 2
ScRa	[mm/h]	Soil heat flow as potential melting rate	0.01 – 0.05
Abso	[-]	Absorption coefficient of the snowpack for short-wave radiation	0.02 – 0.25
A0	[W/m^2 ^{o}C]	Heat exchange at the snow line, independent of the wind	0.5 – 3.5
A1	[J/m^3 ^{o}C]	Heat exchange at the snow line, dependent on the wind	0.8 – 2.5
SRet	[%]	Coefficient for the retention of liquid water in the snow pack	5.0 – 47.0
Soil storage and runoff generation			
A2	[mm/h]	Threshold value for fast and slow surface runoff	0.5 – 4.0
BSF	[-]	Exponent of the soil moisture saturation area function	0.01 – 0.5
Dmax	[-]	Calibration factor for lateral drainage to the interflow storage at saturated conditions	0 – 10
Dmin	[-]	Calibration factor for lateral drainage to the interflow storage at field capacity	0 – 5
β	[1/d]	Drainage index for deep percolation from the lower soil storage	0.000002 – 0.1
WZPf	[-]	Threshold value for the lower soil storage as a fraction of the total soil storage	0.25 – 0.75
WZBo	[-]	Threshold value for the middle soil storage as a fraction of the total soil storage	0.35 – 1.05
Mauf	[mm/d]	Maximum rate of capillary rise	0.9 – 1.1
KFeld	[-]	Correction factor for the field capacity	1.0 – 1.4
Runoff concentration			
EQD2	[-]	Calibration variable for the retention constant of the fast surface runoff storage	10 – 1000
EQD	[-]	Calibration variable for the retention constant of the slow runoff storage	50 – 5000
EQI	[-]	Calibration variable for the retaining constant of the interflow storage	200 – 15000
EQB	[-]	Gauging size for the retaining constant of the basis discharge storage	5000 – 100000
Flood routing			
EKM	[-]	Calibration factor for the roughness coefficient in the main river bed	0.3 – 3.0
EKL / EKR	[-]	Calibration factors for the roughness coefficients on the flood plains	0.3 – 3.0

In the operational model, the measured and simulated discharges can be compared, and the model allows to adjust model parameters as well as model output corrections (using ARIMA corrections), which improves the quality of forecasting. LARSIM is operationally used in the German states of Baden-Württemberg, Bavaria, Hesse, North Rhine-

Westphalia, Rhineland-Palatinate, and Saarland, the Austrian states of Tyrol and Vorarlberg, in Luxembourg and the French regions of Alsace and Lorraine, and currently cover an area of more than 200,000 km² (Laurent et al., 2010; Demuth and Rademacher, 2016).

In this dissertation, the LARSIM model used was provided by the flood forecasting centre for the river Main at the LfU, Hof. A preliminary analysis suggests that it is difficult to calibrate the model parameters to represent satisfactory results for each event at every gauge. Figure 2-4 presents observed vs. simulated peak discharges identified for a duration of eight years (2004-2011) for the gauging stations Ködnitz and Kauerndorf.

(a) Ködnitz   (b) Kauerndorf
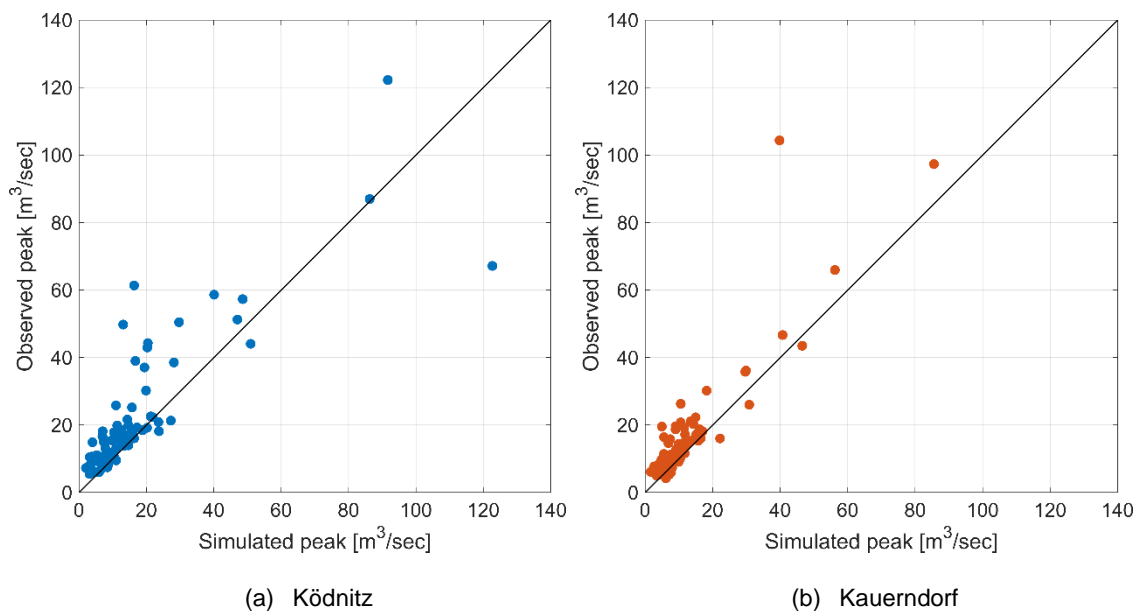
Figure 2-4.Peak discharges of LARSIM for events above a discharge of MQ (arithmetic mean), identified from eight year time series (2004-2011).

It can be observed that with the inputs and parameters set for this LARSIM model, the model generally tends to under-predict the peak of the events. Also, it shows a satisfactory performance for the gauge Kauerndorf but under-predicts the May 2006 flood event by 66 m³/sec. Hence, in order to use the model in flood forecasting, it is important to conduct a comprehensive uncertainty assessment of the model parameters and to develop methods to update the model outputs using an ensemble technique.

The uncertainties in this LARSIM model parameters were quantified and are presented in Chapter 6. In addition, novel methodologies to reduce uncertainty bounds of the LARSIM model outputs such as *Discharge intervals*, *Rising and receding*, and *Slope interval*, were developed in Beg et al. (2018), Beg et al. (2019) and Leandro et al. (2019) but not included in this dissertation.

2.2.2. Hydrodynamic models

HD models are the most important tools required for the flood inundation forecasting, hence various models have been reviewed and tested in my dissertation. Flooding in natural channels is a 3D process that is typically simulated by using HD models that are simplified for idealized environmental systems based on certain assumptions. The structure of an HD model can be described by its governing equations as well as in the dimensions these equations are solved, such as 1D, 2D and 3D (Liu et al., 2019).

Except for catastrophic scenarios of dam breaks where the full dynamic equations must be applied, flood inundation is characterized by a slow-moving phenomenon whereby the inundation can be modelled by the diffusive-wave approximation (Chen et al., 2005). The diffusive-wave approximation neglects the inertial terms allowing, therefore, a simplified set of equations to be solved. In general, terms using a simplified set of equations lead to faster computational times. However, due to the stability criterion, some authors observed that diffusive models can be computationally less effective than dynamic models when high-resolution meshes (i.e. 10 m or less) are used. In urban areas, Maksimovic and Prodanovic´ (2001) suggested values of 1-2 m and Mark et al. (2004) between 1-5 m as optimal grid sizes to capture all the main topographic features. The shallow water equations (mass and momentum conservation) are as follows:

$$\frac{dh}{dt} + \nabla(\boldsymbol{u}h) = R \qquad\qquad (2.1)$$

$$\frac{du}{dt} + (\boldsymbol{u}\nabla)\boldsymbol{u} + \frac{v_t}{h}(h\nabla\boldsymbol{u}) + g\nabla(h+z) = g\boldsymbol{S}_{\mathrm{f}} \qquad\qquad (2.2)$$

$$\begin{bmatrix} S_{fx} \\ S_{fy} \end{bmatrix} = \begin{bmatrix} \frac{n^2|\boldsymbol{u}|u_x}{h^{4/3}} \\ \frac{n^2|\boldsymbol{u}|u_y}{h^{4/3}} \end{bmatrix} \qquad\qquad (2.3)$$

Where h is the water depth (m), $\boldsymbol{u} = [u_x\ u_y]^{\mathrm{T}}$ is the depth-averaged flow velocity vector (ms^{-1}), g is the gravitational acceleration (ms^{-2}), R is source/sink term, such as rainfall, seepage or inflow, and $S_f = [S_{fx}\ S_{fy}]^{\mathrm{T}}$ is the bed friction vector, which can be approximated using Manning's formula given in equation 2.3, in which n is the Manning's coefficient Manning's n (sm$^{-1/3}$).

For diffusive-wave approximation, all the forces, in the momentum equations (Eq. 2.2) can be neglected except the gravity term $g\nabla(h+z)$ and bed friction S_f. $\frac{dh}{dt}$ term is only considered in the continuity equation (eq 2.1). The continuity and momentum equations

can be solved with an explicit or implicit scheme using a discretization technique, such as finite volume, finite element or finite difference on a regular or irregular grid.

HD models are available for various model structures with different levels of simplifications. The differences in model structures, such as the representation of river geometry, governing equations and numerical discretization, as well as model parameterization, lead to different outputs. Furthermore, the assumption of a steady flow, which is typically made for inundation map development, can have a major effect on simulated inundation, as the natural system responds differently to a dynamic flood than to an infinitely long and steady flow. As a result, unsteady flow models may be required in some instances, which is also the case in my dissertation. However, these unsteady models can be challenging to implement operationally due to their high-computational consumption (Bales and Wagner 2009).

Although 1D models have been criticized for representing the flow only between the cross-sections and not across the entire section, lack of available observed data and computational efforts to calibrate restrict the use of 2D models in flood inundation mapping and especially in operational uncertainty analysis. There have been comparative studies on the predictive performance of 1D and 2D models and they have shown that both approaches are equally reliable (Horritt and Bates 2002; Werner et al., 2005). On a catchment scale, a comparative study by Liu et al. (2019) concluded that both 1D and 2D models can give similar results with the right combination of channel and floodplain roughness, especially for a steep topography. Therefore, the impact of the model structure is not critical on a large catchment scale application. However, on an urban scale, this finding might not be applicable, where extreme non-uniformity and spatial variability of flow patterns are common. Flows may occur in sequences of fast-moving shallow flows (possibly supercritical) and in large still ponds, rather than in the form of channels that are well defined over long distances (Néelz et al., 2009). Besides, flow rarely occurs in urban areas along pre-defined routes that could be clearly identified prior to set up a model and running the simulations. Furthermore, it is recommended to incorporate all urban features, such as buildings, roads or dykes carefully (Leandro et al., 2016).

The choice of a model is dependent on the modelling purpose and scale, in the case of a catchment scale, e.g. the Upper Main (4244 km^2), a 1D or a High-performance computing (HPC) model is recommended. In the case of an urban scale, a 2D model can be applied for flood inundation purposes.

An overview of the HD models used for my dissertation is presented in Table 2-2. The table presents, two 1D HD models, for application on a catchment scale (Upper Main), and four 2D HD models with a diffusive- and dynamic-wave equations set up for the city of Kulmbach. The models have been used widely for various flood inundation applications and, given a thorough calibration, they are able to produce satisfactory results. These models were set up for the study areas and based on their performance and study objective, they have been used in various studies. The models were run for a real flood event in January 2011 for a duration of 42 hours. It should be noted that this dissertation does not serve as a comparative study among the HD models or as a guideline to select the best model. All the models presented in Table 2-2 serve a purpose and can simulate equally good results (given a calibration process) and have been used in various studies. Nevertheless, a comprehensive overview of existing HD models has been conducted by Néelz et al. (2009) and/or Teng et al. (2017). A comparison of HD model structures has been conducted by Oberle and Merkel (2007). In addition, a recent study Pflugbeil et al. (2019), compares HD models with the focus on flash flood modelling.

Table 2-2. Overview of hydrodynamic models used for this dissertation.

Model	Numerical scheme	Equations	Access	Min. area	Elements [millions]	Land use	Run-time [hours]
2D hydrodynamic models							
HEC-RAS 2D	Hybrid	Diffusive wave	Open source	6.8 m^2	~0.4	5 & 11	~2
MIKE 21 FM	Finite Volume	Dynamic wave	Commercial	0.2 m^2	~0.6	17	~16
Hydro_AS-2D	Finite Volume	Dynamic wave	Commercial	0.2 m^2	~0.6	17	~22
NUFSAW 2D	Finite Volume	Dynamic wave	In-house code	0.2 m^2	~3.2	11	~2
1D hydrodynamic models							
MIKE 11	Finite difference	Saint-Venant	Commercial	~200 m	-	2	~0.1
HEC-RAS 1D	Finite difference	Saint-Venant	Open source	~200 m	-	2	~0.1

2.2.2.1. 2D HD models

The two commercial 2D models, MIKE 21 FM (DHI, 2017) and Hydro_AS-2D (Nujić, 2006) are well-established codes for solving full shallow water equations and have been used extensively in the field of flood impact assessment. The motivation behind using Hydro_AS-2D is that the model is operationally used by the LfU, Bayern. In addition, flood inundation and risk maps for various exceedance level scenarios are published by

the LfU, Bayern using this model (HND, 2019). Methodologies incorporating this particular model would be more susceptible to potentially be applied in operation-use compared to other models. This model was used in Chapter 5 (Disse et al., 2018) to quantify the propagation of the hydrological model parameter uncertainties.

The models of DHI suites (e.g. MIKE 21 FM) have the advantage that they can be used for complex model structures. The models have the possibility to simulate coupled 1D-2D integrated urban/floodplain processes. In the case of a flash flood, urban drainage plays an important role and its impact on flooding should not be ignored (Leandro et al., 2011). The high run-time required by both the above models limits the application of these models in real-time flood inundation forecasting as well as in performing a comprehensive uncertainty assessment. These models can be used on a licensed version desktop/server associated with a limited number of cores. Although both the models have a Central Processing Unit (CPU) and Graphics Processing Unit (GPU) parallelization, the license costs associated restrict the use of these models. Having said that, given an infrastructure, these models perform exceptionally well as have been successfully applied in many case studies (Patro et al., 2009; Timbadiya et al., 2014). The major advantage of these models is the fast handling of input-output via user-friendly Graphical User Interface (GUI), which reduces the model set up time considerably, especially for a complex mesh containing numerous urban features.

HEC-RAS 2D was used extensively in this dissertation due to its less computational run-time and suitability in flood inundation forecasting and for the possibility of conducting a thorough uncertainty analysis. The model has been widely used for various flood inundation applications (Moya Quiroga et al., 2016; Patel et al., 2017). A disadvantage of the model is that it cannot incorporates internal boundaries for structures, such as buildings (as void), bridges and weirs. In addition, the model is not stable for very fine resolution models (less than 2 m grid size). However, the model employs a sub-grid bathymetry approach to compensate for large grid size and includes buildings as high-elevations or roughness.

Finally, an in-house code NUFSAW2D, which solves full dynamic-wave equations, developed by Ginting and Mundani (2019), was used. Compared to other models, this model has the advantage that it can be used in modern clusters and supercomputers. It is suitable for real-time flood forecasting and for conducting an extensive uncertainty analysis. This model was simulated on CoolMUC-2 cluster with AVX2 (Intel Xeon E5-2697 v3/Haswell), provided by the Leibniz Supercomputing Centre (LRZ, 2019). The model was tested on up to 336 cores and the code can achieve approximately 5.5

Mcell/s/core (for a single-core computation) on this machine, which roughly estimates to up to 2 hours for an event of 42 hours. The model results have been presented and submitted in Bhola et al. (2018) and Ginting et al. (2019).

There are various other 2D HD models worth mentioning, but due to time considerations, they were not investigated. Among the noteworthy ones are TELEMAC-MASCARET (Hervoue, 2000), P-DWave (Leandro et al., 2014), FloodArea (FloodArea, 2017) and LISFLOOD-FP (Neal et al., 2009). Nevertheless, the four models were set up for the city of Kulmbach. In Figure 2-5, the maximum inundation extent is presented for the flood event of January 2011. It should be noted that these model results have not been subjected to calibration and are presented here for the sake of the argument presented by researchers that given a rigorous calibration process an optimal accuracy can be achieved with any model (Horritt and Bates 2002; Werner et al., 2005).
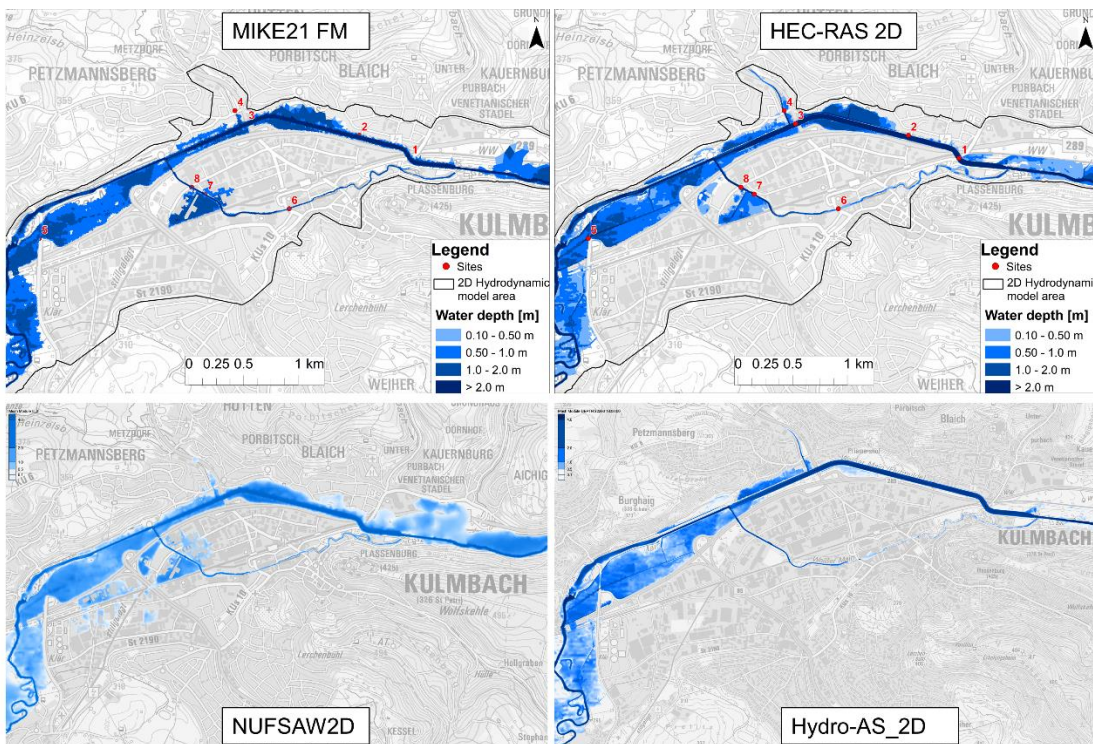
Figure 2-5. Maximum flood inundation maps simulated for the four HD models for the flood event of January 2011.

2.2.2.2. 1D HD models

On the catchment scale, two 1D HD models were set up and coupled with the hydrological model for the entire Upper Main catchment (4244 km^2) with the objective of forecasting flood hazards, such as water depths and flow velocities, on the infrastructures located along the Upper Main river. A preliminary comparison in water levels of MIKE 11 and HEC-RAS 1D is shown in Figure 2-6. It can be observed that,

given a calibration, the measured peaks can be achieved and both models can simulate the peak well. Although, HEC-RAS 1D shows instabilities in the few cases as compared to MIKE 11 (Figure 2-6a), due to its weaker unsteady flow module.

(a) Mainleus   (b) Schwürbitz

(c) Kemmern
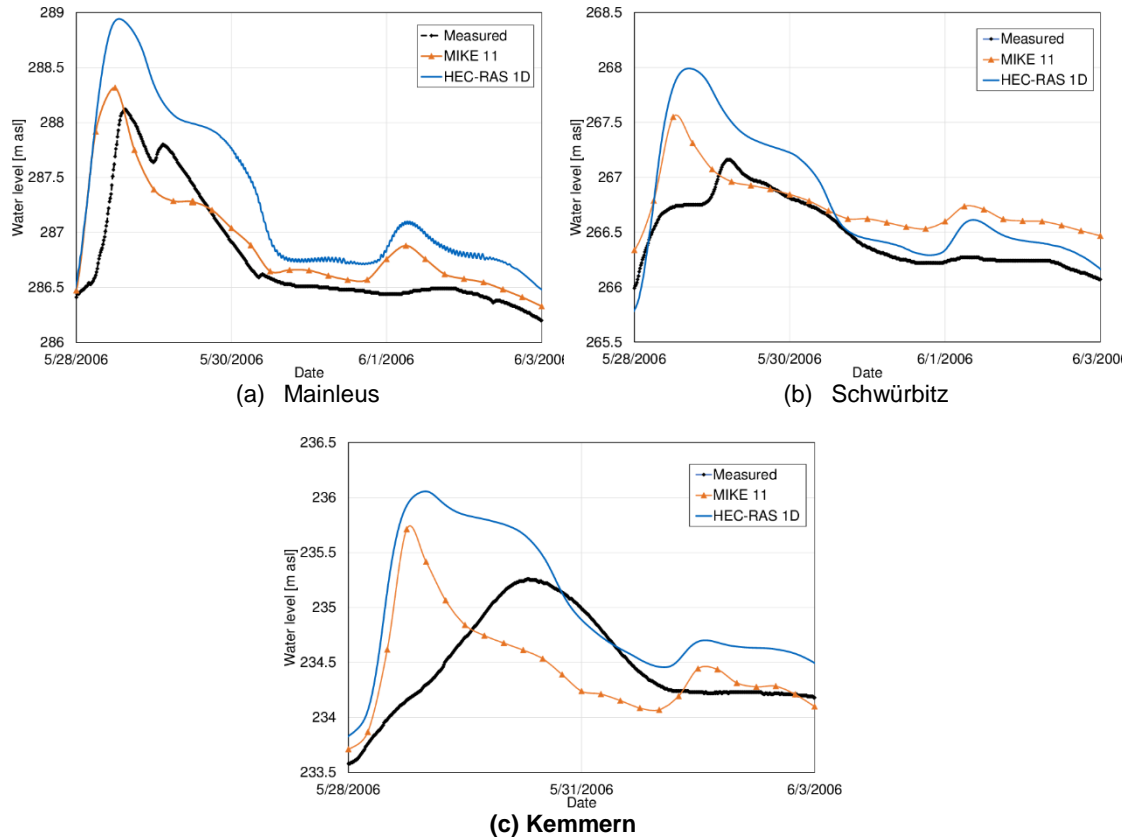
Figure 2-6. Water level comparison at three gauging stations for the flood event of May 2006.
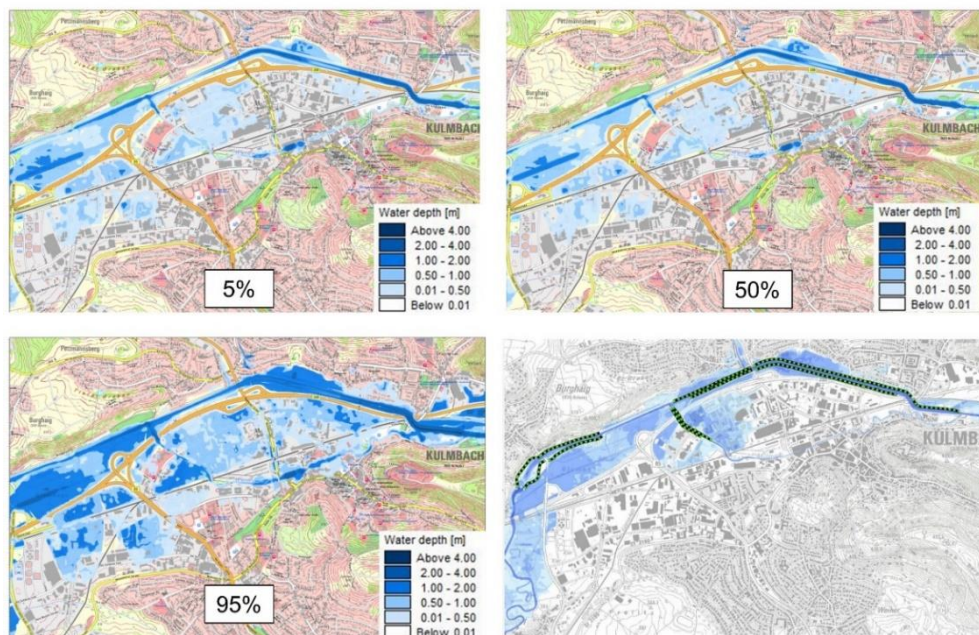
Figure 2-7. Uncertainties in flood inundation of 100-year period discharge using MIKE 11 (presented in Bhola et al., 2016) and 100-year return period flood inundation map obtained from HND (2019).

23

Furthermore, the combined uncertainties in the MIKE11 boundary conditions, elevation and parameters were quantified and presented in Bhola et al. (2016). The main finding is presented in Figure 2-7, which shows a 5%, 50% and 95% confidence interval flood inundation map of a 100-year return period for the city of Kulmbach. Furthermore, the 100-year period flood inundation maps are published for each city by the LfU, Bayern, which are the model results of the Hydro_AS-2D model. The map is presented here as a reference for the MIKE 11 model outcomes. It makes an interesting comparison together with the 1D inundation extents and it can be observed that most of the inundation is captured by the 50% results. It should be noted here again that even with a simple model structure, acceptable flood inundation maps can be achieved. However, the accuracy depends on many factors, such as topography, flow velocities, inundation area and land use (Werner et al., 2005).

In summary, the selection of an HD model is the first step for any flood forecasting framework. Various models are available for a variety of purposes, advantages and limitations; hence, users must select them based on the modelling purpose.

2.3. Flood inundation forecasts – Methods and validation

Flood risk management plans should include flood forecasts and early warning systems that take the characteristics of a river basin or sub-basin into account (European Union, 2007). In a global review of operational flood forecasting, Adams and Pagano (2016), have stated that none of the flood management agencies performs real-time flood inundation mapping due to the fact that the unsteady HD models are data-rich and computationally too expensive to run in real-time. In addition, researchers have also reviewed existing operational flood forecasting systems on a global, continental and local scale (Emerton et al., 2016; Jain et al., 2017). In a few cases, a pre-run library of multiple inundation scenarios based on predictions at river gauging stations is used to provide inundation maps. The *Flood Inundation Mapping and Alert Network* (FIMAN, 2016) for North Carolina in the United States is the most notable example of dynamic flood inundation web-mapping.

In Germany, the federal states are responsible for flood information services. In particular, in Bavaria, early flood warnings are provided in the form of hydrological forecasts by the Flood Forecast Centre of the Federal State of Bavaria (Laurent et al., 2010). However, the forecasting is limited to discharge hydrographs for a lead-time of 12-18 hours without the simulation of HD models. Figure 2-8 presents the state-of-the-art flood warning in Bavaria. The discharge forecasts are converted to water level at

gauging stations based on their respective stage-discharge relation. Hence, an HD model is required to simulate the distributed predictions of flood hazards in terms of water depth, inundation extent, and flow velocity in the form of flood inundation maps (Bates et al., 2014). These maps are a standard tool for designing flood defences and regulating building in the floodplain. In addition, they make the local emergency services aware of structures at risk and spatially distributed flooding hazards in the community.
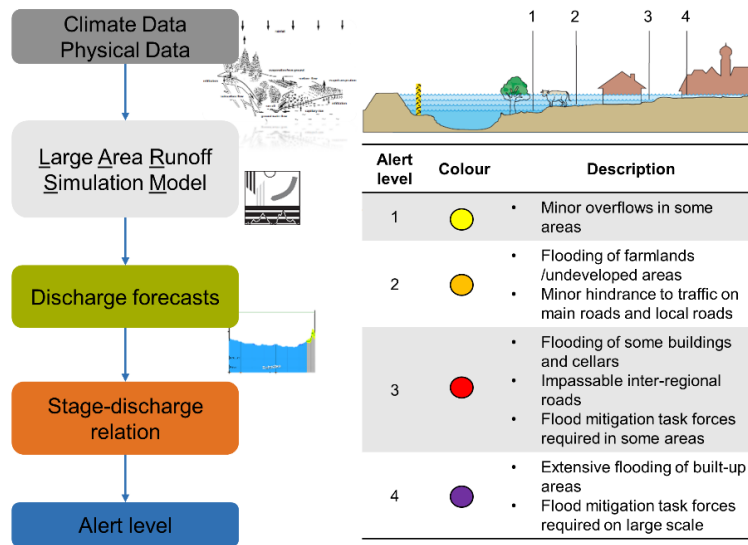
Figure 2-8. State-of-the-art forecasting in Bavaria. Discharge forecasting at gauging stations using the hydrological model *LARSIM* and conversion to alert levels using a stage-discharge relation. Data source: based on HND (2019)

Table 2-3. Overview of existing real-time flood inundation forecast application based on empirical, pre-simulated scenarios and real-time simulation.

Flood	Input	Type	Location	Literature
Empirical scenarios without the use of hydrodynamic models				
River	Rainfall forecast	Dynamic	Kemanman, Malaysia	Chang et al., 2018a
River	Rainfall forecast	Dynamic	Tainan, Taiwan	Chang et al., 2018b
Flash	Rainfall forecast	Static	Havidovre, Denmark	Jenson and Pedersen, 2009
Pre-simulated hydrodynamic scenarios				
River	Gauge level	Static	Sabari river, India	Bhatt et al., 2017
River	Rating curve	Dynamic	Austin, Texas	Buahin et al., 2017
River	Gauge level	Dynamic	North Carolina, USA	FIMAN, 2016
River	Discharge forecast	Dynamic	Sava river, Southern Europe	Dottori et al., 2017
River	Discharge forecast	Static	Regional scale (Europe)	Alfiere et al., 2014
Flash	Rainfall forecast	Dynamic	Nimes, France	Raymond et al., 2006
Real-time hydrodynamic simulations				
Flash	Rainfall forecast	Dynamic	Bangkok, Thailand	Mark and Hosner, 2002
Flash	Rainfall forecast	Dynamic	Barcelona, Spain	Montero et al., 2010
Flash	Rainfall forecast	Dynamic	Wangamo, China	Hu et al., 2018

Flood inundation forecasting is a challenging task due to the lack of validation data and the high computational time required by the HD models for producing dynamic flood maps in real-time. An overview of existing flood inundation forecasting applications in research and operational use is presented in Table 2-3. According to Henonin et al. (2013), flood forecasting systems can be best classified in three categories: (i) empirical scenarios, (ii) pre-simulated scenario (termed as offline), and (iii) real-time simulations (online).

Empirically scenario-based systems do not involve the HD model at any stage. As an alternative, researchers have used surrogate models (Bermúdez et al., 2018) that replace expensive 2D inundation models with data-driven models. In addition, historical satellite images have also been used for flood inundation forecasting (Voigt et al., 2007; Bates, 2012). These alternatives, although practical, do not provide a high spatial-temporal resolution inundation maps that are suitable for reliable flood warning, especially in the case of rapid flood events.

Most prominent conventional method in operational use is pre-recorded flood extent scenarios developed for various water levels or discharges (FIMAN, 2016; Dottori et al., 2017; Bhatt et al., 2017). However, if the scenarios are not designed carefully, the uncertainty associated with this approach is too large (Henonin et al., 2013). The pre-recorded scenario-based systems have mainly been applied to building static flood inundation databases and rules have been developed to select the most probable scenario, using flood stages or rainfall forecast as input (FIMAN, 2016; Dottori et al., 2017; Bhatt et al., 2017). One of these systems has been tested in a flood forecast and warning system: ESPADA (Evaluation et Suivi des Pluies en Agglomération pour Devancer l'Alerte) (Raymond et al., 2007). In this application, 44 pre-existing scenarios were used and successfully tested in a September 2005 storm in Nîmes, Southern France. Another application of such systems has been used in Copenhagen, Denmark, in which a set of rules were used to select the most probable inundation map from a scenario-based catalogue based on local rainfall forecast (Henonin et al., 2013). On a continental scale, a pre-recorded early warning system, EFAS, was tested in the Sava river basin in south-eastern Europe and the results for the flood in May 2014 have highlighted the potential of the system to identify flood extent in urban areas (Dottori et al., 2017).

In real-time systems, HD simulations are required to accurately forecast the inundation (Murphy et al., 2016). However, a full dynamic-wave HD model is computationally

expensive to be simulated in real-time for a lead-time of 6-12 hours. In order to reduce the computational time, simplified model structures, as discussed in the previous section, have also been used. In addition, recent advances in HPC and GPU computing have improved the computational efficiency of HD models (Zhang et al., 2017; Hu and Song, 2018; Xing et al., 2918); however, resources consumption and regular maintenance of such infrastructure is a major issue in operational use (Henonin et al., 2013). The application of such resources might find its use in big cities but cost-effectiveness for smaller counties is a major concern. Furthermore, it is important to develop methods to equip decision-makers with low-cost and resource-friendly methods that do not require lengthy computation of the 2D inundation models in real-time and enable them to analyse inundation patterns well in advance of times of an emergency (Bhatt et al., 2017).

Flood forecasting, although physically deterministic, contains numerous uncertainties in model outputs (Beven et al., 2018). Therefore, it is important to build trust in the forecast by reducing false alarm with the help of validation data. In addition, validation of the inundation forecasting is essential to evaluate its accuracy and predictive capabilities. On catchment-scale, particularly gauged basins, quality measurements of stream flow or water level data is frequent, for example in Bavaria (Roth, 2008). However, in urban areas, spatial and temporal flood validation data is scarce (Leandro et al., 2011). Fortunately, recent developments in technology and crowdsourcing have led to new sources of data. A few researchers have used remote sensing data to validate inundation maps with satellite images (Poser and Dransch 2010; McDougall, 2012). There have also been attempts to gather crowdsourced hydrological measurements using smartphones and to develop a low-cost, practical method of data collection that can be used to predict floods (Kampf et al., 2018). Recent studies have integrated crowdsourced data in the field of inundation modelling in which images and video recordings from smartphones are used to investigate hindcasted flood events (Triglav-Čekada and Radovan, 2013; Kutija et al., 2014; Dapeng et al., 2016) and in real-time modelling frameworks (Smith et al., 2017). In another example, Wang et al., (2018) used a manual approach to detect objects in the images, such as lamp posts and pavement fences, to identify the boundary of the flood extent. Lowry and Fienen (2013) encouraged citizen scientists to participate in capturing stream flows and evaluated the accuracy of citizen measurements.

2.4. Uncertainties in flood forecasting – Quantification and communication

In deterministic flood forecasting, the predictions of forecasting models: precipitation forecasts, hydrological models and HD models, are used to generate flood inundation maps. Although advances are continually being made in real-time forecasting, they are still inherently uncertain (Meyer et al., 2009; Bates et. al., 2014; Beven et al., 2018). The decision-making process based on uncertain predictions can have a huge economic impact and possibly lead to life and death situations (Leedal et al., 2010). Thus, a thorough assessment is required of the extent to which uncertainties affects the predictions of flood hazards. An overview of various components of flood inundation forecasting along with the sources of uncertainties is presented in Table 2-4. A list of selected literature is also provided for each source with the research conducted in the last two decades.

Table 2-4. Sources of uncertainties in flood inundation forecasting

Sources	Selected literature
Precipitation	
Parameters of the atmospheric model	Zappa et al., 2011; Thorndahl et al., 2017
Structure of the atmospheric model	Einfalt et al., 2005; Nester et al., 2012
Initial conditions	Golding, 2000; Park et al., 2008
Hydrological modelling	
Model parameters	Coccia and Todini, 2011; Zhang et al., 2016
Model structures	Butts et al., 2004; Tyralla and Schumann, 2016
Precipitation measurements	Komma et al., 2007
Precipitation interpolation	Mair and Fares, 2011; Ly et al., 2013
Hydrodynamic modelling	
Model roughness	Hall et al., 2005; Werner et al., 2005
Boundary conditions	Pappenberger et al., 2006; Bermúdez et al., 2017
Measurement data	Bates et al., 2014
Model structure	Bach et al., 2014; Liu et al., 2019
Uncertainty techniques	
Methods	Dotto et al., 2012; Beven and Binley, 2014
Ensemble reduction techniques	Dietrich et al., 2009

Researchers have stressed the importance to incorporate uncertainties as an integral part of warnings (Jain et al., 2014). The focus of my dissertation is uncertainties in flood inundation forecasting, especially arising from the HD models. Precipitation is often the most important source of uncertainty considered (Germann et al., 2009; Zappa et al., 2011; Thorndahl et al., 2017). It contains the error components of the parameters and

the structure of the atmospheric model as well as the initial conditions. The discharge generation is usually the first step of inundation forecasting, using the forecasted precipitation. Researchers have addressed various sources of uncertainties in the generation of discharge, such as precipitation measurements, spatial interpolation of the precipitation, model parameter, model structure (Nester et al., 2012; Leandro et al., 2013). Substantial research has thus far dedicated in the field of discharge forecasting. A recent study by Boelee et al. (2018) reviews uncertainty quantification methods to provide practitioners with an overview of the ensemble modelling techniques. An overview of existing ensemble forecasts in operational use can be found in Cloke and Pappenberger (2009) and Todini (2017). In my dissertation, I have focused on the federal state of Bavaria in which discharge ensembles are generated using the COSMO-DE-EPS precipitation ensemble as input for the hydrological model LARSIM (Laurent et al., 2010). Another application of discharge ensemble generation using similar models is found in the federal state of Rhineland-Palatinate as well (Bartels et al., 2017). Although uncertainty in precipitation ensembles are not addressed in my dissertation, precipitation spatial interpolation uncertainty is accounted for by considering conditional geospatial simulation for distributing the precipitation data within the entire catchment (Leandro et al., 2019).

The discharges are then used as input boundary conditions in a 2D HD model to produce flood hazard maps. The major sources of uncertainty in HD models can be categorized as model structure, model input, model parameters, measurement data and the modeller (Matott et al., 2009; Schumann et al., 2011). The HD model structure, as discussed in the previous section (1D, 2D or hybrid 1D-2D HD code) is generally selected based on the purpose and scale of the modelling (Musall et al., 2011; Bach et al., 2014). In addition, there is no general agreement on the best approach to consider model structure uncertainty; hence, it is often neglected (Oubennaceur et al., 2018). Model input consists of boundary conditions and topography data. The boundary conditions can come from a hydrological model, flood frequency analysis or in the case of hindcasting a flood event, from measured discharges or water levels. Recent advances in LIDAR (Light Detection and Ranging) technology have given way to obtain a fine-resolution elevation model with a high vertical accuracy, which tends to reduce uncertainties from topography (Saksena and Merwade, 2015). Furthermore, model parameters, mainly roughness, are a major source of uncertainty in HD models and discussed, in particular, in Chapter 5.

The precise meaning of roughness changes based on a model's physical properties, such as grid resolution and time step (Bates et. al., 2014), and the term is denoted as

Manning's roughness coefficient or simply Manning's n in most of the HD models. The coefficient is either derived from measurements in the field or estimated from the relevant literature on the basis of land use types, but it has proven very difficult to demonstrate that such models can provide accurate predictions using only measured or estimated parameters (Hunter et al., 2007). As this parameter is scale-dependent, the roughness term compensates for varying conceptual errors in the model (Néelz et al., 2009). It is not only related to bottom friction but also includes incorrect representation of turbulence losses, 3D effects and incorrect geometry (profiles); therefore, it cannot be measured exactly.

Various studies point out that HD models can be very sensitive to Manning's n, which implies a higher degree of uncertainty (Aronica et al., 1998; Pappenberger et al., 2005; Werner et al., 2005). Despite uncertainties in flood forecasting models, a single calibrated model or *best-model* approach is used in operational forecast applications (Henonin et al., 2013) instead of using multiple models in forecasting mode. Several studies (e.g. Aronica et al., 1998; Horritt and Bates, 2002; Romanowicz and Beven, 2003; Horritt et al., 2007; Di Baldassarre et al., 2009) have shown that a *best-model* may perform very poorly when it is used to predict events different from those used for the calibration.

(a) May 2006 © Feuerwehr Kulmbach	(b) January 2011 © Feuerwehr Kulmbach	(c) May 2013 © Melitta Burger
(d) July 2015 © Punit Bhola	(e) April 2017 © Punit Bhola	(f) December 2017 © Punit Bhola

Figure 2-9. Characteristics of floods and vegetation over a period in the main channel and flood plains in Kulmbach.

These studies showed that the effective roughness coefficients may be different when evaluated for flood events of different magnitude, even when uncertainty in calibrating roughness coefficients is allowed for. In addition, the values are obtained based on land use, which has seasonal characteristics and changes over time. Both the issues are shown in Figure 2-9 in which flood inundation and vegetation over a long period is shown in White Main in Kulmbach. In the figure, images a-c show three major historical flood events, whereas images d-c show three non-flooding events. For example, images b, c and d are taken from the same bridge and it can be observed that the vegetation or grass length varies over time. As argued by Di Baldassarre et al. (2009), an HD model, calibrated on a hindcasted event, may give a poor prediction on another event, especially on a different or higher magnitude. Therefore, flood inundation forecasting based on a *best-model* approach must be criticised and a range of parameters, which show equifinality in model results must be employed in operational flood risk management.

Another major issue with the generated forecasts is that the uncertainty bounds are too wide and cannot be incorporated into the decision-making processes (Pappenberger and Beven, 2006). This is generally taken care of by employing uncertainty reduction methods, such as the Generalized Likelihood Uncertainty Estimation (Beven and Binley, 2014), Global Sensitivity Analyses (Pappenberger et al., 2008) and the Shuffled Complex Evolution Metropolis Algorithm (Dotto et al., 2012). Dotto et al. (2012) have compared four different uncertainty techniques in their studies and have suggested modeller to select a suitable model based on model purpose, complexity, skill level and available information.

These and similar developments offer a potential framework for quantifying uncertainties. In fact, Beven et al. (2014) have presented a well-defined framework for assessing uncertainties that can be employed in flood inundation forecasting. In addition, Pappenberger et al. (2006) provide a decision tree to find the appropriate method for a given situation. However, the effective communication of the quantified uncertainties to decision-makers is a challenging issue in natural hazards (Doyle et al., 2019). Researchers have questioned how uncertainties should be communicated to reduce the risk of wrong or inappropriate decisions (Bruen et al., 2010; Todini, 2017). Hall and Solomatine (2008) focused on the process of uncertainty analysis, with particular reference to how uncertainty analysis can inform decision-making.

To summarise, this chapter presented an overview of the investigated study area along with the forecasting models and methods used. The chapter provides an overview of the

state-of-the-art and gaps in each research topic. In addition, preliminary models' outcomes are provided to state the gap in research and to support arguments presented in the literature. A more detailed discussion on methods and results is presented in the next chapters.

Chapter

3. Flood inundation forecasts

Flood inundation forecasts using validation data generated with the assistance of computer vision[1].

Forecasting flood inundation in urban areas is challenging due to the lack of validation data. Recent developments have led to new genres of data sources, such as images and videos from smartphones and CCTV cameras. If the reference dimensions of objects, such as bridges or buildings, in images are known, the images can be used to estimate water levels using computer vision algorithms. Such algorithms employ deep learning and edge detection techniques to identify the water surface in an image, which can be used as additional validation data for forecasting inundation forecast. In this study, a methodology is presented for flood inundation forecasting that integrates validation data generated with the assistance of computer vision. Six equifinal models are run simultaneously, one of which is selected for forecasting the inundation based on a goodness-of-fit (least error), estimated using the validation data. Collection and processing of images is done offline on a regular basis or following a flood event. The results show that the accuracy of inundation forecasting can be improved significantly using additional validation data.

3.1. Introduction

Forecasting real-time flood inundation is challenging due to the lack of validation data and high-computational time required by two-dimensional (2D) inundation models for producing flood inundation maps. Thus, researchers have focused on using alternatives to 2D inundation models. A straightforward approach is to generate a large database of inundation maps, using either 2D inundation models (Disse et al., 2018) or historical satellite images (Bhatt et al., 2017), and create rules to select the most likely inundation map, based on forecasted discharges or flood stages (Bhola et al., 2018a). However, the uncertainty associated with this approach is too large (Henonin et al., 2013). Another alternative is the use of surrogate models (Bermúdez et al., 2018) that replace expensive 2D inundation models with data-driven models or more simplified model structures (Razavi et al., 2012).

Inundation models are available with various levels of simplification (Néelz and Pender 2009; Bach et al., 2014). A widely used model is a diffusive-wave model that simplifies full dynamic equations to reduce the computational time (Bates and Roo, 2000; Leandro et al., 2014). These models are suitable when inertial terms are not important, which is often the case for flood inundations in urban areas (Martins et al., 2017). Inundation models are typically calibrated, often using Manning's coefficient, to reproduce a set of observations e.g. water levels, inundation extent. This coefficient represents the resistance to flood flows in the model domain. Various studies point out that inundation models can be very sensitive to these coefficients, which leads to a higher degree of uncertainty (Oubennaceur et al., 2018). Despite uncertainties, a single calibrated model is used in operational forecast applications (Henonin et al., 2013) instead of using multiple models in forecasting mode.

Validation of the inundation forecasting is essential to evaluate its accuracy and predictive capabilities. However, spatial and temporal flood validation data in urban areas is scarce (Leandro et al., 2011). Fortunately, recent developments in technology and crowdsourcing have led to new sources of data. A few researchers have used remote sensing data to validate inundation maps with satellite images (Poser and Dransch 2010; McDougall, 2012). There have also been attempts to gather crowdsourced hydrological measurements using smartphones and to develop a low-cost, practical method of data collection that can be used to predict floods (Kampf et al., 2018).

Computer vision algorithms, such as edge detection and image segmentation, have been used to extract information from images (Zhai et al., 2008) and have been applied to many new areas of research (Uma et al., 2016). For instance, Jaehyoung and Hernsoo (2010) found the water level by measuring the water surface height with reference to an indicator (an invariant feature in the image). Techniques such as Scale-Invariant Feature Transform (SIFT) and automatic adaptive selection of region-of-interest have been used to detect edges and water lines in an image (Hies et al., 2012; Narayanan et al., 2014). In addition, Nair and Rao (2017) estimated flood depth by segmenting humans from a flood scene and detected their face and gender using deep learning algorithms.

Recent studies have integrated crowdsourced data in the field of inundation modelling in which images and video recordings from smartphones are used to investigate hindcasted flood events (Kutija et al., 2014; Triglav-Čekada and Radovan, 2013; Dapeng et al., 2016). In another example, Wang et al., (2018) used a manual approach to detect objects in the images, such as lamp posts and pavement fences, to identify the boundary of the flood extent. Lowry and Fienen (2013) encouraged citizen scientists to participate in capturing stream flows and evaluated the accuracy of citizen measurements. Although several applications of crowdsourced data exist, they are limited to hindcasting the flood events. Hence, there remains a need to use this validation data in improving the forecasting and establishing a back communication from crowdsource to the inundation forecasts.

In this paper, we present a methodology that integrates additional validation data, which is extracted from an image with the assistance of a computer vision algorithm. The main focus is to improve the accuracy of the inundation forecasting by using water levels obtained from images, which are collected on a regular basis or following a flood event. The methodology is tested on three historical flood events and is applied to the city of Kulmbach, Germany.

3.2. Study site and data

3.2.1. Kulmbach

The present study is in the city of Kulmbach (Figure 3-1), which is located in Upper Main river catchment in the North-East of the Free State of Bavaria in Southern Germany. The city has around 26,000 inhabitants. With a population density of 280 inhabitants per km^2 in an area of 92.8 km², it is categorized as a great district city. Traditionally, it has been a manufacturing base for the food and beverage industry. On 28th May 2006, intense

rainfall up to 80 litre/m2 intense rainfall occurred and within a few hours all the streams and rivers were filled (Tvo 2015). The incident prompted decision makers to revisit the flood protection measures for the city.
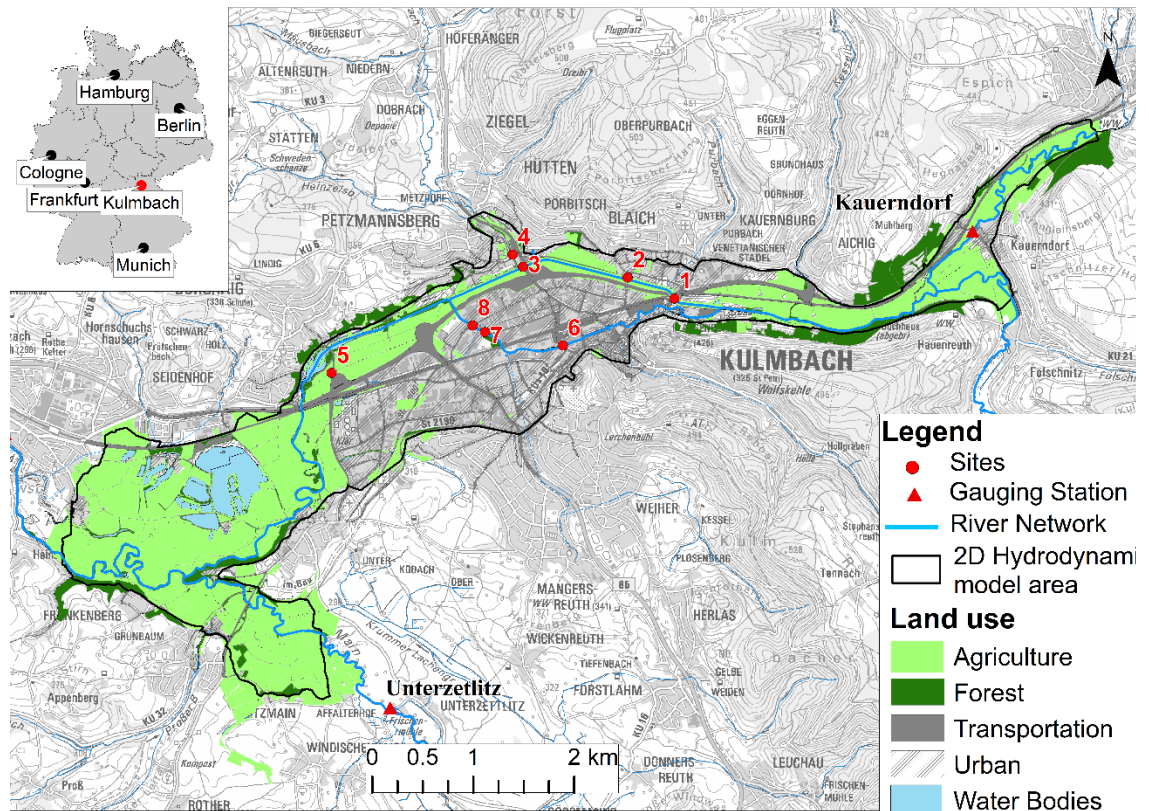
Figure 3-1. The location and land use classes of the study area in the city of Kulmbach, Germany (Data source: Bavarian Environment Agency and Water Management Authority, Hof). The river flows from east to west.

3.2.2. Hydrological data

Three hydrological events are used to assess the methodology. The hydrographs of the events upstream of the city at gauges Ködnitz on the river White Main and Kauerndorf on the river Schorgast are presented in Figure 3-2. Hydrological measurement data for the events were collected by the Bavarian Hydrological Services.
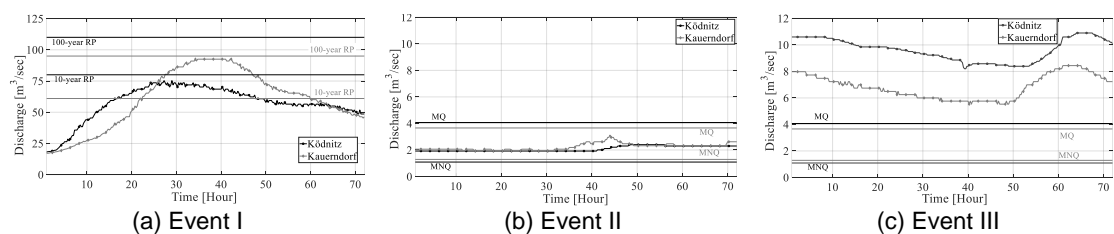
Figure 3-2. Discharge hydrographs at upstream gauges Ködnitz (in Black) and Kauerndorf (in grey) for three events, (a) Event I on 14th January 2011, (b) Event II on 13th April 2017, and (c) Event III on 07th December 2017 (Data source: Bavarian Hydrological Service, www.gkd.bayern.de, accessed 16.03.2018).

The winter flood in January 2011 (event I) was one of the biggest in terms of its magnitude and corresponded to a discharge of 100-year return period at gauge Kauerndorf and 10-year return period at gauge Ködnitz (Figure 3-2a). Intense rainfall and snow melting in the Fichtel mountains caused floods in several rivers of Upper Franconia. Within five days, two peak discharges were recorded. The first one occurred on 9th January and the second peak was measured five days on 14th January that caused even higher discharges and water levels. The maximum discharge of 92.5 m³/s was recorded at gauge Kauerndorf and 75.3 m³/s at gauge Ködnitz. Agricultural land and traffic routes were flooded, but no serious damage was reported. In Kulmbach, dyke in the region of Burghaig was about to collapse due to the large volume of water. The Water Management Authority opened the weir in Kulmbach that saved potential damages (Hof 2011).

Event II and III that occurred on 13th April 2017 and 07th December 2017 respectively, were of relatively smaller magnitudes as compared to event I and corresponded to a discharge of the lowest value of a year (MNQ) and the arithmetic mean (MQ) respectively (Figure 3-2b and Figure 3-2c). During these events, the water was contained well within the floodplains and thus, no inundation was recorded in the urban area.

3.2.3. Measured water levels and available images

The images and water levels were collected in three phases. In the first phase (event I), the Water Management Authority in Hof, Germany collected data during the winter flood and recorded water levels at eight bridges in Kulmbach. Figure 3-1 shows the location of bridges and Figure 3-3 shows the images taken. Based on the locations, the sites are categorized in four groups: sites 1, 2, and 3 at the river White Main; site 4 at Dobrach canal in the north; site 5 at a side canal; and sites 6, 7, and 8 at Mühl canal. Reference dimensions of the bridges were taken from a database SIB-Bauwerke that is developed by the German Federal Highway Research Institute (Bundesanstalt für Straßenwesen) (Bauwerke 2016). The database contains the design and detailed measurements of the infrastructures. The water levels were measured using a levelling instrument Ni 2 (Faig and Kahmen 2012). The instrument was used due to its availability and high accuracy, therefore associated uncertainties were not evaluated in this study. The event was used in calibrating the 2D inundation model and identifying model parameter sets for the inundation forecast.

(a) Site 1   (b) Site 2   (c) Site 3   (d) Site 4

(e) Site 5   (f) Site 6   (g) Site 7   (h) Site 8
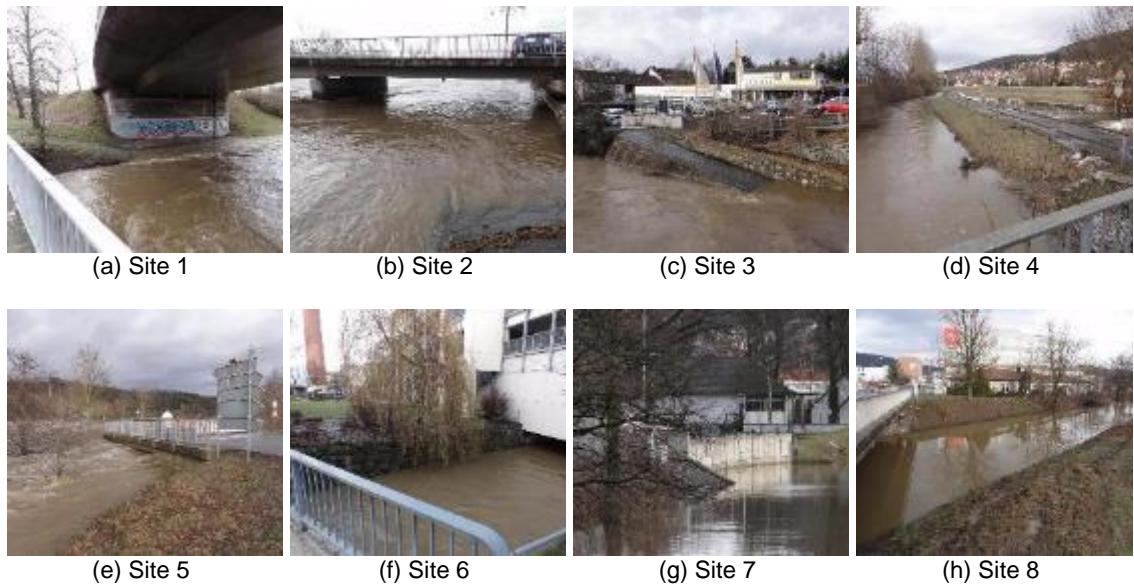
Figure 3-3. Images taken during event I on 14th January 2011 for the eight sites (Source: Water Management Authority in Hof, Germany).

(a) Site 1   (b) Site 2   (c) Site 3   (d) Site 4

(e) Site 5   (f) Site 6   (g) Site 7   (h) Site 8

Figure 3-4. Images taken during event II on 13th April 2017 for the eight sites.

(a) Site 1   (b) Site 2   (c) Site 3   (d) Site 4

(e) Site 5   (f) Site 6   (g) Site 7   (h) Site 8
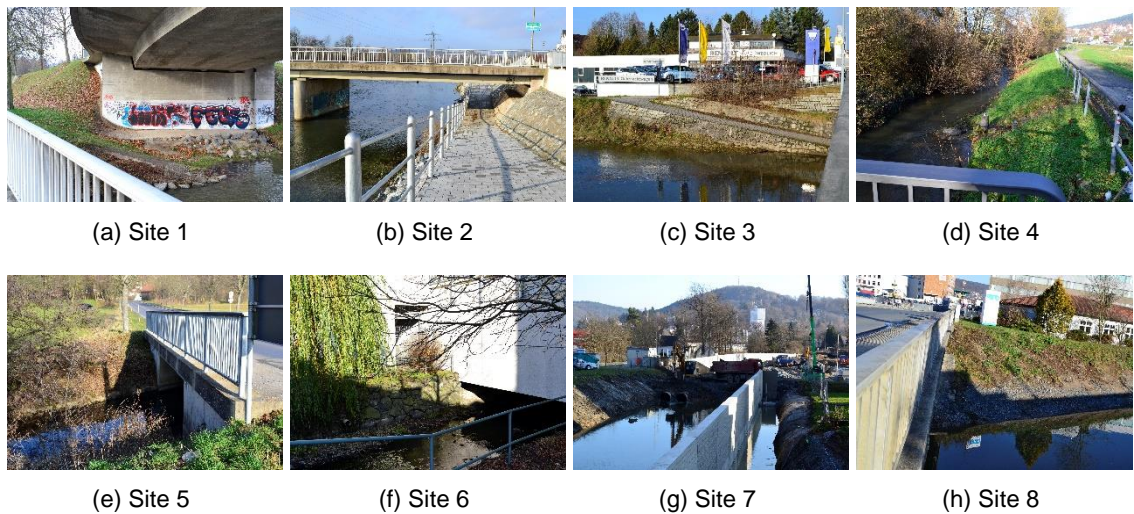
Figure 3-5. Images taken during event III on 07th December 2017 for the eight sites.

For the second phase (event II), images were taken to increase computer vision data set (Figure 3-4). For the third phase (event III), both images and water depths were recorded (Figure 3-5). During the event, the water surface heights were recorded using an electrical contact gauge, which is a measuring tape connected to an electric sensor used to detect water depth in tanks. The heights were measured from the top of the bridges and converted to water levels using the reference dimensions of the bridges. Event III was used in validating the 2D inundation model.

3.2.4. Topography and land use

The quality of inundation maps mainly depends on the topography of the study area. Topography data for this study was provided by the Water Management Authority, Hof. In the digital elevation model, the terrain is determined by airborne laser scanning and airborne photogrammetry, whereas the river bed is mostly recorded by terrestrial survey (Skublics 2014).

The land use of the model domain generally consists of agricultural land, specifically floodplains and grasslands, and covers up to 62% of the total model area. Water bodies make up to 7% and include river channels and lakes. The urban area covers around 26% and includes industrial, residential areas and transport infrastructure, whereas the forests form barely 5% of the total area.

3.3. Methodology

This section briefly describes the methodology used for flood inundation forecast, next the 2D inundation model HEC-RAS used for generating inundation maps, then the computer vision algorithm used to extract the water level from an image, and finally the goodness-of-fit used for model calibration and performance analysis to accomplish the objectives of this study.

3.3.1. Flood inundation forecasting

The conceptual flow chart of flood inundation forecasts integrates the validation data obtained with the assistance of computer vision algorithms (Figure 3-6). The methodology is an extension of the FloodEvac tool (Leandro et al., 2017) in which the discharges are forecasted in real-time at upstream gauging stations. The calibrated inundation model (MCal), determined based on a pre-selected event, is then run based on the forecasted discharges as input boundary conditions. The results of this model are forecasted as inundation maps. The contribution here is the incorporation of n+1 number

of models as well as a computer vision algorithm to improve the selection of flood inundation maps. In real-time, n different model parameter sets are run simultaneously with the calibrated model parameter set (n+1). This is motivated by the concept of equifinality (Beven and Binley, 1992) in which far more models are used as they represent the modelled system equally well. If an image becomes available in the model domain, the computer vision methodology is applied. Goodness-of-fit is calculated between n+1 model results and computer vision results. The model that produces the least error is selected for inundation forecasting. If no image is available, calibrated model parameter results (MCal) are used as a default.
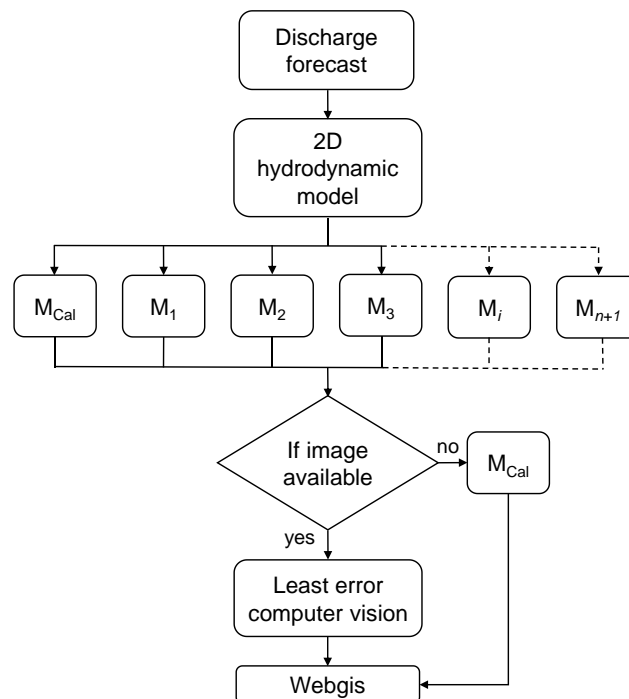
Figure 3-6. Conceptual flow chart of flood inundation forecasts incorporating a computer vision algorithm for n+1 models.

3.3.2. 2D flood inundation model: HEC-RAS

The 2D flood inundation maps were generated using HEC-RAS 2D. It is a non-commercial hydrodynamic model developed by the U.S. Army Corps of Engineers and has been used widely for various flood inundation applications (Moya Quiroga et al., 2016; Patel et al., 2017; Bhola et al., 2018a). The model employs an implicit finite difference scheme to discretize time derivatives and hybrid approximations, combining finite differences and finite volumes to discretize spatial derivatives. The implicit method allows for larger computational time steps compared to an explicit method. HEC-RAS solves either 2D Saint Venant or 2D diffusion-wave equations. The latter allows faster

calculation and has greater stability due to its complex numerical schemes (Martins et al., 2017). Due to these advantages and suitability for use in real-time inundation forecast (Henonin et al., 2013), we have used the diffusive-wave equations in this study. For the diffusive-wave approximation, it is assumed that the inertial terms are less than the gravity, friction, and pressure terms. Flow movement is driven by barotropic pressure gradient balanced by bottom friction (Brunner, 2016). The equations of mass and momentum conservation are as follows:

$$\frac{\partial H}{\partial t} + \frac{\partial (hu)}{\partial x} + \frac{\partial (hv)}{\partial y} + q = 0 \qquad (3.1)$$

$$g\frac{\partial H}{\partial x} + c_f u = 0 \qquad (3.2)$$

$$g\frac{\partial H}{\partial y} + c_f v = 0 \qquad (3.3)$$

$$c_f = \frac{g|V|}{M^2 R^{4/3}} \qquad (3.4)$$

Where H is the surface elevation (m); h is the water depth (m); u and v are the velocity components in the x- and y- direction respectively (ms^{-1}); q is a source/sink term; g is the gravitational acceleration (ms^{-2}); cf is the bottom friction coefficient (s^{-1}); R is the hydraulic radius (m); |V| is the magnitude of the velocity vector (ms^{-1}); and M is the inverse of the Manning's n (m$^{(1/3)}$s^{-1}).

The model was set up for the city of Kulmbach using the gathered data and Table 3-1 summarises the model properties and the details of the mesh size in the model domain. The model parameter consists of roughness coefficient Manning's M for five land use classes. Aronica et al. (1998) suggested to use extreme feasible upper and lower ranges for the parameters because a simple model structure does not reflect the true distribution of the parameters in the basin. Hence, literature-based extreme ranges of the Manning's M are set as: 9.1 – 40.0 for agriculture, which covers a range from short grass to medium-dense brush; 6.7 – 66.7 for water bodies, very weedy reaches to rough asphalt; 5.0 – 9.1 for forest, in dense trees (Chow, 1959); 50.0 – 83.3 for transportation, firm soil to concrete; and 12.5 – 25.0 in urban area, cotton fields to small boulders (Arcement Jr. G. and Schneider, 1989). Sensitivity analysis of the model was performed using one thousand uniformly distributed model parameter sets for event I.

Table 3-1. 2D hydrodynamic model properties of the HEC-RAS 2D model.

Data	Value
Model area	11.5 km^2
Total number of cells	430,485
Δt	20 s
Minimum cell area	6.8 m^2
Maximum cell area	59.8 m^2
Average cell area	24.8 m^2
Downstream boundary condition slope	0.0096

3.3.3. Computer vision

The work flow of the computer vision algorithm used to estimate water level is shown in Figure 3-7. Input images consist of reference and target images. The reference images are collected over a period in known locations and relevant objects, such as bridges and buildings, are identified in the images. The dimensions of the objects are marked in the reference images using the SIB-Bauwerke database.

Target images are obtained as described in section 3.2. Based on their locations, the target images are compared with the reference images and the relevant edges of the objects are mapped in them. The relevant edges to be mapped from the reference image are two horizontal edges corresponding to a known dimension of the bridge and a vertical edge corresponding to a vertical railing on the bridge (Figure 3-7). The water surface line in the target image is then detected. In order to estimate the water levels, the work flow steps include: (1) mapping the relevant edges of the object from the reference image to the target image, and identifying the water line in the target image; (2) measuring the pixel distance between the relevant edges in the target image; (3) correlating the pixel distance with the real-world dimension of the object and calculating the ratio; and (4) estimating the water surface height in m based on the ratio and conversion to water level in m above mean sea level (asl). The procedure was fully automatized except for step 1.

The image processing is performed using computer vision, coded in the programming language Python using OpenCV, which is a library of open-source codes that solves real-time computer vision algorithms. One of the key aspects of the algorithm is mapping pixel dimensions to physical dimensions in the target image. This ratio will be different for each target image and is obtained using the known physical dimensions of the bridge, obtained from the reference image, and the known reference dimensions in pixels, obtained from the target image (see Figure 3-7).
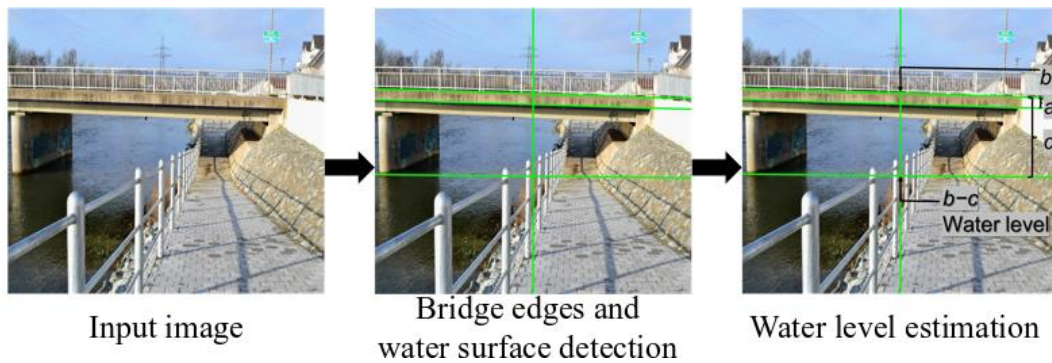
Figure 3-7. Work flow of water level estimation algorithm and annotated image of a flood scene. The reference level (*b*) taken from the SIB-Bauwerke database in metre above mean sea level (m *asl*), the thickness of the slab/object (*a*) in m, and the distance between water surface and reference level (*c*).

To estimate the water level in an image, the parameters marked in Figure 3-7: the thickness of the bridge slab (*a*) in m, and the reference elevation of the bridge (*b*) in m *asl* were used as input to the code. In order to reduce the perspective distortion of the image, a vertical line was drawn to calculate the ratio of pixels to the physical dimension. The line must align with a vertical railing on the bridge to ensure that it is perpendicular to the horizontal edges. Even though it may not appear perpendicular in the image due to the perspective. The perspective distortion was reduced by restricting the drawn edges to coincide with the edges on the bridge, both in horizontal and vertical directions. The distance between the water surface and reference level (*c*) in m was obtained using equation 3.5:

$$c = \frac{c\_pixel}{a\_pixel} * a \qquad (3.5)$$

Where *a_pixel* and *c_pixel* are the pixel distances of the bridge slab and water surface in the image. Their ratio was calibrated for each image using many iterations by manually detecting the edges. In this approach, ten iterations for each image were used to calibrate the ratio. The water level in m *asl* was calculated as the difference of *b* and *c*.

A set of requirements was developed to minimize the error in estimating the water levels. A suitable input image must meet the following three requirements: (1) the edges of the bridge and the water line should be clearly visible in the image; (2) the camera should be placed in front of the bridge to capture the image such that the edges of the bridge and water line appear as three parallel lines, which is important to minimize the perspective distortion; and (3) the image should be taken in proper lighting conditions.

3.3.4. Evaluation metrics

Model selection

For the real-time forecasting, *n+1* number of model parameter sets were selected from one thousand uniformly distributed parameter sets based on the sum of the absolute error between the simulated and the measured water levels at eight sites (Figure 3-1). The goodness-of-fit (*e*) was calculated using equation 3.6, which returns an array of one thousand values. The values were sorted and *n+1* least errors were selected for the inundation forecast.

$$e(r) = \sum_{i=1}^{p} /M_i\text{-}S_i(r)/, \qquad r = 1,\ldots,1000 \qquad (3.6)$$

Where *r* is the number of models, *p* is the number of sites, M_i is the measured water level and $S_i(r)$ is the water level of the rth model at the ith site.

Comparison of inundation maps comparison

For evaluating the performance between predicted and reference inundation extents, Fit-Statistic (*F*) was used. It is widely used for cell-based models (Moya Quiroga *et al.,* 2016). It varies between 1 for a perfect fit and 0 when no overlap exists. It is defined as in the equation 3.7.

$$F = \frac{A_0}{A_{sel} + A_{cal} - A_0} \qquad (3.7)$$

Where A_{cal} is the area of flooded cells in the calibrated model (M_{Cal}), A_{sel} is the area of flooded cells in the selected model and A_0 is the overlap of A_{cal} and A_{sel}. A cell is defined as flooded if the water depth in it is more than 0.10 m (Leandro *et al.,* 2011). In our application, 1 depicts no difference by introduction of computer vision, whereas 0 shows very large differences. The root-mean-square error (*RMSE*) was also calculated for the assessment between the selected and calibrated models. It is calculated using equation 3.8 for flooded cells.

$$RMSE = \sqrt{\frac{\sum_{i=0}^{n}(m_i\text{-}s_i)^2}{n}} \qquad (3.8)$$

Where *n* is the number of flooded cells, m_i and s_i is the water depth in calibrated and selected model respectively.

3.4. Calibration and validation of the HEC-RAS 2D model

The water levels measured in event I were used to calibrate the model parameters. Table 3-2 presents the measured and simulated water levels, along with the maximum water depth at the eight sites. The calibrated inundation model results were in good agreement with the measured data. The sites located at the river White Main (sites 1, 2, and 3) showed a good match with a maximum difference of 0.13 m (measured water depth of 2.93 m) at site 3. A slight over-prediction of 0.08 m (in 1.43 m) was observed at site 4 (Dobrach canal). The water level at site 5 (side canal) was over-predicted the water level by 0.16 m (in 1.75 m). Sites located at the Mühl canal (6, 7, and 8) were under-predicted, with a reasonable agreement of 0.15 m (in 2.31 m) and 0.14 m (in 2.36 m) at sites 7 and 8. However, significant under-prediction of 0.24 m (in 0.89 m) was observed at site 6.

Table 3-2. The performance of the calibration model parameter MCal for event I, on 14th January 2011, and event III, on 07th December 2017. The table shows the time at which the images were captured, measured water depth in m and the difference between measured and the calibrated water levels in m. The positive values show an under-prediction, whereas the negative values represent of the water level by the model.

Site nr.	Event I, 14th January 2011			Event III, 07th December 2017		
	Time	Measured vs. HEC-RAS 2D [m]	Measured water depth [m]	Time	Measured vs. HEC-RAS 2D [m]	Measured water depth [m]
1	14:09	−0.01	2.78	10:02	0.09	1.41
2	14:18	0.01	2.90	10:22	0.27	1.57
3	14:23	−0.13	2.93	10:58	0.40	2.03
4	14:26	−0.08	1.43	11:10	0.40	1.03
5	13:27	−0.16	1.75	11:43	−0.10	0.04
6	14:01	0.24	0.89	12:35	−0.01	0.60
7	14:35	0.15	2.31	13:02	-	-
8	14:35	0.14	2.36	13:02	−0.02	0.96

Validation of the model was done using event III, the non-flood event measured on 7th December 2017. Site 7 located at the Mühl canal was under-construction, hence it was not possible to gather the measured water level for that site. Nevertheless, an exceptional agreement was observed at other two sites (6 and 8), at the Mühl canal. A reasonable agreement was also observed at site 1 with an under-prediction of 0.09 m (in 1.41 m). However, substantial under-prediction of 0.27 m (in 1.57 m) and 0.40 m (in 2.03 m) was observed downstream at sites 2 and 3 respectively. Under-prediction of 0.40 m (in 1.03 m) was also observed at site 4. However, at site 5 no inundation was measured (0.04 m water depth) but it over-predicted the water levels by 0.10 m.

The maximum inundation focussed on the eight sites is shown in Figure 3-8 for the three events. In event I, the floodplains were flooded but as mentioned before, no damage was done as the flood did not overflow the side banks of the White Main. The street, Theodor-Heuss-Allee, at site 5 was flooded as well as the motorway B 289, and the dykes were at their full capacity.
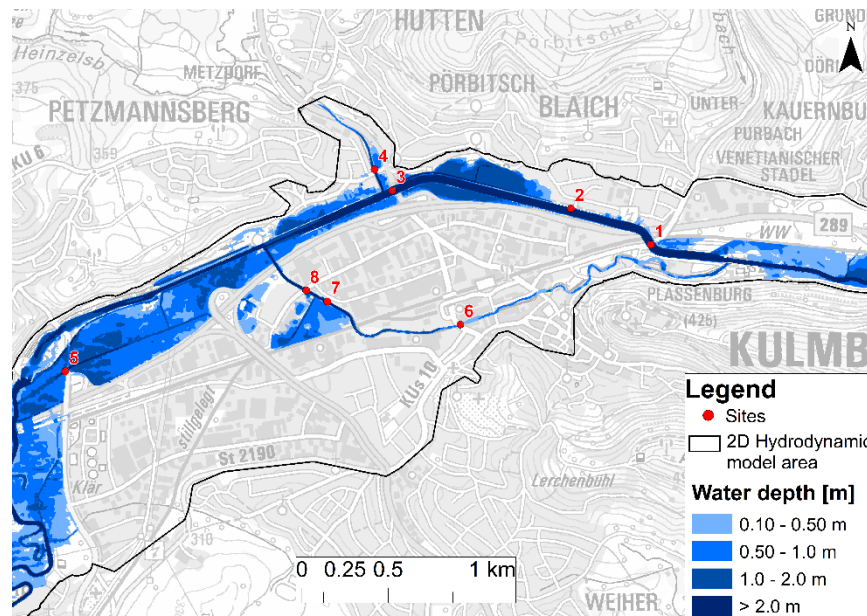
(a) 14th Jan 2011 14:00
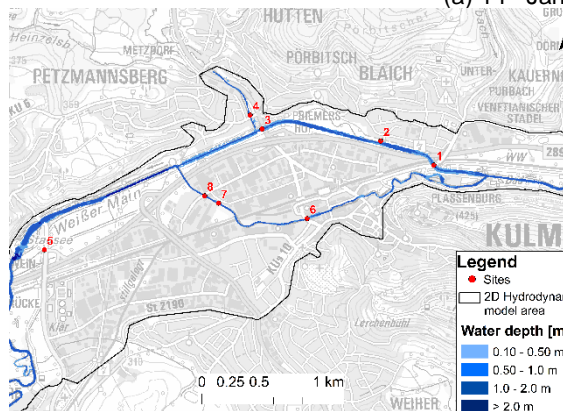
(b) 13th April 2017 14:00
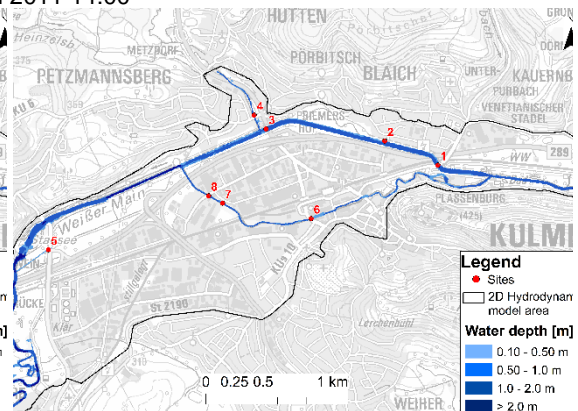
(c) 07th Dec 2017 13:00

Figure 3-8. Maximum flood inundation maps for the three events.

In general, the inundation areas were predicted with good precision. Most of the inundation areas were within the flood plains and inundation extent matched with the observation images and on-field survey.

No inundation outside the main channel was observed during non-flood events II and III (Figure 3-8b and Figure 3-8c). As mentioned before, the events were of smaller magnitude as compared to event I (Figure 3-2b and Figure 3-2c). The simulations were in-line with the measurements. Overall, considering the simple model structure of the

HEC-RAS 2D, which disregards the sewer network and urban key features (Leandro et al., 2016), the results were considered satisfactory. In addition, they show the robustness of the model as it was able to simulate both high and low events within acceptable limits.

3.5. Results of flood inundation forecasts with computer vision

This section presents the water levels extracted from the images using computer vision and the models selected for flood inundation forecasting.

3.5.1. Water levels obtained by computer vision

Computer vision algorithm was applied to the images collected from three different events at eight sites in the city of Kulmbach. The images that were suitable for computer vision are shown in Figure 3-9, Figure 3-10, and Figure 3-11. Images of event II were used as the reference images and events I and III as the target images. The water levels obtained from the algorithm were compared with the measured water levels.

| (a) Site 2 | (b) Site 5 | (c) Site 6 |
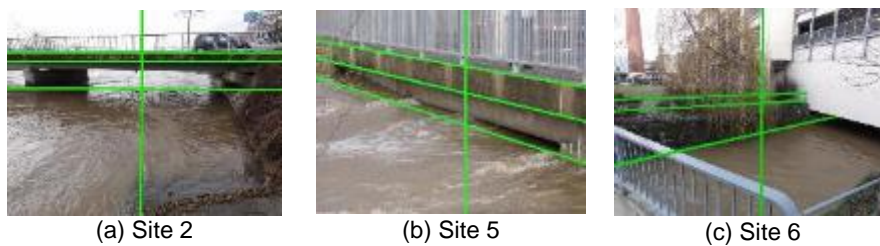
Figure 3-9. Available sites for application of computer vision for event I on 14th January 2011.

(a) Site 2   (b) Site 6
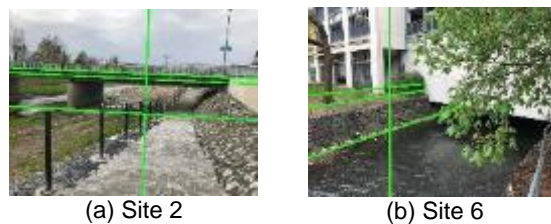
Figure 3-10: Available sites for application of computer vision for event II on 13th April 2017.

(a) Site 2   (b) Site 6
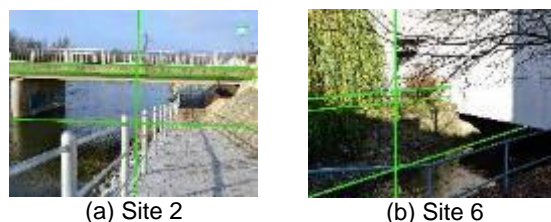
Figure 3-11: Available sites for application of computer vision for event III on 07th December 2017.

A box plot of the pixel distance ratio – division of the distance between the water surface and the height of the referenced object in pixels (*c_pixel*), and the referenced dimension of the object in pixels (*a_pixel*) is shown in Figure 3-12. The ratio was calculated using ten iterations for each image by manually drawing the edges. The figure also shows the

mean and standard deviation (SD) of the iterations that indicates the error in estimating the ratio.
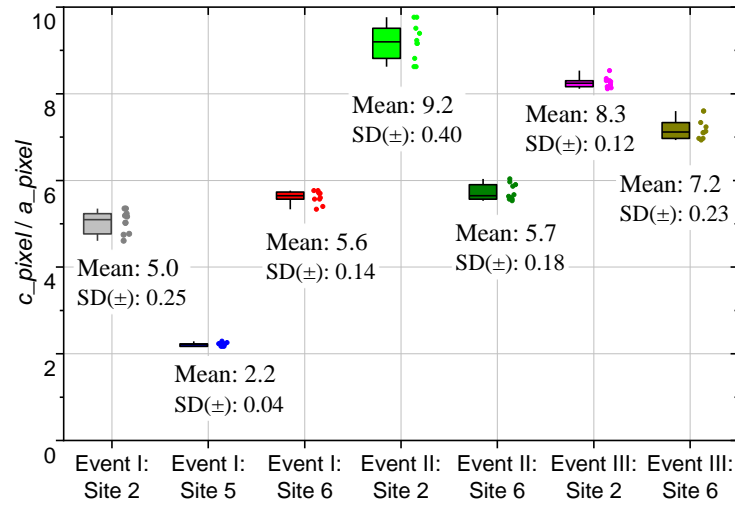
Figure 3-12: Box plot showing the pixel distance ratio of the distance between the water surface and the referenced object in pixels (*c_pixel*) and the height of the referenced object in pixels (*a_pixel*) for ten iterations.

The height of referenced objects (*a*) are same for all three events: 0.43 m, 0.35 m, and 0.30 m for sites 2, 5, and 6 respectively. Thus, the water surface height (*c*) was calculated in m using equation 3.5. Furthermore, the mean of the *c* was converted to water level. The difference of the water levels between the measured and predicted by computer vision for the seven images is shown in Table 3-3. As mentioned before, no measurement was performed for event II, hence the difference cannot be calculated.

Table 3-3. Difference between the measured and the computer vision water levels predicted for events I and III.

Event	Site nr.	Measured vs. computer vision [m]	Measured water depth [m]
I	2	−0.01	2.90
I	5	0.17	1.75
I	6	−0.07	0.89
III	2	0.04	1.57
III	6	0.12	0.60

3.5.2. Flood inundation forecasting

The total number of models to be simulated in real-time is restricted by the computational resources. Given a large infrastructure, a large number of models can be realized with this methodology, however, in our case, existing resources limited the number of models to six (1+5). To conclude, out of one thousand models, we have selected six models that

produced least error in the water levels. As mentioned above, the sensitivity analysis was performed for a single event (event I) based on pre-determined ranges of the 2D inundation model parameter. Figure 3-13 presents the six models that return the least error in the water levels at the eight sites. The radar plot shows the variability of the Manning's *M* for each land use class. It is evident from the figure that the parameter space is different in each model, which results in different output. The output of the models is presented in Table 3-4, which shows the difference between the measured and the simulated water levels resulted from the six models for event I. A threshold value of ±0.15 m is used for highlighting the differences in the model results.

To select the most suitable model out of the six, water levels obtained using computer vision are used as the validation data. The goodness-of-fit (equation 3.6) is calculated for the three events for the six model and one least error model is selected for the real-time forecast for each event. If there was no validation data, inundation maps of the calibrated model (M_{Cal}) would have been used as the final forecast.
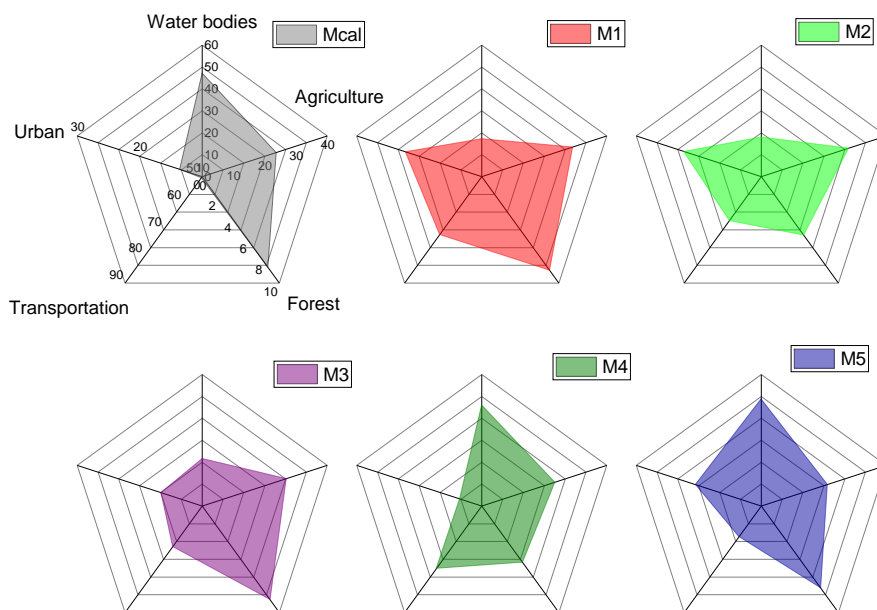
Figure 3-13. Six model parameter sets for five land use classes. The figure shows the Manning's *M* in m $^{(1/3)}$/s resulting from the sensitivity analysis of one thousand HEC-RAS 2D model runs.

Table 3-4. Difference in water levels between measured and six HEC-RAS 2D models in m. The threshold value of up to ±0.15 m is highlighted in the table.

Site nr.	Measured Water depth [m]	Measured vs. M_{cal} [m]	Measured vs. M_1 [m]	Measured vs. M_2 [m]	Measured vs. M_3 [m]	Measured vs. M_4 [m]	Measured vs. M_5 [m]
1	2.78	−0.01	0.01	0.02	−0.07	−0.03	0.00
2	2.90	0.01	0.06	0.04	−0.01	−0.01	0.05
3	2.93	−0.13	0.06	−0.11	0.02	−0.12	0.05
4	1.43	−0.08	0.11	−0.06	0.08	−0.07	0.10
5	1.75	−0.16	0.08	−0.15	0.09	−0.13	0.08
6	0.89	0.24	0.44	0.23	0.45	0.28	0.44
7	2.31	0.15	0.60	0.16	0.62	0.21	0.57
8	2.36	0.14	0.58	0.14	0.60	0.19	0.56

To assess the difference between the calibrated and selected models, goodness-of-fits Fit-Statistic (*F*) in percentage and root-mean-square error (*RMSE*) in m (equations 3.7 and 3.8) is presented in Table 3-5. For events I and III, the calibrated model was not the selected model, hence the difference is reported. For event II, the calibrated model produced the least error using the computer vision water levels. Large differences were found in event I. The spatial distribution of the error for event I is shown in the Figure 3-14.

Table 3-5. Selected model and goodness-of-fit between the calibrated and the selected model (M_{cal}) for the peak inundation time step.

Event	Model selected	Fit-Statistics [%]	RMSE [m]
I	M_3	89	0.40
II	M_{Cal}	100	0
III	M_4	99	0.03
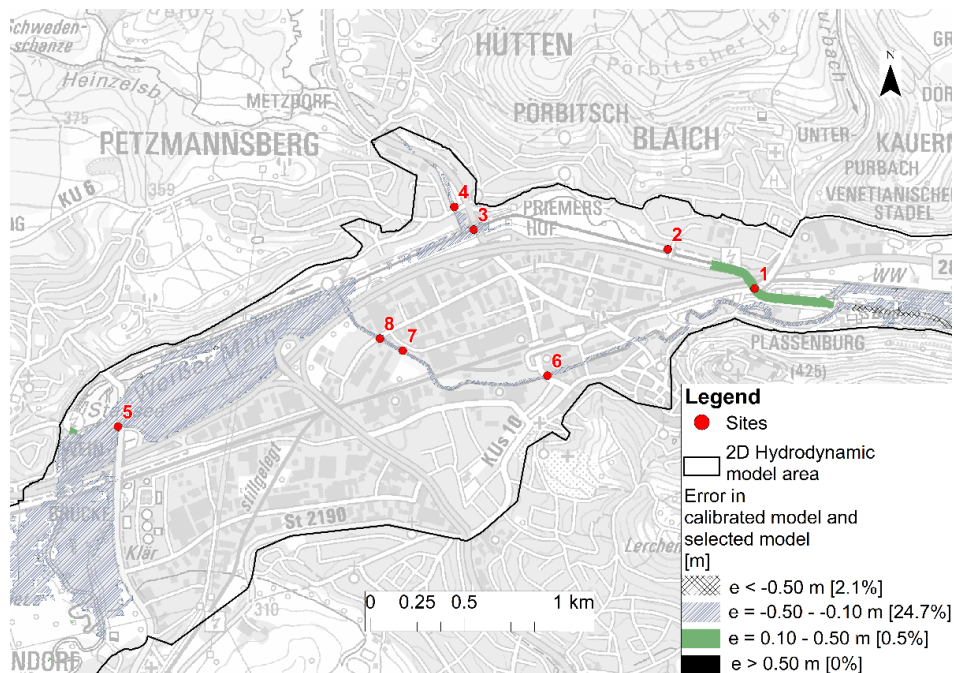
Figure 3-14. Difference in the water depths between the calibrated and the selected model using computer vision for event I (14th January 2011).

3.6. Discussion

3.6.1. Computer vision

For event I, only the images of sites 2, 5, and 6 were amenable for analysis using computer vision. The images from the other sites did not satisfy the specified requirements for analysis (section 3.3.3): Figure 3-3a(site 1) the water line is not clearly visible on the image; in Figure 3-3d and Figure 3-3g (sites 4 and 7), the reference lines of the bridges are not visible; in Figure 3-3c and Figure 3-3h (sites 3 and 8), the reference lines and the water line are not parallel to each other. Whereas, in Figure 3-3f (site 6), the railings are right on top of the vertical embankment of the river, so the three reference lines are practically in the same vertical plane, thus it can be used for computer vision. Furthermore, for events II and III, only the images of Figure 3-4b, Figure 3-4f, Figure 3-5b, Figure 3-5f (sites 2 and 6) were deemed suitable for computer vision. The water level is very low in Figure 3-4e and Figure 3-5e (site 5) and thus, the water line is not clearly visible. These examples indicate that the local conditions may constrain the application of computer vision and it should be ensured that the requirements are met while capturing images.

Uncertainty was quantified based on the edge detection in an image. We assumed an error of ±0.50 mm in the detection of each reference line, which results in an error of ±1 mm in the estimation of a reference dimension. The images used have a high resolution

of 300 dpi. Each millimetre corresponds to 11.8 pixels. Based on the ratio of pixels to physical dimensions (0.011 m per pixel), the error in physical dimension was calculated to be 0.13 m. Therefore, the uncertainty in the computer vision-based water level was estimated at ±0.13 m. In some cases, the side surface used as the reference for drawing the edges is not entirely vertical, as in site 6 (Figure 3-9c, Figure 3-10b and Figure 3-11b), which could introduce additional errors since the algorithm assumes the surface to be entirely vertical.

The calibrating parameter c_pixel / a_pixel and a were used to estimate c for the ten iterations. The maximum standard deviation of ±0.18 m in the value of c was observed for Figure 3-10a (Event II: site 2) and ±0.11 m for Figure 3-9a (Event I: site 2). The values of the mean were converted to the water level in m asl. These values compare well with the value of ±0.13 m estimated previously.

A reasonable match was found in the measured and the computer vision water levels on five images: sites 2, 5, and 6 in event I and sites 2 and 6 in event III. The water levels predicted from computer vision for event II (Figure 3-10a and Figure 3-10b) were 1.12 m and 0.92 m for sites 2 and 6 respectively. In the absence of measured water levels, the calibrated HEC-RAS model results at those sites, 1.2 m and 0.65 m, can be used as good estimates to evaluate the performance of computer vision. The image for site 2 is more in line with the requirements than the image for site 6. This has potentially resulted in better results for site 2 than site 6. If the images are captured as per the requirements, computer vision has the potential to be a good validation tool for flood inundation forecasting.

One of the limitations of these methodologies (as in Wang $et\ al.,$ 2018) is the manual approach used to map the edges from the reference images and to detect the water surface line, which is not automatized. However, this step would only be a crucial step if it had to be run continuously in real-time. This is not the case in this study, since the procedure for selecting the forecast model (section 3.3.1) can be done offline on a regular basis or following a flood event. In our methodology, the model that produces the least error is selected for inundation forecasting only if images become available, otherwise the calibrated model (M_{Cal}) is used as a default.

If locations that have not been referenced are included in this procedure, it might be difficult to generate the reference elevation or measurements. The images would first need to be referenced manually using the database and the location can then be used for as a target location in our methodology. The locations could include either hotspots

in the city or major bridges that are easily accessible and regularly monitored via social media or CCTV cameras.

3.6.2. Flood inundation forecasting

It can be seen from the model parameter distribution (Figure 3-13) that six different sets of parameters were selected based on the least error. Equifinality can be observed from Table 3-4 where multiple model parameter sets represent the modelled system equally well and the six models can be accepted. However, depending on the sites where computer vision is applied (i.e. where images are available), equifinality will be reduced, because this will now become the main criteria for the selection of the model used for forecasting inundation. The additional validation will ensure that the number of false alarms can be reduced significantly by the forecasting framework. The error can be minimized using back communication from computer vision to the inundation forecast. If no computer vision is available, the calibrated model M_{Cal} is used.

Comparison between the 2D model and computer vision was done on the available sites (see Table 3-4). For event I, the model M_3 was selected based on the least error (Table 3-5). For event II, there was no change in the selected model. Based on the comparison, the calibrated model was selected. For event III, the selected model was M_4. To assess the differences in the forecasted inundation extents between using or not using computer vision, the Fit-Statistic (*F*) and root-mean-square error (*RMSE*) is used (see section 3.3.4). Larger differences can be observed in event I (Figure 3-14) since the *F* is 89% and the *RMSE* is 0.40 m. The selected model generally had higher water depths as compared to the calibrated model as 24.7% of the total flooded cells contains higher water depths (range of −0.10 – −0.50 m). Furthermore, 72.8% of the flooded cells had a minimal difference in the range of −0.10 – −0.10 m as compared to the calibrated model. Very few cells showed water depths smaller than the calibrated model.

For event III, model selected using computer vision was very similar to the calibrated model hence the differences were minimal. This can be explained by the similar Manning's *M* values of M_{Cal} and M_4 in the main channel and the floodplain. As the discharges were considerably low in event III, the water did not leave the main channel and hence not much of a difference was observed. In event II, there was no change in the selected model by applying computer vision.

These examples show that the inclusion of computer vision can produce changes in the forecasted inundation extent. In this study, we assumed that computer vision was the prevailing source of accurate data.

3.7. Conclusion

We present a methodology for real-time flood inundation forecasts incorporating additional crowd-sourced validation data generated with the assistance of the computer vision algorithm. Six 2D diffusive wave models (HEC-RAS 2D) are run in parallel. The selection of models used for the inundation forecasting is based on one thousand models run for a single event. In this study, validation of the methodology is carried out using three events on eight sites located in the Kulmbach inner city. Model selection (one out of six) for flood forecasting is based on the least error using computer vision at available sites. The computer vision algorithm is used to estimate the water levels of the images that meet the requirements of the proposed guidelines. The algorithm uses specific features, such as bridges and water surfaces, to estimate water levels in the images. Since the procedure is not fully automated, we suggest collecting images on a regular basis or following a flood event for model selection.

The major advantage of the forecast framework is its fast run-time and easy application to other study areas. The framework of the back communication from computer vision to the forecasts shows how alternative data sources can improve inundation forecasts. Furthermore, equifinality can be reduced by employing computer vision validation for the selection of the appropriate model for forecasting inundations. The validation data can be in the form of georeferenced images captured by citizens (Lowry and Fienen, 2013), security cameras or the fire fighters at referenced locations.

The results obtained from computer vision can be used as additional point source validation data and substantially improve flood inundation forecasting. However, the procedure is not yet entirely automated, requiring the user to detect the edges manually. In future, edge detection should be automatized using e.g. SIFT or image segmentation algorithms as described by Narayan et al. (2014), Nair and Rao (2017) and Geetha et al. (2017). Moreover, the method should include image enhancement techniques, such as power-law and logarithmic transformation (Maini and Aggarwal, 2010), to deal with the issue of poor lighting conditions in an image. The enhancement will mitigate one of the requirements concerning the proper lighting conditions and allow more images to be

processed. Furthermore, setting up a network of pre-installed CCTV cameras that fulfils the requirements should be explored.

The inundation model should be extended to simulate urban pluvial flooding (Arnbjerg-Nielsen et al., 2016) in future by including of a 1D-2D sewer/overland flow coupled-model structure. With ever-increasing computational performance and the introduction of cloud computing, the integration of more complex models will become feasible. In addition, analysing additional model outputs, such as flow velocities and hazards, should improve the existing forecasting framework by incorporating flood risk assessments.

Chapter

4. Offline flood forecasting

Framework for offline flood inundation forecasts for two-dimensional hydrodynamic models[2].

The paper presents a new methodology for hydrodynamic-based flood forecast that focuses on scenario generation and database queries to select appropriate flood inundation maps in real-time. In operational flood forecasting, only discharges are forecasted at specific gauges using hydrological models. Hydrodynamic models, which are required to produce inundation maps, are computationally expensive, hence not feasible for real-time inundation forecasting. In this study, we have used a substantial number of pre-calculated inundation maps that are stored in a database and a methodology to extract the most likely maps in real-time. The method uses real-time discharge forecast at upstream gauge as an input and compares it with the pre-recorded scenarios. The results show satisfactory agreements between offline inundation maps that are retrieved from a pre-recorded database and online maps, which are hindcasted using historical events. Furthermore, this allows an efficient early warning system, thanks to the fast run-time of the proposed offline selection of inundation maps. The framework is validated in the city of Kulmbach in Germany.

---

[2] Bhola, P. K., Leandro, J., and Disse, M.: Framework for offline flood inundation forecasts for two-dimensional hydrodynamic models, Geosciences, 8, 346, https://doi.org/10.3390/geosciences8090346, 2018a.

4.1. Introduction

Floods are posing an increasing threat worldwide and have severe social and economic impacts (European Union, 2007). Recent extreme precipitation events in central Europe, for example, highlighted the vulnerability of settlements and infrastructures to flooding. The extensive 2016 summer floods that hit Southern Germany and its neighbouring countries led to monetary losses of more than 2.6 billion euros (Munich Re, 2017). Therefore, improvement in the field of flood management, including the qualitative assessment of existing flood forecast and early warning systems, is urgently required.

According to the EU Floods Directive, flood risk management plans should include flood forecasts and early warning systems that take the characteristics of a river basin or sub-basin into account. In Germany, the federal states are responsible for flood information services. The operational strategies of flood risk management in Germany include, in particular, an increased flood hazards in spatial planning and urban development, comprehensive property-level mitigation and preparedness measures, a targeted maintenance of existing flood defence systems, and an effective flood warnings and improved coordination of disaster response (Thieken et al., 2016)

Early flood warnings in the study area is provided in the form of hydrological forecasts by the Flood Forecast Centre of the Federal State of Bavaria (Laurent et al., 2010). However, the forecast is limited to hydrological discharge hydrographs for 12–18 h without the simulation of two-dimensional (2D) inundation models. The inundation models provide the basis for the decision-making in flood risk management as they transform the bulk discharge outputs from hydrological models into distributed predictions of flood hazards in terms of water depth, inundation extent, and flow velocity (Bates et al., 2014).

Flood inundation forecasting is a challenging task because of the high computational time required for producing dynamic flood maps in real-time. With the introduction of multi-core CPU-based and graphics processing unit (GPU) based hardware architecture, the computational efficiency of numerical models has been improved significantly (Zhang et al., 2017; Hu and Song, 2018). However, resources consumption and regular maintenance of such infrastructure is a major issue in operational use (Henonin et al., 2013). Furthermore, it is important to develop methods to equip decision-makers with low cost and resource-friendly methods that do not require lengthy computation of the 2D inundation models in real-time and enable them to analyse inundation patterns well in advance of times of emergency (Bhatt et al., 2017).

In the past, historical satellite images have been used for flood inundation forecasting as an alternative to 2D inundation models (Voigt et al., 2007; Bates, 2012). Researchers have also developed a database of modelled flood extents for communities over a range of potential flood levels to be applied in disaster management (Bales and Wagner, 2009; Henonin et al., 2013; René et al., 2014). These pre-recorded scenario-based systems have mainly been applied to building static flood inundation databases and rules have been developed to select the most probable scenario, using flood stages or rainfall forecast as the input (Chen et al., 2006; Henonin et al., 2013; Schulz et al., 2015). These systems have been tested in a flood forecast and warning system: ESPADA (Evaluation et Suivi des Pluies en Agglomération pour Devancer l'Alerte) (Raymond et al., 2007). In the system, 44 pre-existing scenarios were used and successfully tested in a September 2005 storm in Nîmes, Southern France. Another application of such systems has been used in Copenhagen, Denmark, in which a set of rules were used to select the most probable inundation map from a scenario-based catalogue based on local rainfall forecast (Henonin et al., 2013). On a continental scale, a pre-recorded early warning system, EFAS, was tested in the Sava river basin and the results of the flood in May 2014 have highlighted the potential of the system to identify flood extent in urban areas (Dottori et al., 2017).

The limitations of the existing approaches are that they identify inundated areas associated with floods as having identical exceedance levels, usually a 100-year return period (Alfieri et al., 2014) or various levels of reference return periods (Dottori et al., 2017). What is needed, however, is a dynamic flood inundation forecasting framework based on a wide range of forecasted discharge. Moreover, existing studies' pre-recorded flood inundation forecasts have a coarse spatial and temporal resolution. One major improvement would be to assess the performance at finer resolutions. Furthermore, there is no readily available way to relate the discharge forecast to the inundation maps produced for specific exceedance levels.

In our study, we built a high-resolution spatial-temporal inundation database using a 2D hydrodynamic model for a wide range of discharge hydrographs. Our focus was to develop an efficient framework for offline flood inundation forecast that selects inundation maps in real-time from the database for fluvial flood forecasts. The selection of the optimal maps was based on real-time discharge forecast on upstream gauges. The performance of the framework was assessed by comparing offline and online inundation maps for a lead time of 12 h and updating the maps selection at every three-hour interval.

Offline here refers to maps retrieved from a pre-recorded database as opposed to online, in which maps are produced using real-time discharge forecast.

4.2. Methodology

4.2.1. Framework for offline flood inundation forecast

The forecast framework consists of two components: Pre-recorded, where the database was generated and stored; and real-time, in which the optimal inundation map is selected based on real-time discharge forecast (Figure 4-1).
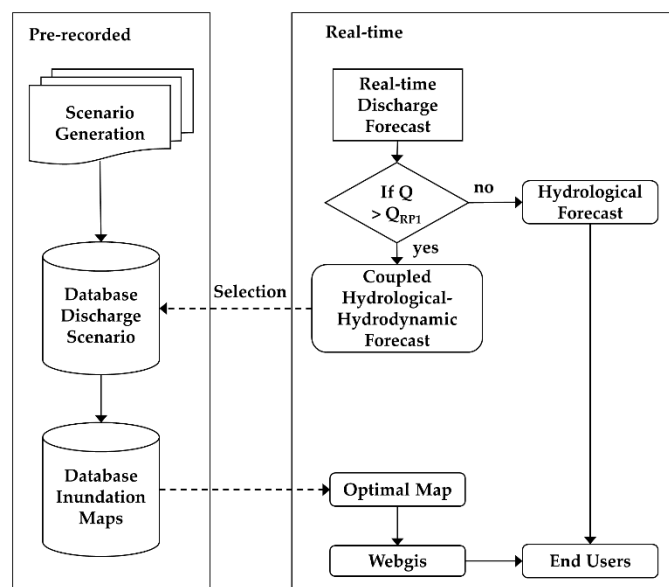
Figure 4-1. Framework of the offline flood inundation forecast including the pre-recorded and real time component. The coupled hydrological-hydrological forecast is activated once a one-year return period (QRP1) is exceeded.

The pre-recorded component contains databases of the discharge hydrographs and the inundation maps. Synthetic rainfall scenarios were used as an input to generate the discharge database. The scenarios were generated using rainfall intensities, duration, and distributions. Discharge scenarios were generated in two steps: first, the genesis of the discharge hydrograph was modelled using the hydrological model LARSIM (Large Area Runoff Simulation Model) (Ludwig and Bremicker, 2006). The model is operationally used in the flood forecasting centre for the river Main at the Bavarian Environment Agency (Disse et al., 2018). In the next step, various synthetic convective and advective discharge hydrographs (explained in section 4.3.2) were selected from the existing hydrographs based on the peak discharge ranging between the one-year return period and the extreme event, which is 1.5–1.6 times the 100-year return period. The selected hydrographs were further used as the input boundary conditions for the 2D

hydrodynamic model HEC-RAS 2D, version 5.0.3 (Hydrologic Engineering Center - River Analysis System, Davis, California, USA). Altogether, 180 convective and advective scenarios were realised and stored in the discharge database. The maps for the scenarios were stored in the inundation maps database. The generated maps contain high-resolution spatial and temporal (15 min) information of water depth and velocity in the study area. To automatize the component, a tool "FloodEvac" was developed in MATLAB R2018a (version 9.4.0.813654, 64 bit, MathWorks Inc., Natick, MA, USA) (Leandro et al., 2017).

In real-time, the discharge is forecasted for the upstream gauges by the Water Management Authority, Hof, and can be obtained from the LARSIM (Large Area Runoff Simulation Model) model (Laurent et al., 2010). If the peak of the forecasted discharge is lower than the threshold of a one-year return period (Q_{RP1}), only the discharge forecast is shown to the end users. Coupled hydrological-hydrodynamic forecast is activated if the forecasted discharge exceeds the threshold. The threshold of Q_{RP1}, which is less than the bankful discharge, is carefully selected to ensure that all the maps begin with the similar initial inundation extent and are not over-spilling the river banks. To select the optimal map from the database, the forecasted hydrograph for the next 12 h is compared to the discharge database and the index of the best match is recorded. Furthermore, the inundation maps corresponding to the recorded index are published for the next 12 h with 15-min intervals and can be accessed by end users via a webgis server. The maps are updated every three hours and the forecasted discharge is matched with the discharge database repeatedly for the next 12 h.

4.2.2. Evaluation metrics

To identify similarities between the real-time discharge forecast and the pre-recorded discharge database, two goodness of fit were identified: Nash-Sutcliffe efficiency (*NSE*) and weighted coefficient of determination (wr^2) (Krause and Bäse, 2005). The metrics are calculated as in Table 4-1.

The query to find the best match follows a sequential if-then order. It first selects the best *NSE* value of more than 0.85 from the database. If no match is found, it selects the best wr^2 values of more than 0.85. The value of 0.85 was based on the review for model evaluation criteria between the simulated and measured discharge (Krause and Bäse, 2005; Moriasi et al., 2007); however, the value can be changed depending on the case study. Furthermore, if no optimal match is found, it selects the best *NSE* and a warning note is issued to the end-user along with the *NSE* value reported.

The hindcasted inundation maps for four historical events were generated from the 2D hydrodynamic model. These maps are termed online forecasts in this study. The historical discharges at the upstream gauges were used as the input boundary conditions for the 2D hydrodynamic model. Due to the absence of the real observed flood extents (Leandro et al., 2011), the online inundation maps were used to validate the framework. The results between the selected optimal offline inundation maps were compared to the online maps. To assess the differences in the forecasted inundation extents in the offline and the online maps, Fit Statistic (*F*) (Moya et al., 2016) and absolute error (*e*) was used for flooded cells. A cell is defined as flooded if the water depth in it is more than 0.10 m.

Table 4-1. Evaluation metrics used in the study.

Evaluation Metrics	Equation	Terms
Nash-Sutcliffe efficiency (*NSE*)	$1-\dfrac{\sum_{i=1}^{n}(O_i-P_i)^2}{\sum_{i=1}^{n}(O_i-\bar{O})^2}$	n—the number of samples O—the forecasted discharge P—the discharge of the database b—the gradient of the regression line
Weighted coefficient of determination (*wr²*)	$x\left(\dfrac{\sum_{i=1}^{n}(O_i-\tilde{O})(P_i-\tilde{P})}{\sqrt{\sum_{i=1}^{n}(O_i-\tilde{O})^2}\sqrt{\sum_{i=1}^{n}(P_i-\tilde{P})^2}}\right)^2$	$x=\begin{cases}\lvert b\rvert & \text{if } b\leq1\\ \lvert b\rvert^{-1} & \text{if } b>1\end{cases}$ $b=\dfrac{\sum_{i=1}^{n}(O_i-\tilde{O})(P_i-\tilde{P})}{\sum_{i=1}^{n}(O_i-\tilde{O})^2}$
Fit Statistic (*F*)	$\dfrac{A_0}{A_{offline}+A_{online}-A_0}$	A_0—the overlap of flooded cells in the online (A_{online}) and offline ($A_{offline}$) maps
Absolute Error (*e*)	$\dfrac{\sum_{i=1}^{nf}\lvert d_i^{offline}-d_i^{online}\rvert}{nf}$	nf—the number of flooded cells $d^{offline}$ and d^{online}—the water depth in the offline and online maps

Moreover, the absolute error does not provide information if the offline selected map is over- or under-predicting the inundation. Therefore, errors between the offline and online water depths are also included in the assessment. Positive values indicate an over-prediction and negative values indicate an under-prediction of the water depths. The goodness of fit was calculated over time for the intervals of 15 min as the hydrodynamic model output interval was 15 min.

4.3. Study Area, data and models

4.3.1. Study area

The proposed methodology was applied in the city of Kulmbach located in the North-East of the Free State of Bavaria in Southern Germany. The city is crossed by the river White Main and a diversion canal for flood protection, the Mühl canal. Schorgast is one of the main tributaries that meets the White Main upstream of the city. In the north, the small tributary Dobrach meets the White Main and from the south side, two stormwater

canals meet the Mühl canal. The river Red Main merges with the White Main near Kulmbach from the South to form the river Main, the longest tributary of the Rhine. Main gauging stations upstream of the city are Ködnitz at White Main and Kauerndorf located at the river Schorgast. For the study, a virtual gauge (Figure 4-2) was added just after the confluence of the rivers for discharges comparison purposes (section 4.4).

The land use is shown in Figure 4-2a and it generally consists of agricultural land (62%) that includes floodplains and grassland. The water bodies make up 7% of the total model area and include river channel and lakes. The urban area covers around 26% and includes industrial and residential areas as well as transport infrastructures like roads and railway tracks, whereas forests form barely 5% of the total area. The quality of inundation maps depends crucially on the topography. Topography data for this study was provided by the Water Management Authority, Hof (Figure 4-2b).

4.3.2. Case study data

Rainfall probability data was available from the computer program KOSTRA-DWD 2000 (KOordinierte STarkniederschlags-Regionalisierungs-Auswertungen; itwh GmbH Hannover, Germany), which is distributed by the German Meteorological Services (DWD). It provides rainfall intensities for different annual probabilities and durations. It was primarily developed for the design of water management systems such as urban drainage infrastructure or flood retention basins. Precipitation heights were extrapolated using PEN-LAWA 2000 (Praxisrelevante Extremwerte des Niederschlags; itwh GmbH, Hannover, Germany) (Verworn, 2006) for the higher return periods. Figure 4-3 shows the duration and intensities of the precipitation for the city of Kulmbach.
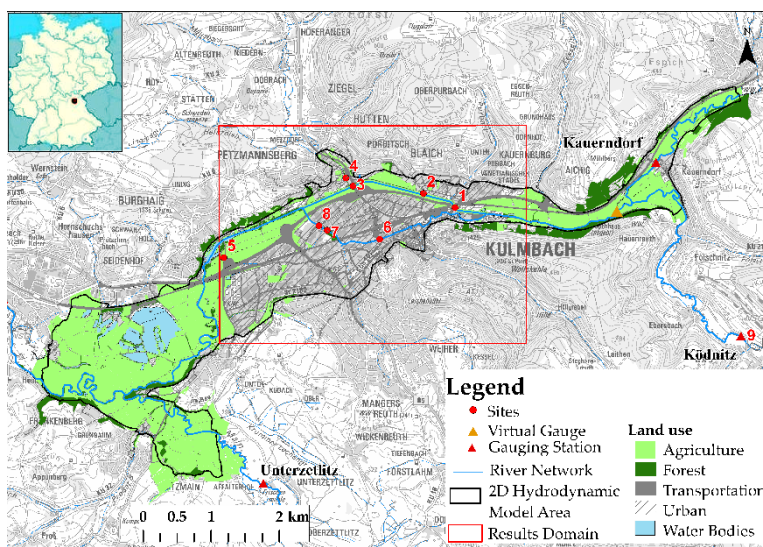
(a) Land use
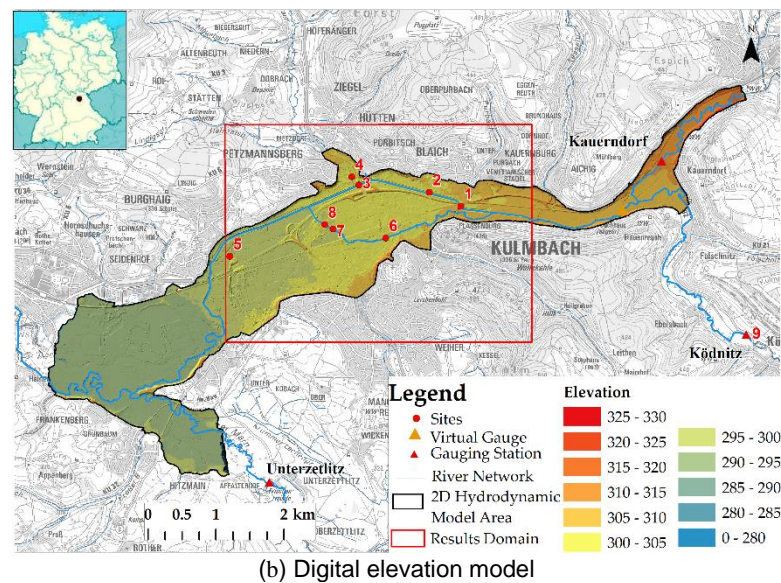
(b) Digital elevation model

Figure 4-2. Study area (a) Land use and (b) digital elevation model of the city Kulmbach. Data source: Water Management Authority Hof.

Hydrological measurement data for the historical events were gathered by the Bavarian Hydrological Services and via field surveys. Figure 4-4a and 4b shows four historical discharges at two gauges upstream of the city, Ködnitz and Kauerndorf, respectively. The figures also indicate the flood frequency estimations of 1, 5, 20, 50 and 100-year return period discharges along with the extreme event. The historical discharges were used as the input boundary conditions to the online 2D hydrodynamic model, which is later used to show the performance of the offline maps. The events have seasonal characteristics based on convective and advective precipitation input. The hydrographs resulting from a convective precipitation are categorised by higher peaks and shorter duration (May 2006 and May 2013), where the precipitation event can take 25–120 m and rain intensity can vary between 5–60 mm/h (Maniak, 2010). May 2006 and May 2013 had higher peaks and shorter durations and were of convective nature. In May 2013, only the gauge Ködnitz was flooded. The two events that occurred in winter (February 2005 and January 2011) had low peaks but longer durations and were categorised as advective events. An advective precipitation event can last up to 3–4 days and the intensity is often less than 2–3 mm/h (Maniak, 2010). The two categories give a clear indication of convective storm generated from a cloud-burst and snowmelt-rainfall induced flood event. The four events were used to validate the proposed offline forecast.
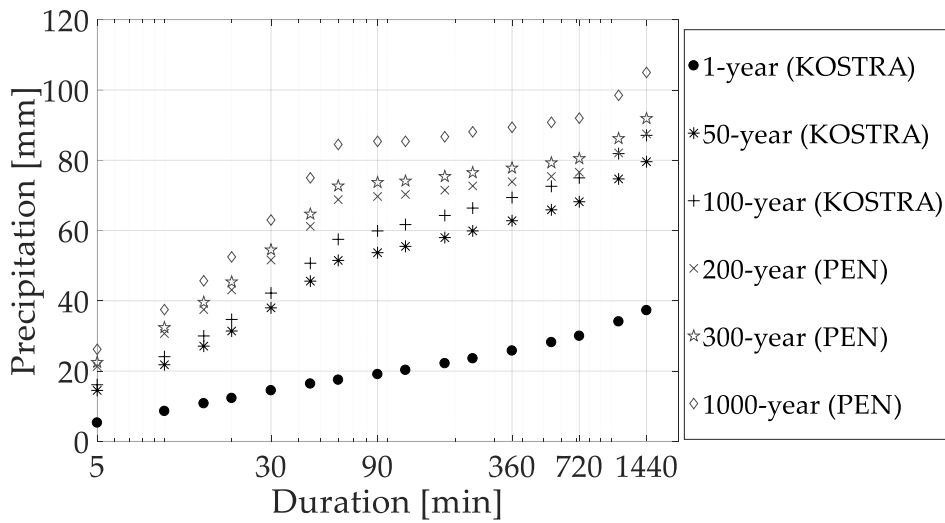
Figure 4-3.Precipitation values in mm for various durations (in min) and various return periods. PEN method used to extrapolate precipitation values above 100-year return period. Data source: KOSTRA-DWD 2000 (Kulmbach: Column 47, Row 67).
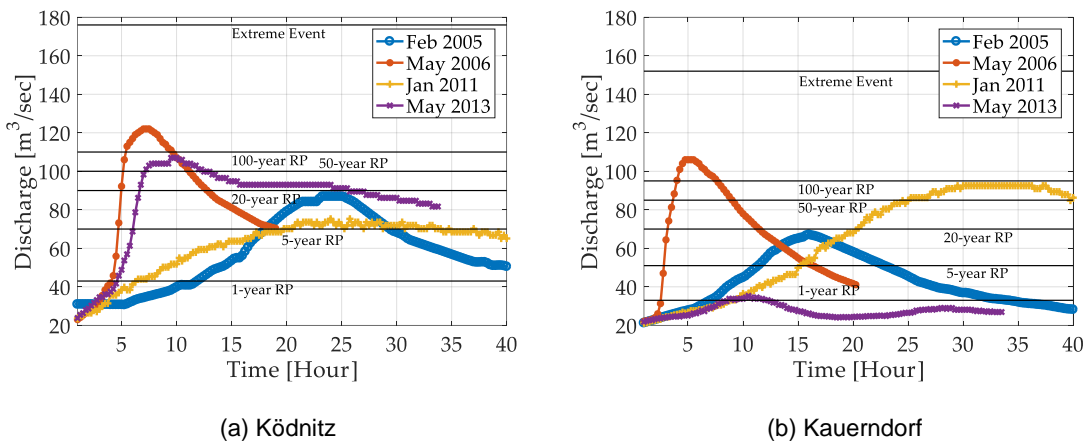
Figure 4-4. Discharge hydrographs at the upstream gauging stations (a) Ködnitz and (b) Kauerndorf. Data source: Bavarian Hydrological Service (www.gkd.bayern.de).

4.3.3. Pre-calibration and validation of the 2D flood inundation model

HEC-RAS 2D was used as the 2D hydrodynamic model to produce the inundation maps. The model uses an implicit finite difference solution algorithm to discretise time derivatives and hybrid approximations, combining finite differences and finite volumes to discretise spatial derivatives (Brunner, 2010). We used the diffusive wave equations to generate the database due to the less complex numerical schemes and faster calculations (Leandro et al., 2014). The governing equations are as follows:

$$\frac{\partial H}{\partial t} + \frac{\partial (hu)}{\partial x} + \frac{\partial (hv)}{\partial y} + q = 0 \qquad (4.5)$$

$$g\frac{\partial H}{\partial x} + c_f u = 0 \tag{4.6}$$

$$g\frac{\partial H}{\partial y} + c_f v = 0 \tag{4.7}$$

$$c_f = \frac{g|V|n^2}{R^{4/3}} \tag{4.8}$$

Where H is the surface elevation (m), h is the water depth (m), u and v are the velocity components in the x− and y−direction, respectively (m/s), q is a source/sink term, g is the gravitational acceleration (m/s^2), cf is the bottom friction coefficient (/s), R is the hydraulic radius (m), |V| is the magnitude of the velocity vector (m/s) and n is the Manning's roughness coefficient (s/m$^{(1/3)}$).

Table 4-2. 2D hydrodynamic model properties.

Data	Value
Model area	11.5 km^2
Total number of cells	430,485
Number of cells in results domain	193,161
Δt	20 s
Minimum cell area	6.8 m^2
Maximum cell area	59.8 m^2
Average cell area	24.8 m^2

Table 4-3. Manning's M for each land use class.

Land Use	Calibrated Manning's n [s/m$^{(1/3)}$]	Ranges of Manning's n [s/m$^{(1/3)}$]
Water bodies	0.022	0.015–0.149
Agriculture	0.043	0.025–0.110
Forest	0.189	0.110–0.200
Transportation	0.014	0.012–0.020
Urban	0.074	0.040–0.080

The model was set up using data provided by the Water Management Authority in Hof and field surveys. The water enters the model domain from the east at rivers White Main (Ködnitz) and Schorgast (Kauerndorf) and flows through the city and meets river Red Main (Unterzetlitz) after the city. The hydrograph boundary conditions represent the observed discharges that enter the simulation domain. Along with the major rivers, four canals were also represented as discharge hydrograph type. Besides the flow hydrograph, an energy slope value of 0.0096 mm^{-1} was used for distributing the discharge over the cells that integrate the boundary. Table 4-2 shows the model

properties and information of the cell size. The roughness parameter was selected based on a sensitivity analysis. Table 4-3 shows the calibrated parameter for each land use class (Figure 4-2a).

The authority also carried out data collections during the winter flood on 14 January 2011. Water levels were measured at eight bridges in the city of Kulmbach. Since the measured water levels were available for the winter event in January 2011, it was used to calibrate the hydrodynamic model to produce the inundation maps. Figure 4-5 presents the error between the calibrated HEC-RAS 2D water levels and measured water levels for the eight sites in the city. The model results are in good agreement with the measured data. The sites lying directly on the river White Main (sites 1, 2 and 3) have a good match with a maximum over-prediction of 0.12 m at site 3. Underestimation of up to 0.28 m was observed in the Mühl canal at site 6 and an over-prediction of 0.13 m in the side canal at site 4.
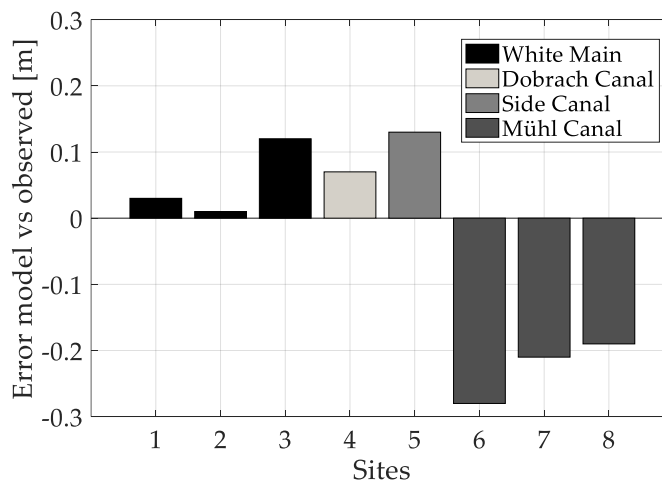
Figure 4-5. Error in m between the water levels resulting from the calibrated model and the measured water levels on 14 January 2011 at eight sites.

The validation was conducted using binary information of the flood extent that is collected from newspaper articles and press releases from the water authority. Figure 4-6 shows the resulted inundation map of the city Kulmbach, focused on the eight sites. In the January 2011 event, agricultural land and traffic routes were flooded, but no serious damage was reported. The street Theodor-Heuss-Allee at site 5 was flooded, as well as motorway B 289; the dykes were at their full capacity (WWA, 2011). Inundation was also reported at sites 7 and 8 around the street E.-C.-Baumann-Straße (Wolf, 2011), as supported by the modelling results. Most of the inundation areas are within the floodplains and inundation extent matches with on-field measured data. In general, considering the simple model structure of the HEC-RAS 2D, which disregards the sewer

network and urban key features (Leandro et al., 2016), the results were considered satisfactory.
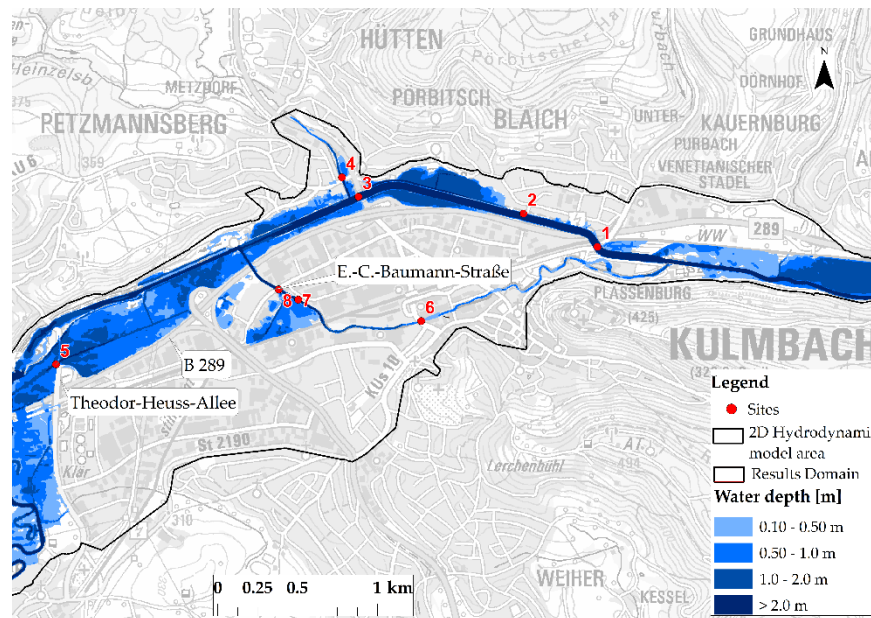
Figure 4-6. Inundation map of the city of Kulmbach on 14 January 2011 at 14:00.

4.4. Results and discussion

4.4.1. Discharge comparison

The proposed methodology was validated on four historical hydrological events. Since the discharge forecast in real-time is given for 12 h in advance on the upstream gauges, the inundation forecast duration was set the same and the selection of the maps was updated at every three-hour interval. To incorporate the contribution of both the rivers—Schorgast and White Main—a virtual gauge (Figure 4-2) was added just after the confluence of the rivers for discharge comparison. The goodness of fits between the forecasted discharge and discharge database at the virtual gauge for the events at every three-hour interval are summarized in Table 4-4. The discharge dataset was available at every 15 minutes' interval, which gives 12 data samples to calculate the goodness of fit for each three-hour forecast. The optimal map for each event was found by the query (section 4.2.2). Only once was the NSE reported lower than 0.85 and the maps with wr^2 of 0.87 were selected at the twelfth hour in May 2013. Figure 4-7 presents the discharge hydrographs that are resulted from the rainfall scenario at the virtual gauge and the optimal ID for the 12-hour forecast window with the three-hour update interval of the four events. The selection of new maps (ID) can be seen in the figure. It also shows the different databases for the advective and convective events. It is worth mentioning that

the excellent agreement between the offline and online discharge hydrographs is a result of the suitability of the variety of synthetic scenarios generated from the KOSTRA and PEN rainfall simulation to fit the observed data. The quality of the database is therefore considered equally important as the methodology for selecting the maps, as presented in order to cover possible future events.

Table 4-4. Goodness of fit for discharge comparison.

Duration	No. of Data Samples	Goodness of fit [-]			
		February 2005	May 2006	January 2011	May 2013
0–3 h	13	0.98 (NSE)	0.91 (NSE)	0.96 (NSE)	0.97 (NSE)
0–6 h	25	0.99 (NSE)	0.95 (NSE)	0.97 (NSE)	0.96 (NSE)
0–9 h	37	0.99 (NSE)	0.95 (NSE)	0.95 (NSE)	0.91 (NSE)
0–12 h	49	0.94 (NSE)	0.95 (NSE)	0.97 (NSE)	0.87 (wr^2)

(a) February 2005

(b) May 2006

(c) January 2011
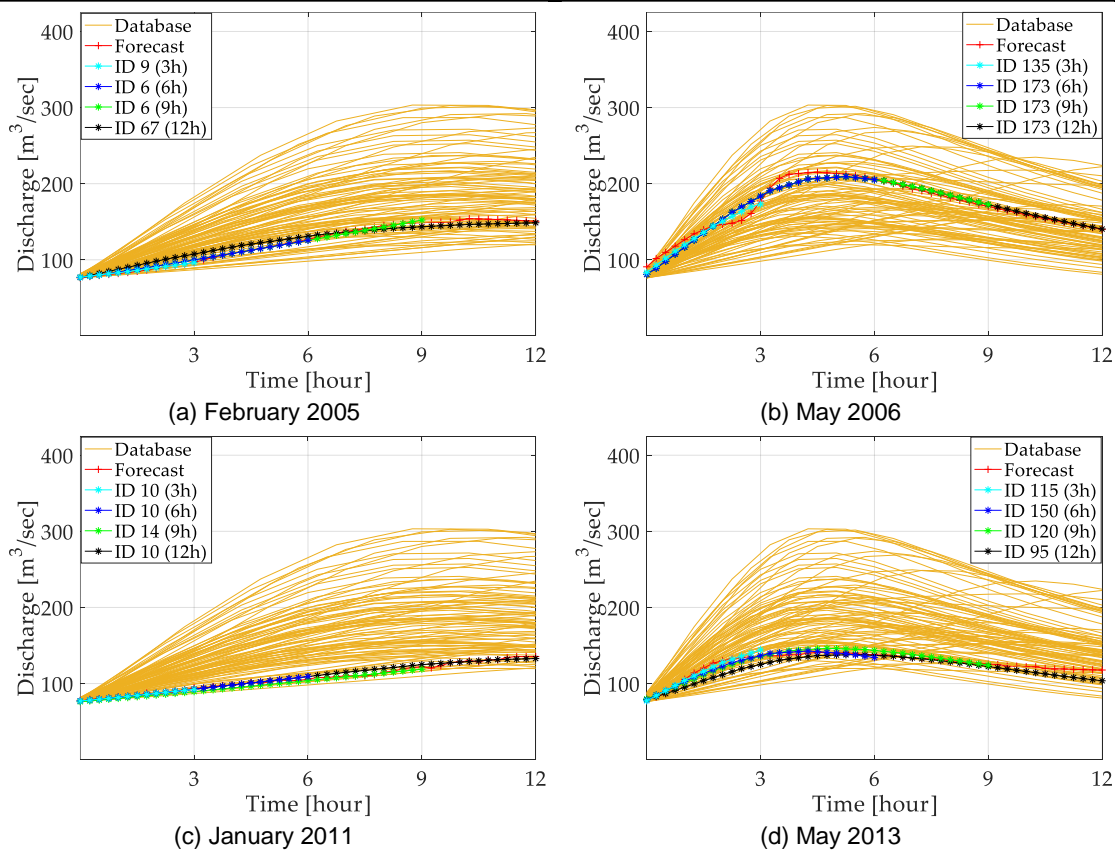
(d) May 2013

Figure 4-7. Comparison of discharge hydrographs at the virtual gauge: (a) and (c) advective events in February 2005 and January 2011, (b) and (d) convective events in May 2006 and May 2013.

4.4.2. Inundation forecast comparison

The offline and online inundation maps were compared in the result domain shown in Figure 4-2. The offline inundation maps produced using the discharge comparison are valid only for the area downstream of the virtual gauge. The inundation maps in the regions between the existing gauges and virtual gauge is produced by comparing the

discharge at their respective gauge. Table 4-5 shows the Fit Statistics and absolute error averaged for the update interval of three hours. In the paper, we assume a deviation up to 0.25 m between offline and online water depth as a threshold, although this value can be changed depending on the requirements of the end-user. Figure 4-8 shows the metrics with time intervals of 15 min. The spatial extent of the error between offline and online forecast maps are also plotted to see the over- and under-prediction of water depths. Information on the number of flooded cells and the distribution of error in the cells is given in Table 4-6 and Table 4-7. The results will be further discussed in the following subsections.

Table 4-5. Average Fit Statistics and absolute error for the four events at the end of the forecast update interval of three hours.

Duration	Average Fit Statistics [-]				Average Absolute Error [m]			
	February 2005	May 2006	January 2011	May 2013	February 2005	May 2006	January 2011	May 2013
0–3 h	0.97	0.75	0.97	0.76	0.06	0.14	0.06	0.27
0–6 h	0.96	0.84	0.97	0.80	0.07	0.11	0.06	0.22
0–9 h	0.96	0.89	0.97	0.92	0.07	0.09	0.07	0.12
0–12 h	0.93	0.90	0.95	0.93	0.11	0.08	0.07	0.11
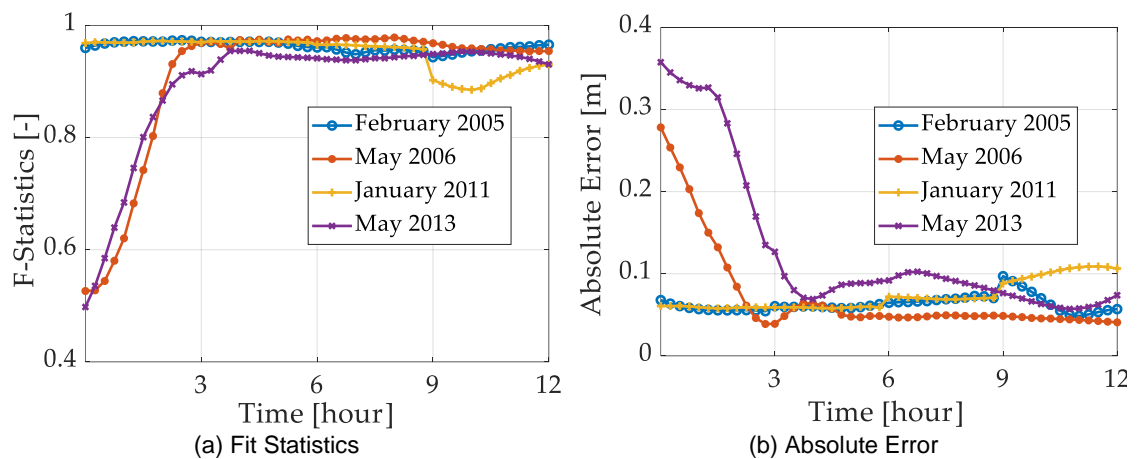
Figure 4-8. Goodness of fit (a) Fit Statistics and (b) Absolute Error between offline and online flooded cells for each time step for the forecast duration of 12 h.

4.4.2.1 Convective events

The events in May 2006 and May 2013 were categorised as convective events and the results for both events show similar trends. They start with a poor average F (0.75 and 0.76) and average e (0.14 and 0.27 m), but as the time increases, the performance gets better. Figure 4-7b and Figure 4-7d show that the discharge compared well with NSE value of 0.91 and 0.97 at the third hour in May 2006 and 2013 respectively. However,

the inundation maps show discrepancies between offline and online maps. This was induced from the one-year return period threshold at the beginning of the forecast. As we look further—the spatial extent of the error between offline and online maps—the results show a satisfactory agreement.

May 2006 was an extreme hydrological event and both the upstream gauges reached a discharge corresponding to the 100-year return period (Figure 4-4). The protection structures were breached, and critical infrastructure was flooded. Almost 31% of the cells in the result domain were flooded at the twelfth hour (Table 4-6), which is the highest amount in all four events. The spatial extent of error in Figure 4-9 and Table 4-6 show that the difference was mostly within the acceptable limit of 0.25 m at all times. Only 3% of cells lying in the Mühl canal were found under-predicting the water depths by more than 0.25 m. The water depths were under-predicted at initial hours but as the peak of the flood passed and the number of flooded cells increased (after the sixth hour), the water depths were over-predicted. It can be concluded that the extreme event was predicted quite well using the offline forecast.

Table 4-6. Percentage of cells inundated at the convective event in May 2006.

Time	Flooded Cells	May 2006 [%]			
		< −0.25 m	−0.25–0 m	0.25–0 m	> 0.25 m
T = 3 h	36,865	3	48	49	0
T = 6 h	55,550	3	96	1	0
T = 9 h	60,012	3	11	86	0
T = 12 h	60,418	3	13	84	0

Table 4-7. Percentage of cells inundated at the convective event in May 2013.

Time	Flooded Cells	May 2013 [%]			
		< −0.25 m	−0.25–0 m	0.25–0 m	> 0.25 m
T = 3 h	34,493	8	92	0	0
T = 6 h	44,553	5	4	84	7
T = 9 h	45,864	4	6	89	1
T = 12 h	44,204	8	88	3	1

(a) T = 3 h
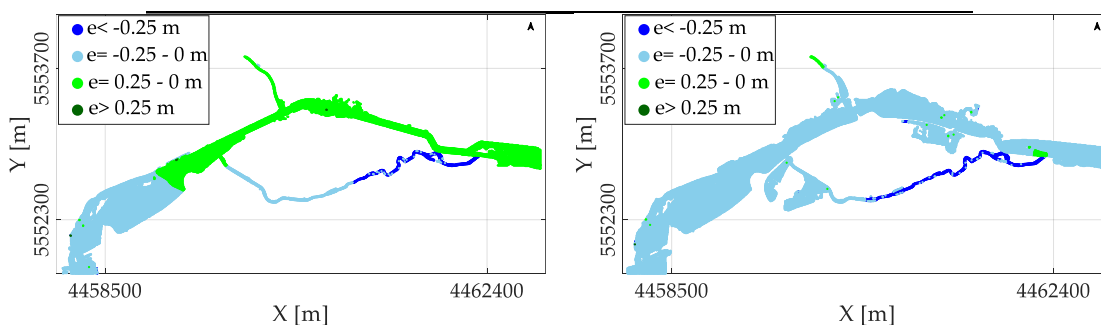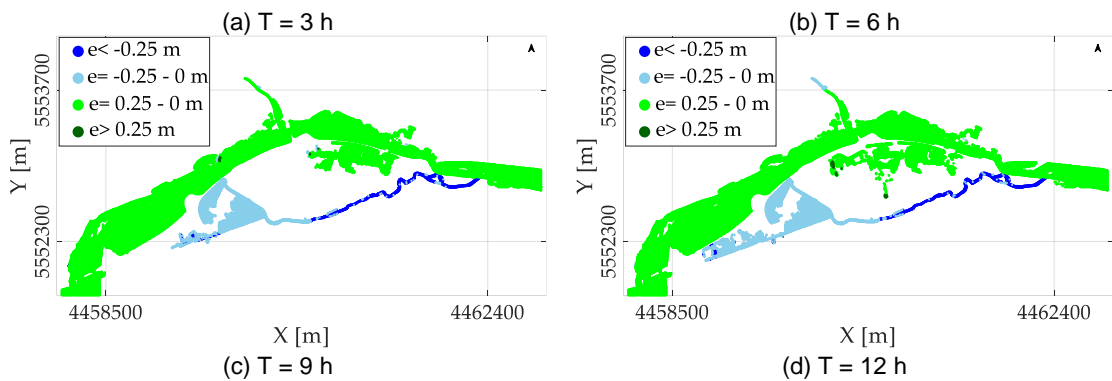
(b) T = 6 h

(c) T = 9 h

(d) T = 12 h

Figure 4-9. Water depth error between offline and online maps for May 2006. Positive values indicate over-prediction and negative values indicate under-prediction: (a) T = 3 h, (b) T = 6 h, (c) T = 9h and (d) T = 12 h.

(a) T = 3 h
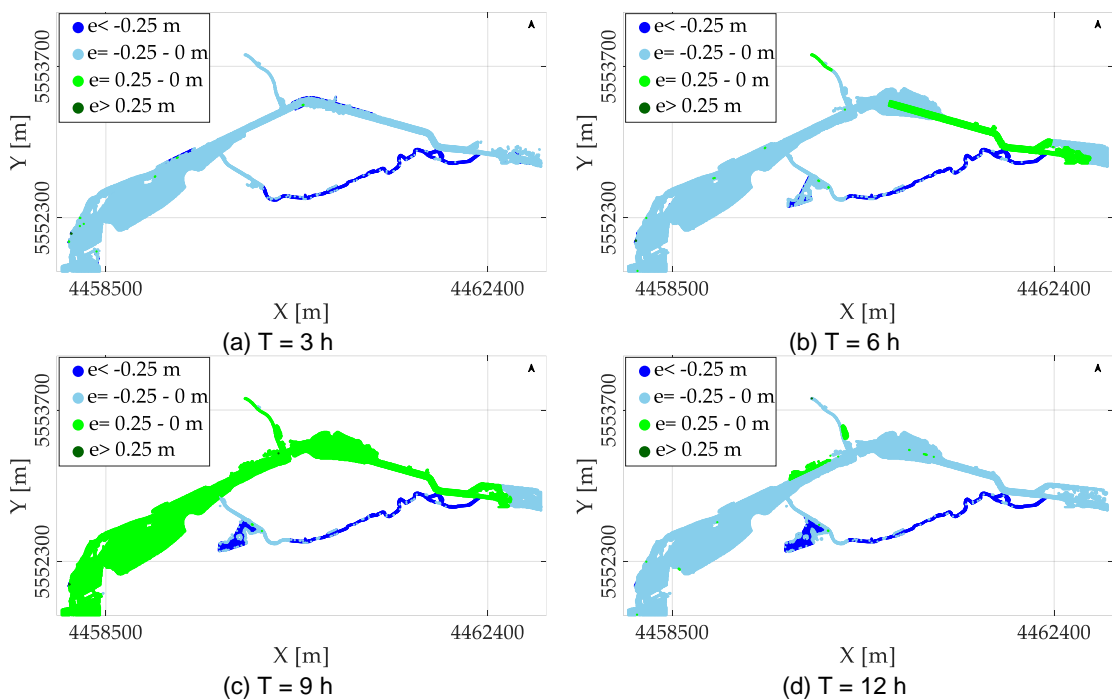
(b) T = 6 h

(c) T = 9 h

(d) T = 12 h

Figure 4-10. Water depth error between offline and online maps for May 2013: (a) T = 3 h, (b) T = 6 h, (c) T = 9h and (d) T = 12 h.

In May 2013, however, only one of the upstream gauges at Ködnitz was flooded (Figure 4-4b), therefore discharge was considerably low at the virtual gauge. The number of flooded cells is also lower than in May 2006. F and e show average performance at initial stages with average F values of 0.76, 0.80 and average e values of 0.27 and 0.22 m at the third and sixth hour. As the time increases, the performance gets better. The spatial extent of error (Figure 4-10) and Table 4-7 suggest under-prediction at the third hour, with 8% of the cells with an error of more than 0.25 m. At the sixth hour, 7% of the cells over-predicted the water depths on the river Upper Main and 5% of the cells that lie on the Mühl canal did the same. At the ninth and twelfth hour, performance improved in the river and only 4% and 8% of cells, respectively, under-predicted the water levels at the Mühl canal. Additional under-predicted cells are clustered at the junction of the Mühl

canal and E.-C.-Baumann-Straße and over-predicted cells in the floodplains on the river Upper Main.

4.4.2.2 Advective events

The advective events exhibit similar characteristics such as long duration and flatter peak (Figure 4-4). Unlike the convective events, both goodness of fits F and e are good from the beginning and stay much within the acceptable limits, with a minimum value of average F of 0.93 and 0.95, and minimum average e of 0.11 and 0.07 m at the twelfth hour for the two events in 2005 and 2011, respectively., a good agreement was reached between offline and online inundation maps. In Figure 4-8, both F and e after the ninth hour indicate a decrease in the performance for January 2011. F returns to an acceptable value at the twelfth hour; however, the error remains the same. Similar trends can be seen in February 2005, in which e deviates after the ninth hour but returns to 0.05 m.

Table 4-8. Percentage of inundated cells at the advective event in February 2005.

Time	Flooded Cells	February 2005 [%]			
		< −0.25 m	−0.25–0 m	0.25–0 m	> 0.25 m
T = 3 h	30,915	6	7	87	0
T = 6 h	37,426	5	2	87	5
T = 9 h	43,691	5	12	76	7
T = 12 h	46,790	7	91	2	0

Table 4-9. Percentage of inundated cells at the advective event in January 2011.

Time	Flooded Cells	January 2011 [%]			
		< −0.25 m	−0.25–0 m	0.25–0 m	> 0.25 m
T = 3 h	30,825	6	70	24	0
T = 6 h	32,348	6	69	25	0
T = 9 h	37,097	6	3	87	4
T = 12 h	42,603	5	4	81	10

(a) T = 3 h
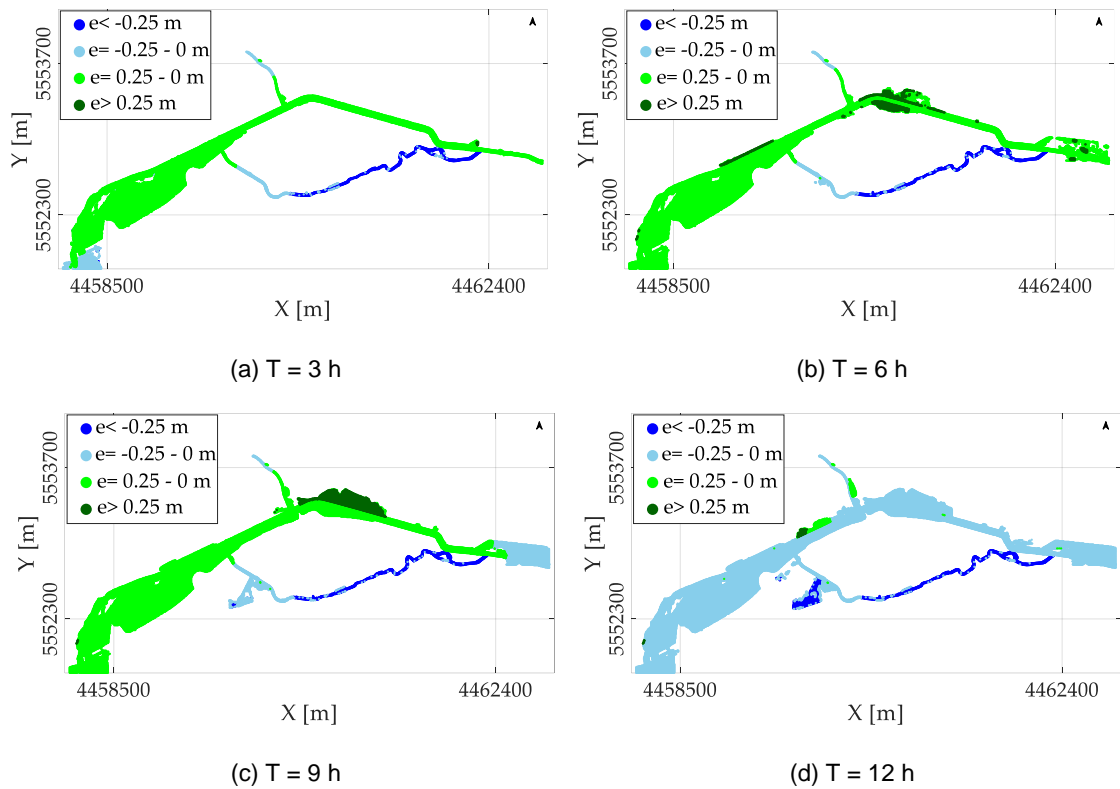
(b) T = 6 h

(c) T = 9 h

(d) T = 12 h

Figure 4-11. Water depth error between offline and online for February 2005: (a) T = 3 h, (b) T = 6 h, (c) T = 9h and (d) T = 12 h.

(a) T = 3 h
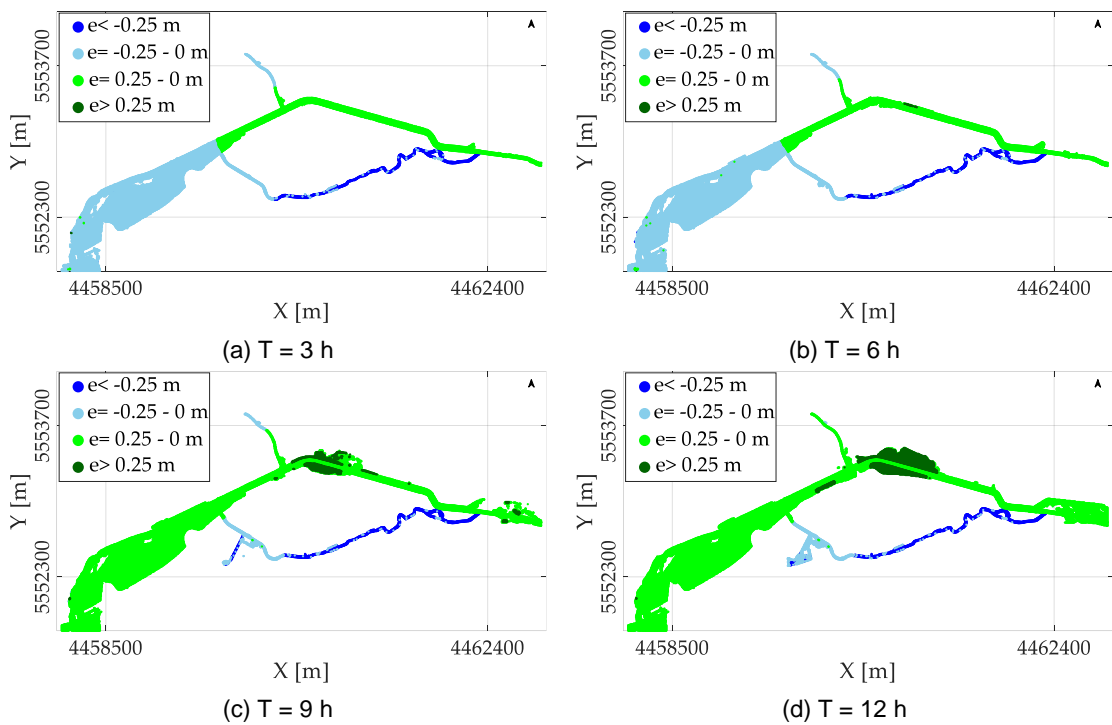
(b) T = 6 h

(c) T = 9 h

(d) T = 12 h

Figure 4-12. Water depth error between offline and online for January 2011: (a) T = 3 h, (b) T = 6 h, (c) T = 9h and (d) T = 12 h.

Spatial distribution of error (Figure 4-12Figure 4-11 and Figure 4-12) suggests slight under-prediction in all time steps in the Mühl canal and slight over-prediction at the river

Upper Main. Table 4-8 and Table 4-9 show the percentage error distribution of the advective events. In February 2005, only 7% of the cells were over-predicted more than 0.25 m at the ninth hour (similar pattern for May 2013). In January 2011, the agreement was good until the ninth hour, when the over-prediction of water depth started (10% at the twelfth hour). However, it was restricted to the floodplain of the river at the northern part. Overall

4.4.3. Update map selection

Updating the selection of maps is an important step to avoid selecting offline inundation maps that do not provide optimal results. With an update, a new set of maps was selected every three hours for the next twelve hours. The changes in the performance of the four validation events are plotted in Figure 4-13 and Figure 4-14 for convective and advective events, respectively. The figures show F and e values of the events at every time step along with the index (ID) of the database. It also shows the best match or the maps selected for the forecast duration. For the convective events, as described in the previous section, the start was not perfect, but the performance improves with time.

In the convective event of May 2006, only two indexes—ID 135 for 0–3 h and ID 173 for 6–12 h—were selected. The change in the third hour was important in order to find the optimal maps available with the highest F and least e. In May 2013, for the initial 0–3 h, better performance maps (ID 95) were available, but it selected ID 115 because of the high threshold for which the forecast starts (76 m^3/s). This value was decided on the river overflowing the banks. Since the inundation extents are within the main channel, they are not affected by this initial discharge. It would be possible to reduce this value and optimise the forecasts. The optimal maps were selected from 3–12 h.

The update was also successful in advective events. In February 2005 (Figure 4-14a), at all the time steps, it selected the best performance maps with the highest F and least e. In January 2011, optimal maps were selected for 0–9 h, however, for 9–12 h, the optimal maps were not selected (Figure 4-14b). This happens because the map selection is based on the optimal discharge hydrographs selection. This may not be the case for the corresponding inundation maps. The online inundation maps may be closer to another discharge scenario in the database. The difference between the maps was however not drastic and both maps were well within the threshold of 0.25 m (section 4.4.2).
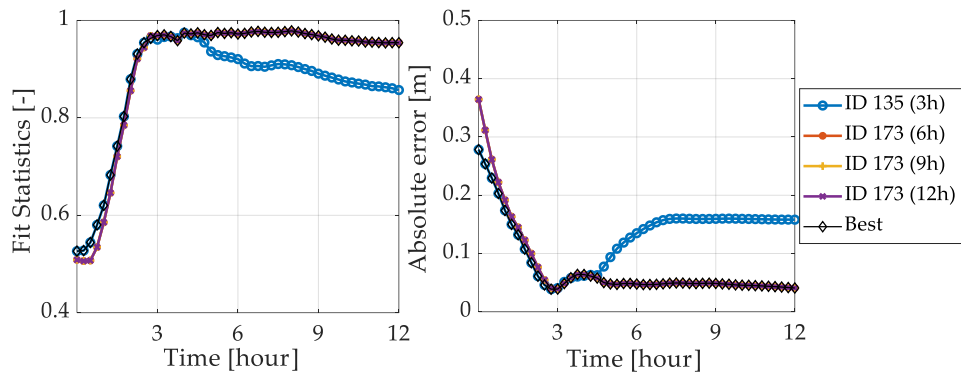
(a) May 2006
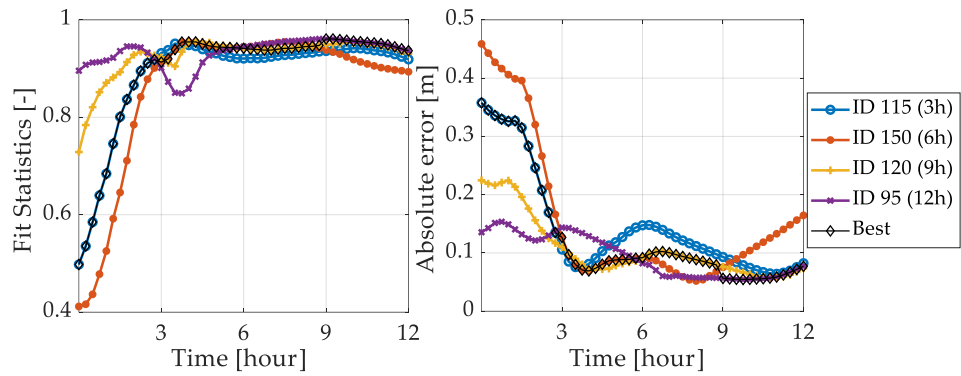
(b) May 2013

Figure 4-13. Update of the map selection for the convective events: (a) May 2006 and (b) May 2013.
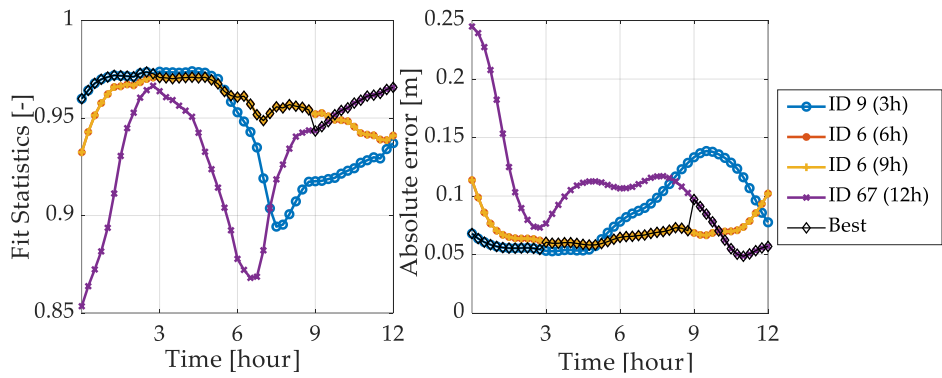
(a) February 2005
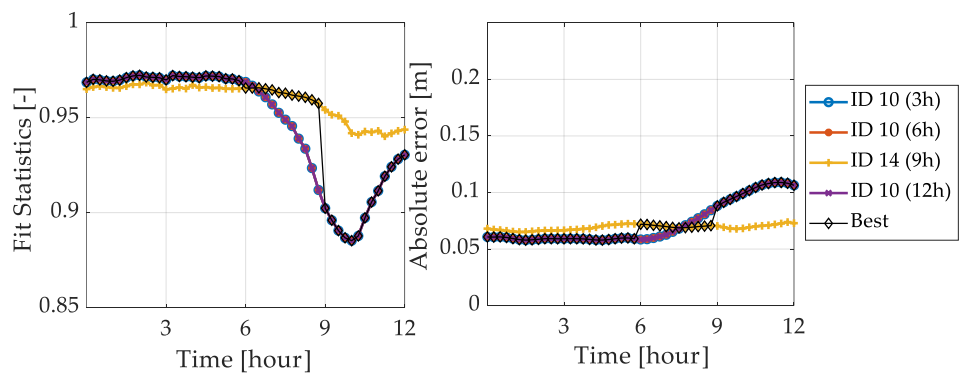
(b) January 2011

Figure 4-14. Update of the map selection for the advective events: (a) February 2005 and (b) January 2011.

4.5.   Framework performance

The framework has shown to be robust and efficient for operational flood forecast, both in terms of time and cost-effectiveness, when compared to an online inundation forecast. Indeed, this methodology overcomes the main constraints of online forecast, namely the need for the use of supercomputers and maintenance of infrastructure (Henonin et al., 2013), as well as the limitation on the computational time required by 2D hydrodynamic models. In addition, the resolution (cell size) or scale of the maps are not a limiting factor in this offline methodology; in principle, the resolution is limited by available data. Had we used online modus, the 2D hydrodynamic model would have required 30 min to simulate a real-time event of 12 h on an 8-core, 2.4 GHz (Intel E5-2665), including the initial start. Post-processing of the model results and update of the maps on the webgis server would consume an additional 15 min. Therefore, online inundation maps would only be delivered to decision makers 45 min after the discharge forecast at the upstream gauges for the next 12 h. The proposed offline framework, by contrast, runs in seconds to find the best selection of the maps and as such, it can be used as an early warning system. The maps are forwarded to a webgis server, where they are published, and end-users can see them in fine resolution.

A disadvantage of the framework is the error in water volume introduced by the update of the map selection. The water volume changes every time a different discharge is selected. This issue does not occur for online forecasts. The jump in the map outputs (water depth and velocities) occurs after every three-hour update and will be more or less pronounced, depending on the difference between the previous and the new discharge scenarios. We acknowledge that this is an additional source of uncertainty when compared to online forecasts. However, only 0–10% of the flooded cells exceeded 0.25 m. This difference can nonetheless be minimised by increasing the number of scenarios. In addition, regular updates of the inundation database are required in case of major land use, construction changes in the city, and climate change. In any case, the current database can be easily improved by including the simulation of historical events as well as performing a continuous update of new events.

4.6.   Conclusions

A framework for an offline flood forecast has been presented, which overcomes the high computational time required by hydrodynamic flood forecasting. The framework was validated using four extreme historical hydrological events. A total of 180 convective and

advective scenarios were simulated, as compared to the 44 scenarios used in the ESPADA system (Raymond et al., 2007). The forecast duration was 12 h and a new set of inundation maps was selected every three hours using real-time discharge forecasts as input. Furthermore, the map selection in real-time can improve the given forecast and substantially reduce errors. We thus conclude that the methodology works for both convective and advective events with a threshold of 0.25 m water depth. The current database has limitations and it needs to be enlarged to incorporate multiple peak events. Future work will see the generation of additional discharge scenarios based on historical data to strengthen the proposed framework.

A major advantage of the forecasting framework is its fast run-time and its easy application to other study areas, regardless of their size. This methodology can be applied to virtually any catchment size. The 2D hydrodynamic model run-times are not a limitation since all runs are prepared beforehand. In the study, the inundation maps were compared downstream at a virtual gauge that is introduced to incorporate the contribution of both the rivers. In a complex river system, an ensemble of inundation maps can be provided by comparing the discharge at existing gauges and at virtual gauges, introduced at the confluence of rivers. The ease of operational practise of the offline systems is well documented in previous applications such as ESPADA system in France, the Zambezi FloodDSS in Mozambique, in which the inundation database was produced using a 1D hydraulic model (Schulz et al., 2015), and EFAS in Sara river basin (Dottori et al., 2017). Furthermore, there are major challenges in operational application of these systems, in particular: Recompilation of the database in major land-use changes, an exhaustive database to cover all possible scenarios, validation of the query to select the most optimal scenario, and real-time validation of the forecast.

At an urban scale, the availability of real-time inundation maps would substantially improve emergency responses by assessing potential consequences of forecasted events (Molinari et al., 2014), and the end users of early warning systems would indeed benefit from prioritising and coordinating evacuation planning. Typical end-users are disaster relief organisations, such as the Federal Agency for Technical Relief (THW), the German Red Cross, and the Bavarian Water Authorities. For advanced users such as decision-makers in water management authorities, the published inundation maps should furthermore serve as a tool for better risk assessment.

In addition, even though we applied a simpler model (diffusive wave), it can easily be adapted to full dynamic models, since there is no limitation on the computational time.

Future work will see the inclusion of a 1D-2D sewer/overland flow coupled-model and extend the method to forecasting urban pluvial flooding (Leandro et al., 2011), including radar rainfall as an additional input in the query (Henonin et al., 2013).

A further promising application that is being tested is to incorporate both offline and online in one framework. In cases where a satisfactory goodness of fit is not found (<0.85) between the real-time discharge forecast and the discharge database, the online modus is activated, the 2D hydrodynamic model is run in real-time, and maps are made available. This will lead to fewer resource consumption as compared to a complete online forecast and reduced errors in the outputs. Furthermore, pre-calculated dynamic inundation maps can help to visualise the uncertainties in the hydrodynamic modelling and support rescue services. Better flood mitigation and flood forecast planning strategies can be developed by visualising inundation scenarios for different magnitudes of floods and associated potential damage for various quantiles of discharge hydrographs.

Chapter

5. Uncertainty quantification – Model parameter

Reducing uncertainties in flood inundation outputs of a two-dimensional hydrodynamic model by constraining roughness[3].

The consideration of uncertainties in flood risk assessment has received increasing attention over the last 2 decades. However, the assessment is not reported in practice due to the lack of best practices and too wide uncertainty bounds. We present a method to constrain the model roughness based on measured water levels and reduce the uncertainty bounds of a two-dimensional hydrodynamic model. Results show that the maximum uncertainty in roughness generated an uncertainty bound in the water level of 1.26 m (90 % confidence interval) and by constraining roughness, the bounds can be reduced as much as 0.92 m.

5.1. Introduction

Uncertainties in flood risk assessment have received increasing attention from researchers over the last 2 decades. In Germany, flood risk management plans rely on hydrodynamic (HD) models to determine the impact of flooding for areas of potential flood risk (Thieken et al., 2016). Two-dimensional (2D) HD models are widely used to simulate flood hazards in the form of water depth, inundation extent, and flow velocity (Disse et al., 2018). The hazard maps depict inundated areas for floods above certain exceedance levels, which leads to an improvement in flood risk assessment through increased spatial planning and urban development (Hagemeier-Klose, 2007).

Even though HD models are physically deterministic, they contain numerous uncertainties in model outputs (Bates et al., 2014; Beven et al., 2018). Information about the type and magnitude of these uncertainties is crucial for decision-making and for increasing confidence in model predictions (Oubennaceur et al., 2018). Despite uncertainties, decision-making in practice is based on first-hand data, expert judgement, and/or a calibrated model output (Henonin et al., 2013; Uusitalo et al., 2015). Uncertainties associated with exceedance level scenarios are usually not quantified for at least five reasons: (1) most of the sources of uncertainty are not recognized (Bales and Wagner, 2009), (2) the data required to quantify uncertainty are seldom available (Werner et al., 2005a), (3) high computational resources are required to perform an extensive uncertainty assessment, (4) the wide uncertainty bounds cannot be incorporated into the decision-making process (Pappenberger and Beven, 2006), and (5) the uncertainty analysis is complex and is not considered for the final decision (Merwade et al., 2008).

The major sources of uncertainty in HD models can be categorized as model structure, model input, model parameters, and the modeller (Matott et al., 2009; Schumann et al., 2011). The model structure, essentially either 1D, 2D, or hybrid 1D–2D HD code, is generally selected based on the purpose and scale of the modelling (Musall et al., 2011; Bach et al., 2014). In addition, there is no general agreement on the best approach to consider model structure uncertainty; hence, it is often neglected (Oubennaceur et al., 2018). In the case of hindcasting a flood event based on measured discharges or water levels as the input boundary conditions and a fine-resolution elevation, roughness remains the main source of uncertainty in HD models; hence we focus this study on roughness uncertainty.

The precise meaning of *roughness* changes based on a model's physical properties, such as grid resolution and time step (Bates et al., 2014), and the term is denoted as Manning's roughness coefficient or simply Manning's *n* in most HD models. Various studies point out that HD models can be very sensitive to Manning's *n*, which implies a

higher degree of uncertainty (Aronica et al., 1998; Pappenberger et al., 2005; Werner et al., 2005a). The coefficient is either derived from measurements in the field or estimated from the relevant literature on the basis of land use types, but it has proven very difficult to demonstrate that such models can provide accurate predictions using only measured or estimated parameters (Hunter et al., 2007). In addition, Manning's n is not only related to bottom friction but also includes incorrect representation of turbulence losses, 3D effects, and incorrect geometry (profiles); therefore, it cannot be measured exactly. The spatial distribution of the Manning's n in floodplains is challenging and depends on many factors, such as vegetation type, soil surface, and imperviousness (Sellin et al., 2013). Traditionally, this coefficient can be best estimated based on lookup tables of land use types (Werner et al., 2005b).

Table 5-1. A summary of selected publications including the maximum uncertainty bound reported. GLUE, PEM, GSA and SD stands for *Generalized Likelihood Uncertainty Estimation*, *Point Estimate Method*, *Global Sensitivity Analyses*, and standard deviation respectively.

Model dimension	HD Model	Identified sources	Method	Sample size	Max bound	Literature
1D	HEC-RAS	Manning's n	GLUE	10000	~	Pappenberger et al., (2005)
1D	HEC-RAS	Flow Topography Manning's n	GLUE	5000	~2.5 m (95%) in 8 m	Jung and Merwade (2012)
1D-2D	SOBEK	Topography Manning's n	GLUE		1.64 m (90%) in 1.51 m	Werner et al., (2005)
2D		Manning's n	GLUE	1000	~7m (90%) in 10.5 m	Aronica et al., (1998)
2D	H2D2	Flow Topography Manning's n	PEM	108	0.27 m SD in 12.06 m	Oubennaceur et al., (2018)
2D	Lisflood-FP	Flow Topography Manning's n Channel width	GSA	1792	6 m SD in 11 m	Hall et al., (2005)

In order to understand views on uncertainty analysis, it is important to look at the different modeller types. According to Pappenberger and Beven (2006), there are different modeller types: physically based modellers believe that their models are physically accurate and that the roughness must not be adjusted under any circumstances, the second modeller type believes that the roughness should be calibrated within a strictly known range (Wagener and Gupta, 2005), and the third modeller type uses effective roughness beyond the accepted range (Pappenberger et al., 2005). The first modeller type would reject any calibration or uncertainty analysis; however, HD models make simplifying assumptions and do not consider all known processes that occur during a flood event (Romanowicz and Beven, 2003). Hence, models are subjected to a degree of structural errors that are typically compensated for by calibrating Manning's n (Bates et al., 2014). However, effective roughness identified for one flood event might not hold true for another (Romanowicz and Beven, 2003), and a range of parameters should be defined where equifinality can be observed. Beven (2006) argued that the prior selected

for the range of parameters should potentially cover all the accepted or behavioural models (modeller type 2 or 3). In HD models, selecting such a prior distribution for model parameter introduces the issue of too wide bounds.

Significant work has been carried out thus far in the quantification of HD model uncertainties and an overview of selected publications, including model roughness, is presented in Table 5-1. The major issue of wide uncertainty bounds raised by researchers and practitioners is reflected in the table. It shows the maximum bounds reported in each publication and in some cases these bounds are more than 50 % of the available water depth (Aronica et al., 1998; Hall et al., 2005; Werner et al., 2005a; Jung and Merwade, 2012). This is indeed an issue but not a reason to ignore uncertainties in predicting hazards. Moreover, decision makers must be made aware of potential risks associated with the possible outcomes of predictions, such as water levels and inundation extent (Pappenberger and Beven, 2006; Uusitalo et al., 2015).

The associated uncertainties can be constrained on measured data, if available, using a suitable goodness of fit or with the help of a sophisticated framework for assessment (Werner et al., 2005a). Few researchers have used frameworks, such as generalized likelihood uncertainty estimation (GLUE), the point estimate method, and global sensitivity analysis, to reduce the bounds. These methods, although widely used in research, are not employed in operational practice, and a straightforward approach is needed to reduce the bounds. Furthermore, there is a need to ensure efficiency in searching model parameter spaces for behavioural models (Beven, 2006).

This study investigates the use of measured water levels to reduce uncertainty bounds of HD model outputs. We begin with the approach of the third modeller type and select extreme ranges of model roughness in literature and gradually shift to the approach of the second modeller type by reducing the uncertainty bounds based on the measured data. The main focus of this paper is to constrain literature-based ranges of roughness using measured water levels and to assess uncertainties in water levels. Uncertainty is quantified for the flood event of January 2011 in the city of Kulmbach, Germany.

5.2. Methods

To investigate the effect of measured data on constraining parameters, an ensemble of parameter sets was sampled using a prior distribution. In the HD model, distributed roughness values were used based on land use and a single value was used for each land use class. The model domain was spatially discretized based on the classification of land use and parameter sets were sampled using a prior. The choice of the distribution influences the outcome; hence it should be selected carefully. The 2D HD model was then run with each parameter set. The acceptance of each simulation was assessed by

comparing the model outputs and measured data. The measured data can be static or time series water level measurements in the model domain and/or inundation extent gathered by field survey or post-event satellite images.

The performance of the simulations can be accessed using a suitable goodness of fit, such as Nash–Sutcliffe efficiency, the coefficient of determination, absolute error, etc., based on the purpose of application and measured data available. A behaviour threshold was applied to divide simulations with acceptable performances from those with unacceptable performances. Parameter sets that perform below the threshold were then selected at each location and an intersection at all the locations resulted in the final number of accepted simulations (*r*) using equation 5.1:

$$r = \bigcap_{i=1}^{n} P_i(\text{GoF} \leq e) \qquad (5.1)$$

where *n* is the total number of observations, GoF is the goodness of fit used, *e* is the threshold, and *P* is the array of models that satisfy the criteria of GoF below the threshold.

5.3. Materials

5.3.1. Study area and land use

The city of Kulmbach is located in the north-east of the federal state of Bavaria in southern Germany. The city is categorized as a great district city with around 26 000 inhabitants and a population density of 280 inhabitants per square kilometre in an area of 92.8 km^2. The city is crossed by the river White Main and Mühl canal, which is a diversion canal for flood protection. Schorgast and Red Main are two main tributaries that meet the White Main upstream and downstream of the city respectively. In the north, the small tributary Dobrach meets the White Main and from the south side two storm water canals join the Mühl canal (see Figure 5-1a). The main gauging stations upstream of the city are Ködnitz at White Main and Kauerndorf located at the river Schorgast.

The land use is shown in Figure 5-1a and it generally consists of agricultural land (62%) that includes floodplains and grassland. The water bodies make up 7% of the total model area and include rivers, canals and lakes. The urban area covers around 26% of the land and includes industrial and residential areas as well as transport infrastructures like roads and railway tracks, whereas forests form barely 5% of the total area. Figure 5-2 shows images of the main channel and flood plain of the river White Main near site 1.
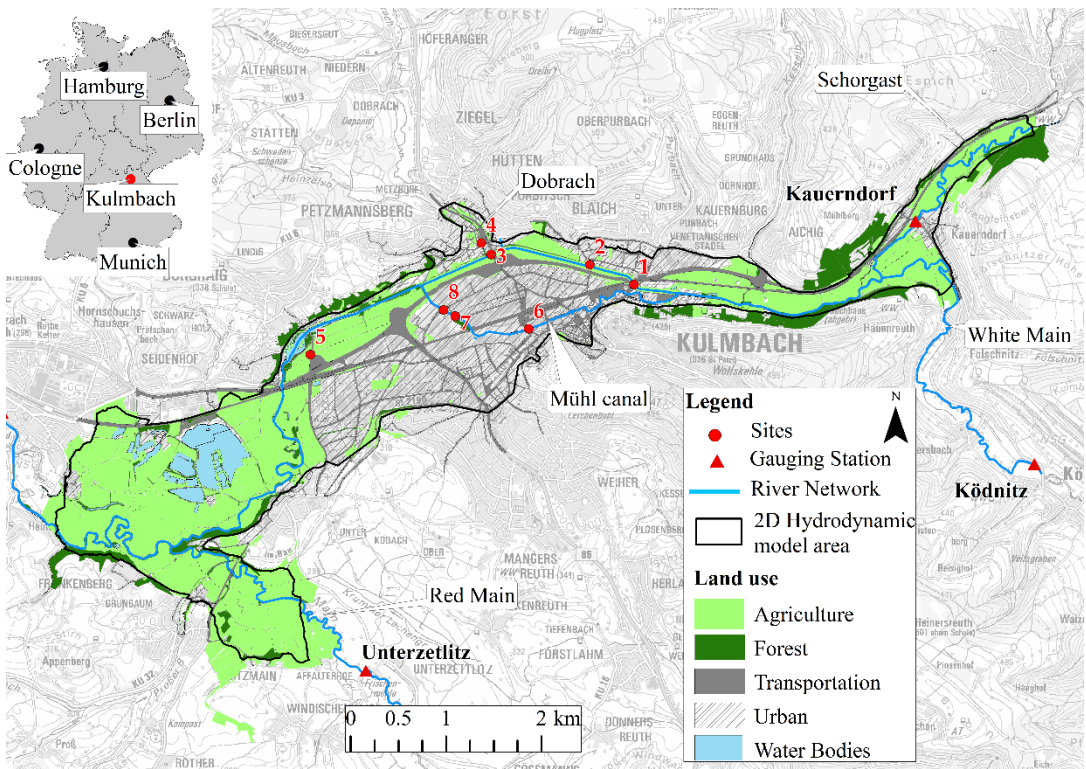
(a) Land use
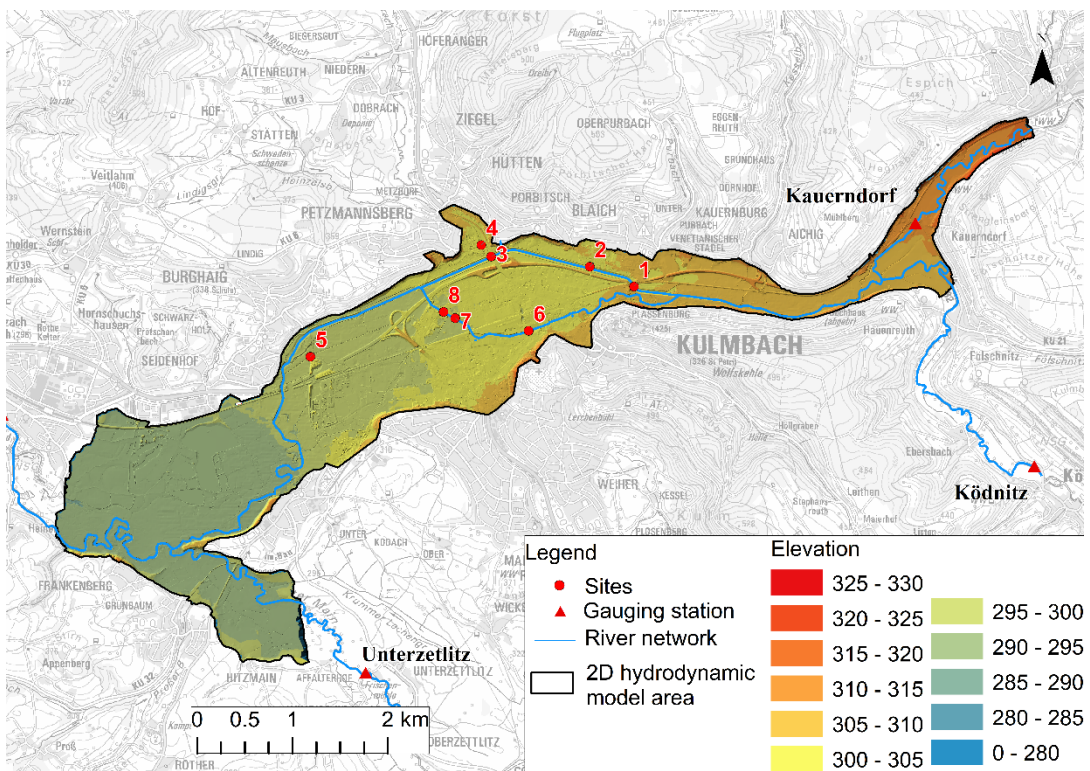
(b) Digital elevation model

Figure 5-1. Land use and the digital elevation model of the city of Kulmbach. Data source: Hof water management authority.

Figure 5-2. Main channel and flood plain of the river White Main near site 1 (image taken on 23.07.2015).

5.3.2. Measured discharges and water levels

Hydrological measurement data for the winter flood event of January 2011 were collected by the Bavarian Hydrological Services. Figure 5-3 shows the discharge at the main two gauges upstream of the city, Ködnitz and Kauerndorf. Intense rainfall and snow melting in the Fichtel Mountains caused floods in several rivers of Upper Franconia. On 14 January, the maximum discharge of 92.5 $m^3\,s^{-1}$ was recorded at gauge Kauerndorf and 75.3 $m^3\,s^{-1}$ at gauge Ködnitz. It was one of the biggest in terms of its magnitude and corresponded to a discharge of the 100-year return period at gauge Kauerndorf and the 10-year return period at gauge Ködnitz. Agricultural land and traffic routes were flooded, but no serious damage was reported. In Kulmbach, a dyke in the region of Burghaig was about to collapse due to the large volume of water. The water management authority opened the weir in Kulmbach, which prevented potential damages (Hof, 2011).
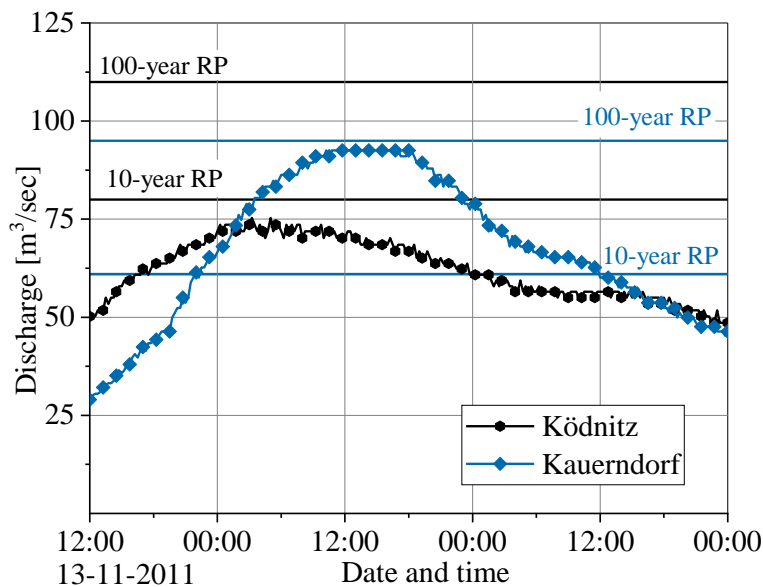
Figure 5-3. Discharge hydrographs at gauging stations upstream of the city, Ködnitz and Kauerndorf. RP stands for return period. Data source: Bavarian Hydrological Service (www.gkd.bayern.de).

Water levels at eight sites during the winter flood of January 2011 were collected by the water management authority in Hof, Germany, in Kulmbach (see Figure 5-1a). The water levels were measured using a levelling instrument *Ni 2* (Faig and Kahmen 2012). Based on the locations, the sites are categorized in four groups: sites 1, 2, and 3 at the river White Main; site 4 at the Dobrach canal in the north; site 5 at a side canal; and sites 6, 7, and 8 at the Mühl canal.

5.3.3. 2D HD model

HEC-RAS 2D was used as the 2D hydrodynamic model to quantify uncertainties in the inundation. The model uses an implicit finite-difference solution algorithm to discretize time derivatives and hybrid approximations, combining finite differences and finite volumes to discretize spatial derivatives (Brunner, 2010). Table 5-2 shows the model properties and information of the cell size. We have used the unsteady diffusive wave model presented in previous work in Bhola et al. (2018a, b).

Measured discharge hydrographs described in the previous section were used as the upstream boundary condition at river gauges Ködnitz and Kauerndorf, and an energy slope value of 0.0096, based on the river slope, was used at the downstream boundary where the water flows out of the model domain. Along with the major rivers, canals were also represented as a discharge hydrograph type.

Digital elevation model for this study was provided by the Hof water management authority and presented in Figure 5-1b. In the provided elevation model, the terrain is determined by airborne laser scanning and airborne photogrammetry with a high resolution of 1 m, whereas the riverbed was mostly recorded by the terrestrial survey. The combined elevation data were used to generate a triangulated irregular network (TIN) of the topography, which was then resampled to an irregular mesh of the 2D HD model. Special attention was given in resampling in order to preserve important features, such as rivers, dykes, buildings, and roads.

Table 5-2. 2D hydrodynamic model properties.

Data	Value
Model area	11.5 km^2
Total number of cells	430,485
Δt	20 s
Minimum cell area	6.8 m^2
Maximum cell area	59.8 m^2
Average cell area	24.8 m^2

5.4. Results and discussion

For the study, we have performed 1000 simulations based on uniformly distributed parameter sets for five land use classes. The sample size does contain enough samples of different behavioural models and the estimate was based on the recommendation in the literature (Aronica et al., 1998; Romanowicz and Beven, 2003) as well as the computational resources available. The HD models were simulated starting from 13 January 2011 00:00 central European summer time (time zone in Munich, GMT+2) to 14 January 2011 18:00 central European summer time (time zone in Munich, GMT+2), which requires approximately 5 h to simulate an event of 42 h on an eight-core, Intel® Core™ 2 Duo CPU T7700 @ 2.40 cloud computer with 64 GB RAM. Eight cloud computers using the LRZ Compute Cloud, provided by the Leibniz Supercomputing Centre of the Bavarian Academy of Sciences and Humanities, were used to complete 1000 simulation in 2 weeks. Measured water levels at eight sites (see section 5.3.2) were used for the analysis of the model output. The absolute error between the simulated and measured water level is used as the goodness of fit to reach the objective.

5.4.1. Roughness range and distribution

The model parameter consists of roughness coefficient Manning's *n* for five land use classes. A simple model structure, such as diffusive wave approximation, does not represent the accurate values of roughness as this parameter is a scale-dependent effective value that compensates for varying conceptual errors in the model (Néelz et al., 2009). Hence, it is recommended to use feasible extreme upper and lower ranges for the parameters in the literature (Aronica et al., 1998; Bhola et al., 2018b). In this study, ranges of Manning's *n* were set as 0.015–0.15 for water bodies, which covers a range from very weedy reaches to rough asphalt; 0.025–0.110 for agriculture, short grass to medium-dense brush; 0.110–0.200 for forests, dense trees (Chow, 1959); 0.012–0.020 for transportation, firm soil to concrete; and 0.040–0.080 for parks to gravels in urban areas (Arcement and Schneider, 1989). Latin hypercube sampling was used to generate 1000 parameter sets using the upper and lower ranges of Manning's *n* set as the prior and the HEC-RAS 2D model was simulated for each set.

5.4.2. Error tolerance

For the analyses, the absolute error between the simulated and the measured water levels was calculated at eight sites. The simulations that produced an absolute error below a threshold at all the sites were selected. Figure 5-4 shows that as we increase the threshold, the number of accepted simulations increases. To find one calibrated

parameter set, the least value of tolerance can be set at 0.20 m that gives two simulations that result in the least error at all sites. Having said that, the calibrated roughness set will probably hold true only for the January 2011 event as discussed in the study (Romanowicz and Beven, 2003). In order to generalize the results to other events and collect enough samples to produce uncertainty bounds, the tolerance needs to be increased. In this study, we have used 1.5, 0.70, and 0.50 m as the tolerance at sites to evaluate the roughness sensitivity, which results in 1000, 339, and 143 selected simulations respectively. Nevertheless, tolerance can be changed depending on the requirements of the user. To summarize, three thresholds are used to evaluate the performance of the method in order to reduce the uncertainty bounds and are termed as follows.

- *Case I.* Absolute error of 1.5 m resulting in 1000 simulations
- *Case II.* Absolute error of 0.7 m resulting in 339 simulations
- *Case III.* Absolute error of 0.5 m resulting in 143 simulations
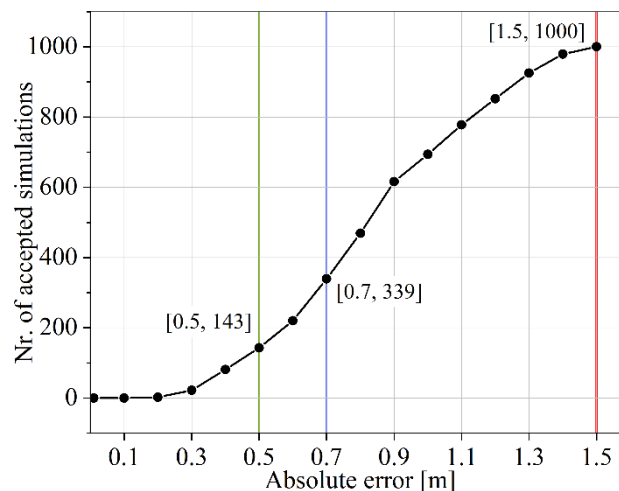
Figure 5-4. Accepted number of simulations vs. absolute error.

5.4.3. Roughness sensitivity

The sensitivity of the model roughness was investigated, and it was observed that the sites were only sensitive to land use of water bodies and agriculture and no sensitivity was observed with respect to urban, transportation, and forest. Table 5-3 presents the coefficient of determination (R^2) between Manning's n for all the land uses and absolute error for case I. Site-specific dependency in Manning's n and sites was observed for the cases in which the value of R^2 is found to be above 0.18 (in italic). The main reason for the lack of sensitivity can be explained by the location of the sites since they were mainly

located next to bridges upstream from water bodies or agriculture land uses. Nonetheless, there are other influencing factors, such as the inundation area, velocity, and topography that could also play a role (Werner et al., 2005b). Figure 5-5 shows the maximum flood inundation map for the January 2011 flood event simulated using the optimal model parameters, which were obtained by the least absolute error of 0.20 m. The inundation upstream to the sites is mainly constrained in the water bodies and agricultural land uses, which explains the impact on sensitivity of water levels to these two land uses.
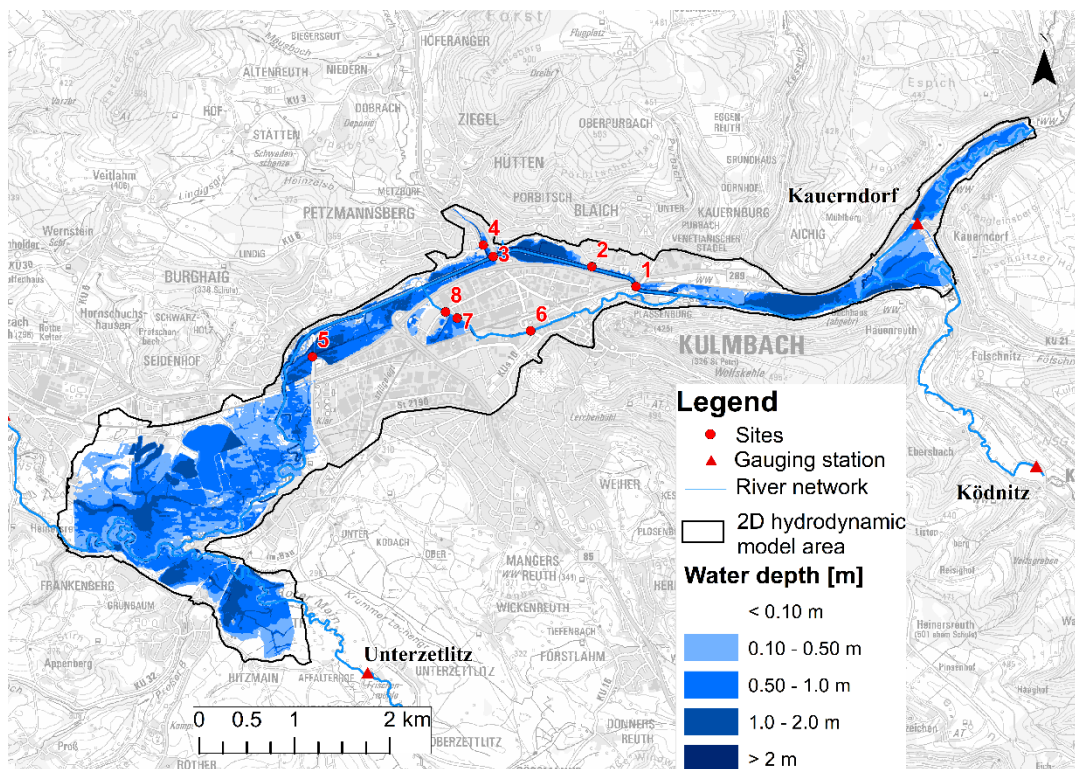
Figure 5-5. Inundation map for the flood event of January 2011 using the optimal model parameters, obtained using a least absolute error of 0.20 m.

The sensitivity to the land uses is apparent in the scatter plots between the absolute error and Manning's n shown in Figure 5-6. In the figure, it can be observed that cases II and III (with 339 and 143 accepted simulations) result in an absolute error of less than 0.70 and 0.50 m at the sites respectively. The selected simulations were further used in refining the uncertainty bounds. Sites 1, 2, and 3 (White Main) show a pattern with agriculture (flood plain): as Manning's n increases, the error decreases until an optimal roughness is obtained and further increase in the roughness value results in an increased error. Sites 6, 7, and 8, located at the Mühl canal, show similar sensitivity towards water bodies. In the case of sites 4 and 5, sensitivity is observed for both land use types. The sensitivity found here is also reflected in other studies, such as sensitivity

to flood plains (agriculture) (Aronica et al., 1998) and main channels (water bodies) (Hall et al., 2005), and insensitivity to other land uses for flood events (Horritt and Bates, 2002; Werner et al., 2005a).

Table 5-3. Coefficient of determination (R^2) between Manning's n and absolute error for case I. The value above 0.18 are shown in italic.

Site	Coefficient of determination [-]				
	Water bodies	Agriculture	Forest	Transportation	Urban
1	0.04	*0.89*	0.00	0.00	0.00
2	0.05	*0.85*	0.00	0.00	0.00
3	*0.18*	*0.69*	0.00	0.00	0.00
4	*0.34*	*0.54*	0.00	0.00	0.01
5	*0.45*	*0.37*	0.00	0.00	0.00
6	*0.97*	0.00	0.00	0.00	0.00
7	*0.23*	*0.18*	0.00	0.00	0.00
8	*0.19*	*0.22*	0.00	0.00	0.00

(a) Site 1: Water bodies

(b) Site 1: Agriculture

(c) Site 2: Water bodies

(d) Site 2: Agriculture

(e) Site 3: Water bodies

(f) Site 3: Agriculture

(g) Site 4: Water bodies

(h) Site 4: Agriculture

(i) Site 5: Water bodies

(j) Site 5: Agriculture

(k) Site 6: Water bodies

(l) Site 6: Agriculture

(m) Site 7: Water bodies

(n) Site 7: Agriculture

(o) Site 8: Water bodies   (p) Site 8: Agriculture
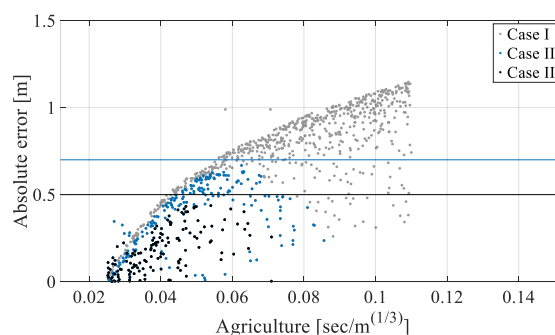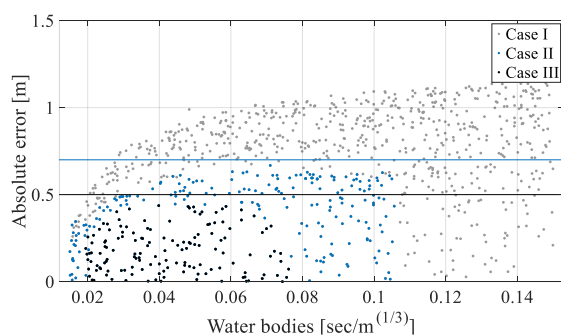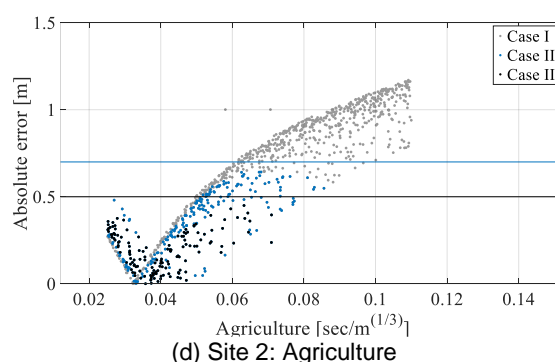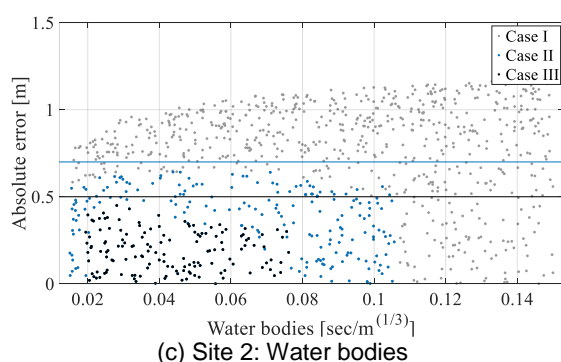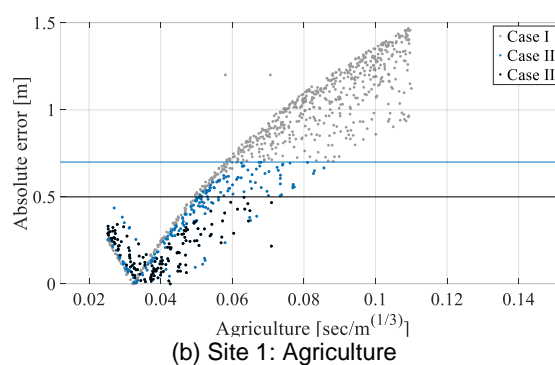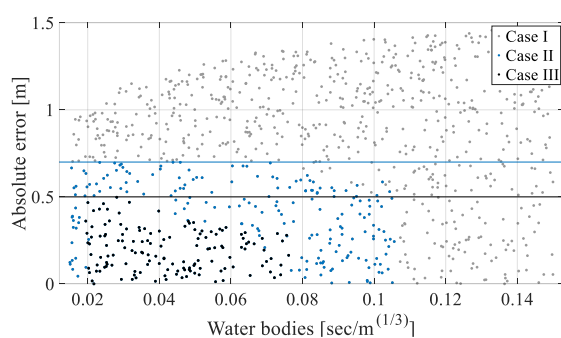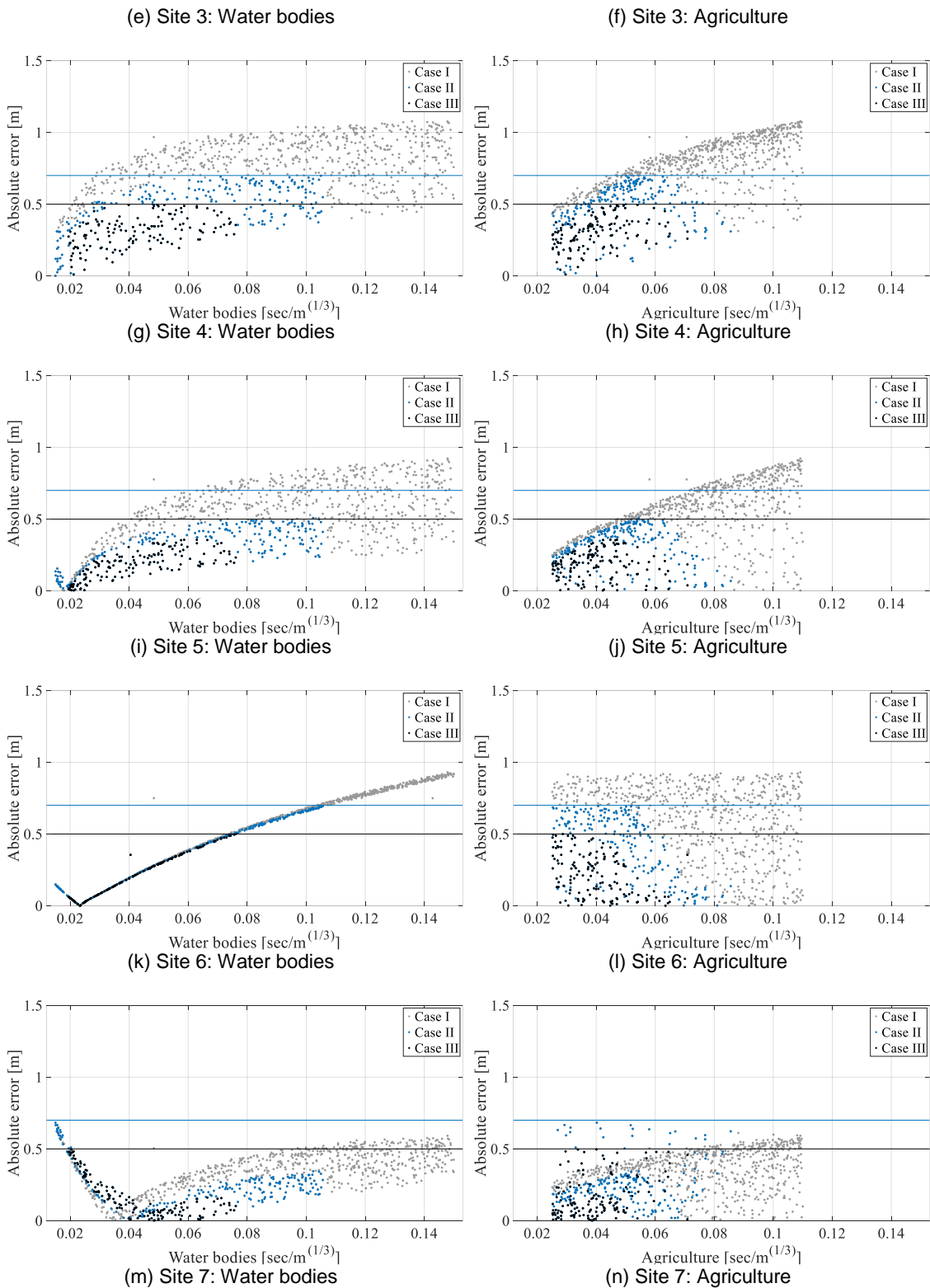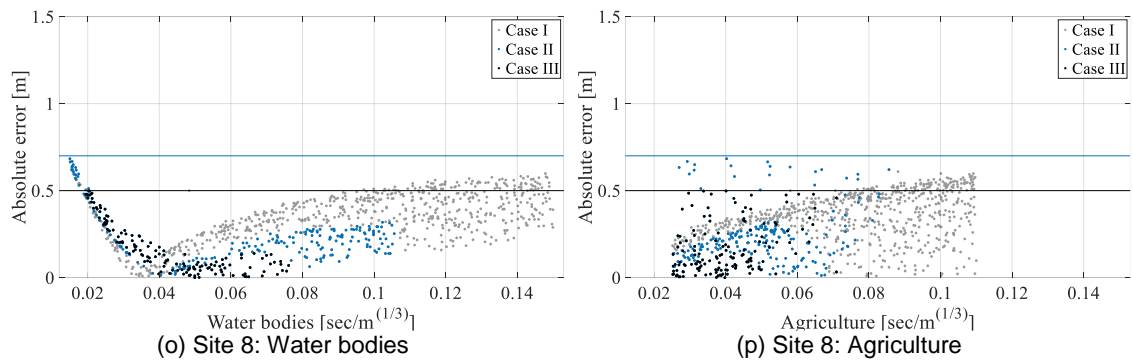
Figure 5-6: Scatter plot of the absolute error of 1000 simulation in relation to water bodies and agriculture. Three cases I, II and III shows accepted simulations based on threshold values of 1.5, 0.7 and 0.5 m respectively.

5.4.4. Uncertainty of water levels

Table 5-4 shows the 90 % confidence interval of the absolute error bounds of the simulated and measured water levels for three cases along with the measured available water depth. The impact of reducing the uncertainty is clear in the simulated flood inundation for the city of Kulmbach; the average uncertainty bound was 0.87 m and after constraining with the measured data, it was reduced to 0.55 m for case II and further reduced to 0.38 in case III. The maximum bound of 1.26 m was observed at site 1, which was reduced to 0.59 and 0.34 m in cases II and III respectively. Sites 7 and 8, located on the Mühl canal, showed the least effect of 0.12 and 0.11 m reduction in the bounds respectively (case III). Figure 5-7 presents a box plot of the difference in the simulated and measured water levels. The preselected literature values of Manning's n tend to over-predict the water levels as the mean water level is well above zero at sites in case I. After constraining Manning's n, the mean drops considerably and is still above zero for all sites except 7 and 8 in both cases II and III. The figures also suggest that the simulations can both under- and over-predict the inundation, which might not be desired in some applications, such as early warning and evacuation planning.

(a) Case I   (b) Case II   (c) Case III
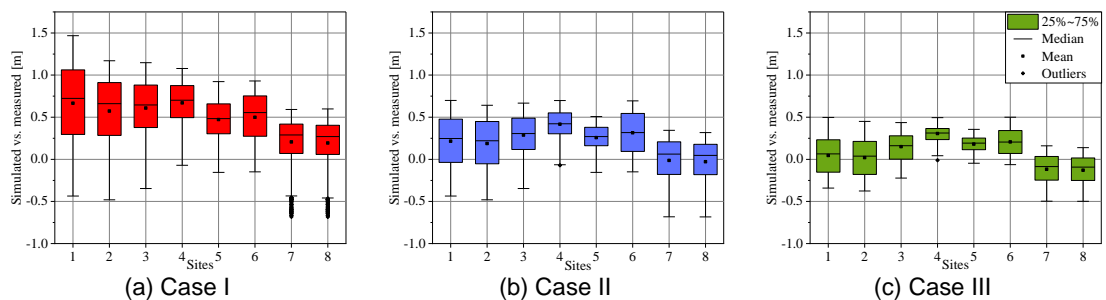
Figure 5-7. Error in simulated vs. measured water levels for a) Case I, b) Case II, and c) Case III.

Furthermore, in situations where a few sites are more sensitive/important than others, a weighted goodness of fit can also be used. However, in this study, we have focused on the overall uncertainties, both positive and negative, for a comprehensive assessment.

Table 5-4. The 90 % confidence interval absolute error bounds (m) for three cases along with measured water depth (m) at eight sites for the January 2011 event.

Site	Measured water depth[1]	90% absolute error bounds		
		Case I	Case II	Case III
1	2.78	1.26	0.59	0.34
2	2.90	1.04	0.55	0.34
3	2.93	1.01	0.59	0.36
4	1.43	0.97	0.64	0.46
5	1.75	0.78	0.46	0.32
6	0.89	0.85	0.65	0.43
7	2.31	0.52	0.46	0.40
8	2.36	0.51	0.46	0.40

[1]Data source: water management authority in Hof, Germany.

5.4.5. Constrained parameter set

The main objective of this study was to reduce the uncertainty bounds of the model output by constraining the prior set for the roughness. In this section, it is shown that the literature-based prior used for Manning's n can be reduced using measured water levels. Figure 5-8 presents the box plot of water bodies and agriculture roughness for three cases (1000, 339, and 143 accepted simulations). As stated in the previous section, no sensitivity was observed between the sites and other three land use types. Hence, the uncertainty bounds for other land use classes remain the same after the analysis.

In the case of water bodies, Manning's n gradually concentrated in the range of 0.029–0.055 (25 %–75 %, case III). The physical interpretation of the constrained coefficient ranges in the main channels with stones to sluggish reaches (Chow, 1959). However, for agriculture, the mean dropped considerably from case I to case II and remains consistent in case III. The 25 %–75 % bounds of the coefficient were 0.032–0.047 (case III) and can be interpreted as high grass to medium brush in the flood plains (Chow, 1959). This compares well to the results of Horritt and Bates (2002) in which they achieved an optimum in the range of 0.03–0.05 for the main channel and 0.02–0.10 for the flood plain roughness of the 2D HD models.
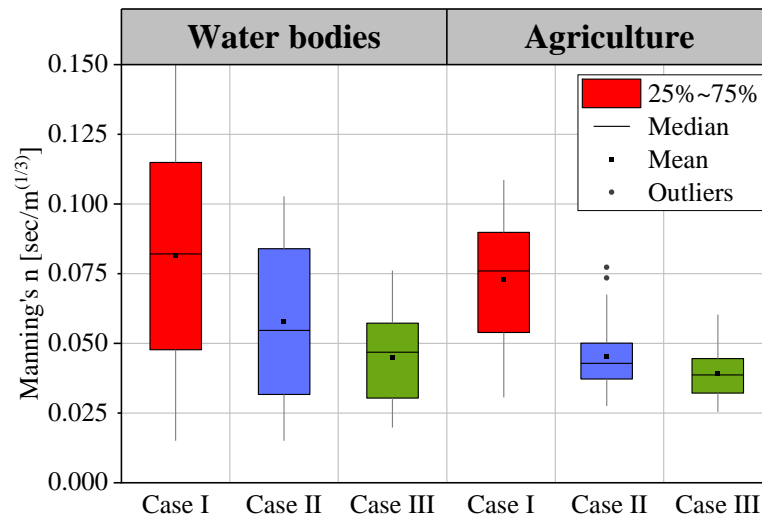
Figure 5-8. Box plot of Manning's n of water bodies and agriculture for three cases.

Both the main channel and flood plains are homogenous in the model area and the presence of stones and high grass is observed in the field (see Figure 5-2). It was discussed previously in the Introduction, that the second modeller type believes that Manning's n should be varied in a strictly known range based on field experiments. But these ranges can also be defined using a data-driven approach with the method presented. However, a detailed field experiment in the study area will be required to make a conclusive remark for a comparison between the field and evaluated coefficients. Furthermore, these ranges may vary for summer and winter events and various HD models can be built up depending on the season.

5.5. Conclusions

We have quantified the uncertainty associated with the model parameter for the flood event of January 2011 in the city of Kulmbach, Germany. Moreover, the study provides a comprehensive review of HD model uncertainty and explores the issue of high uncertainty bounds, which hinder users from analysing uncertainties. We have provided a straightforward approach to practitioners for searching model parameter spaces for behavioural models and subsequently reduce the flood inundation uncertainty bounds. Extreme ranges of model roughness in the literature were selected and 1000 uniformly distributed models were run, which resulted in wide uncertainty bounds of up to 1.26 m (90 % confidence interval). To reduce the bounds, measured water levels at eight sites were used and three cases were selected on the basis of absolute error threshold values of 1.5, 0.7, and 0.5 m, which resulted in 1000, 343, and 143 accepted simulations respectively. By constraining the roughness, the bounds were reduced to a maximum of

0.34 m. In addition, the model roughness was constrained, and the physical interpretation of the constrained roughness was discussed. The model roughness was spatially distributed based on five land uses and the model was sensitive only to water bodies and agriculture.

The method is easy to incorporate into other study areas, provided that there are measured water levels available. The uncertainty analysis presented in this study allows a better understanding of the model roughness variability in HD models. The ranges researched for Manning's n in this study can represent a good starting point (prior distribution) for other studies. Our study has shown that there are significant uncertainties in HD model roughness and should be considered in decision-making. In addition, the study highlights the importance of field surveys for reducing the uncertainty in flood inundation outputs.

On an urban scale, the uncertainty assessment presented would substantially improve emergency responses by assessing the potential consequences of flood events (Molinari et al., 2014), and disaster relief organizations, such as the Federal Agency for Technical Relief (THW), the German Red Cross, and the Bavarian Water Authorities, would indeed benefit from prioritizing and coordinating evacuation planning. For advanced users such as decision makers in water management authorities, the uncertainty assessment should further serve as a tool for enhanced risk assessment. In addition, by visualizing inundation scenarios, improved flood mitigation and flood forecast planning strategies can be developed using a multi-model ensemble (Bhola et al., 2019) and potential damage can be estimated for various quantiles.

Under-prediction of a simulated inundation is not desired in most case studies; therefore, the goodness of fit used in this study could be a critical issue. Future work should include other evaluation measures to constrain the parameter ranges. As the high-computational resources hinder a comprehensive uncertainty assessment of a full dynamic HD model, it is worth exploring transferability of the evaluated uncertainty bounds of Manning's n of the simple model structure (diffusive wave) to a complex model structure. Furthermore, other sources of uncertainty, such as model input (hydrological model in Disse et al., 2018), discharge measurement error, or flood frequency estimations, and digital elevation map and measured water level, which is assumed to have no error, should also be incorporated for a comprehensive assessment. The parameter ranges were constrained based on a single event in this study; however, the values can be further validated using another flood event of higher magnitude. Land use in this study is divided

into five classes; in future, further reclassification of land use, especially in urban areas, will help further reduce the bounds (Bhola et al., 2018c).

The inundation model should be extended to simulate urban pluvial flooding in future by including a 1D–2D sewer/overland flow coupled-model structure (Leandro et al., 2011). This will bring other sources of uncertainties as there are numerous uncertain parameters associated with this model structure (Djordjević et al., 2014). With an ever-increasing computational performance and the introduction of cloud computing, the integration of more complex models will become feasible.

Chapter

6. Uncertainty quantification – Model input

Uncertainty assessment for the calculation of dynamic flood maps – case study Kulmbach[4].

The project FloodEvac, funded by the German Federal Ministry of Education and Research (BMBF), aims at providing spatial and temporal information on the flood risk in the event of a flood. In the subproject presented here, flood maps of water depths and flow velocities are calculated including model uncertainties. The effects of different uncertain inputs on the flooding areas are presented. These uncertainties include the spatial interpolation of the precipitation as well as the model parameters of the hydrological model LARSIM and of the hydrodynamic model Hydro-AS_2D. The floods areas are visualized in an hourly time step in order to determine evacuation paths more effectively. This information will support the rescue forces for optimizing their alert and evacuation plans.

---

[4] Disse, M., Konnerth, I., Bhola, P. K., and Leandro, J.: Unsicherheitsabschätzung für die Berechnung von dynamischen Überschwemmungskarten – Fallstudie Kulmbach, in: Vorsorgender und nachsorgender Hochwasserschutz: Ausgewählte Beiträge aus der Fachzeitschrift WasserWirtschaft Band 2, edited by: Heimerl, S., Springer Fachmedien Wiesbaden, Wiesbaden, 350-357, 2018.

6.1. Presentation of the project FloodEvac

The German-Indian project FloodEvac is funded by the Federal Ministry of Education and Research (BMBF, FKZ 13N13196 (TUM)) since 2015 and aims to improve the safety of people and transportation for extreme flooding events. For this purpose, risk-based methods, technologies and processes are being developed in order to assess the vulnerability of transport infrastructures that are crucial in the case of a disaster for transport and evacuation.

FloodEvac has the following partners with their associated work packages

*   Coordination and administration as well as evaluation of critical transport infrastructures: University of the Federal Armed Forces Munich, Prof. Norbert Gebbeken
*   Flood modelling and flood plains: Technical University of Munich, Prof. Markus Disse
*   Smartphone-based sensor fusion: University of Applied Sciences, Prof. Thomas Haenselmann
*   Underwater robot: Jacobs University Bremen, Prof. Andreas Birk
*   Robust evacuation and civil protection planning: University of Kaiserslautern, Prof. Horst W. Hamacher
*   Cultures and catastrophe in Germany and India in climate change: Freie Universität Berlin, Prof. Martin Voss
*   Monitoring and management of urban flooding using the crowd-sourcing technique: Amrita Vishwa Vidyapeetham University (India), Prof. Maneesha V Ramesh
*   The drainage system: Indian Institute of Technology Delhi, Prof. Ashwin K. Gosain

More information about FloodEvac can be found at: http://www.floodevac.org/

6.2. The FloodEvac tool for coupling the flood model chain

As part of the subproject *Flood modelling and flood plains*, FloodEvac tool was developed. It allows the coupling of different models in a single interface. Interface applications include inter-model data exchange, quantifying uncertainties within the model chain, and model calibration. The interface is written in MATLAB™ and structured in subroutines. MATLAB was chosen to facilitate the replacement of subroutines and to benefit from the graphical capabilities of MATLAB in presenting results. Three types of subroutines can be distinguished: the first allows the coupling and exchange of data between the models, the second one is responsible for the calibration of the models and the quantification of the uncertainties, and the third involves the presentation and analysis of the results (see Figure 6-1).
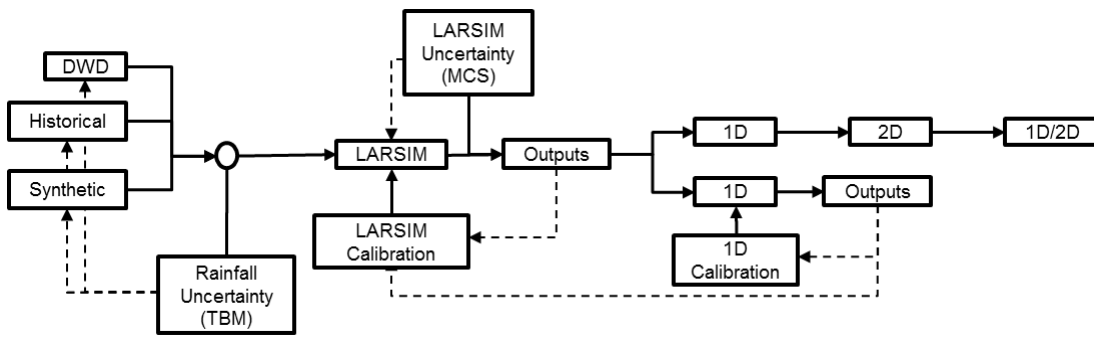
Figure 6-1. FloodEvac tool and model chain.

6.2.1. The hydrological model LARSIM

LARSIM (Large Area Runoff Simulation Model) is a conceptual water balance model (WHM) that calculates complex processes in the water cycle using simple mathematical equations (Figure 6-2). The model consists of a soil module and area storage that regulate the distribution of water supply to direct runoff, interflow and base runoff. The model enables the linking of continuous long-term simulations of the water balance with the event-related flood forecast. Input data of the model are meteorological measurement and forecast data, spatially distributed land use and soil properties, as well as discharge measurements and information on water management measures, such as the operation of dams or retention basins (Gerlinger et al., 2003). The model was provided to the Chair of Hydrology and River Basin Management of the Technical University of Munich by the Bavarian Environment Agency for use in the FloodEvac project.
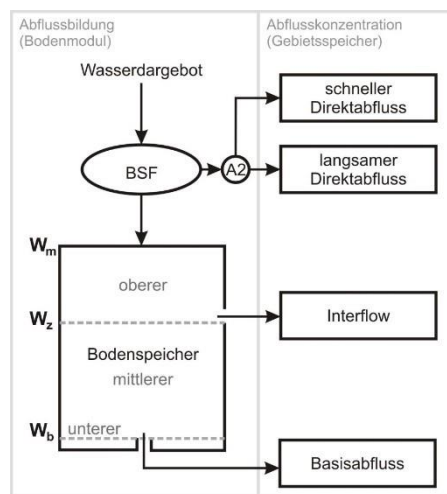
Figure 6-2. Scheme of the LARSIM water balance model.

6.2.2. Hydro_AS-2D

Hydrodynamic modelling is performed with the commercial flow model Hydro-AS_2D. The model is based on the depth-averaged shallow-water equations and uses the finite-volume method to discretize an unstructured mesh, which consists of triangular and rectangular elements (Nujić, 2014). The model is used in Bavaria to provide flood hazards and flood risk maps. The FloodEvac project uses a calibrated model of the Water Management Authority, Hof.

6.2.3. FloodEvac tool uncertainty visualisation

A significant advantage of the FloodEvac tool is the ability to estimate the predictive uncertainty. Since the model chain includes a hydrological and hydrodynamic model, it is possible not only to propagate the uncertainties from precipitation data but also to consider the uncertainties of model parameters of the various models. In fact, uncertainties can arise from different sources: input data, model calibration and model uncertainties. Although this paper examines only the uncertainties of the model parameters of the hydrological model, the various methods implemented in FloodEvac-Tool are briefly explained.

The interpolation of precipitation is a source of uncertainties of the input data. FloodEvac uses the Turning Bands method (TBM, Mantoglou and Wilson, 1982) with hourly aggregated precipitation data. To quantify the uncertainty of interpolation, a large number of TBM simulations are performed. This produces various precipitation rasters that have the same total area precipitation. This procedure ensures to quantify the influence of precipitation interpolation uncertainties on the results of the hydrological and hydraulic models. Another source of uncertainty arises from the calibration parameters of LARSIM. Uncertainty is determined using Monte Carlo simulations (MCS) by varying the parameters within the limits set for calibration (Leandro et al., 2013). The specified limits are based on Haag et al. (2016) and have been adjusted to the values used in the provided LARSIM model. In this paper, only the uncertainties of the model parameters of the hydrological model are investigated.

6.3. Parameter uncertainty of the LARSIM model Upper Main

The inaccuracy of the flood forecast for the city of Kulmbach, which results from the uncertainty in the LARSIM, becomes clear by visualising a longer time series. Figure 6-3 shows the simulated and measured discharges from 2006 to 2008 of the White Main (gauge Ködnitz) and the Schorgast (gauge Kauerndorf), which flow together upstream

of Kulmbach. The flood at the end of May 2006 is not simulated by the model at any of the gauges, and smaller discharge peaks in the simulation period are only rarely achieved by the model. Overall, the model under-predicts discharge peaks at both the gauges. First, the parameter uncertainty of the model was determined using MCS and then uncertainty bands for the event May 2006 were determined (see Figure 6-4).

(a)   (b)
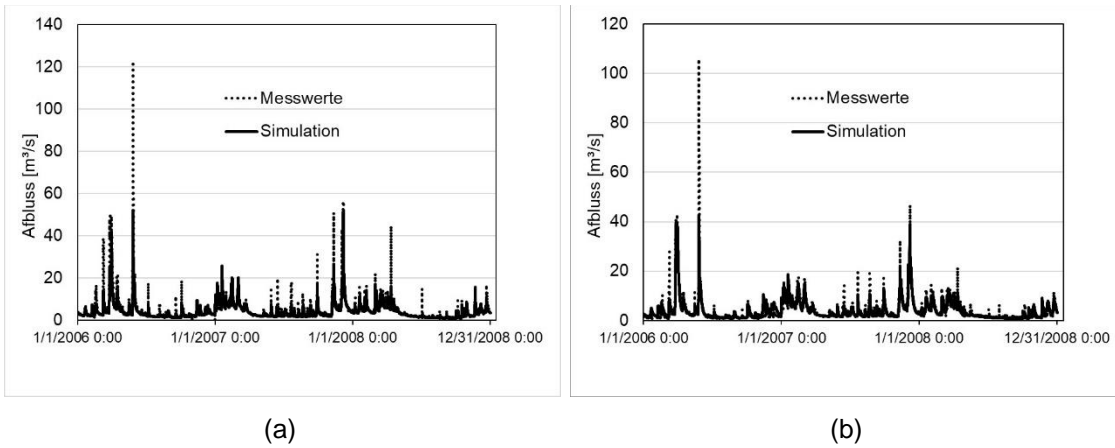
Figure 6-3. Measured and simulated discharge at gauges Ködnitz (left) and Kauerndorf (right).

(a)   (b)
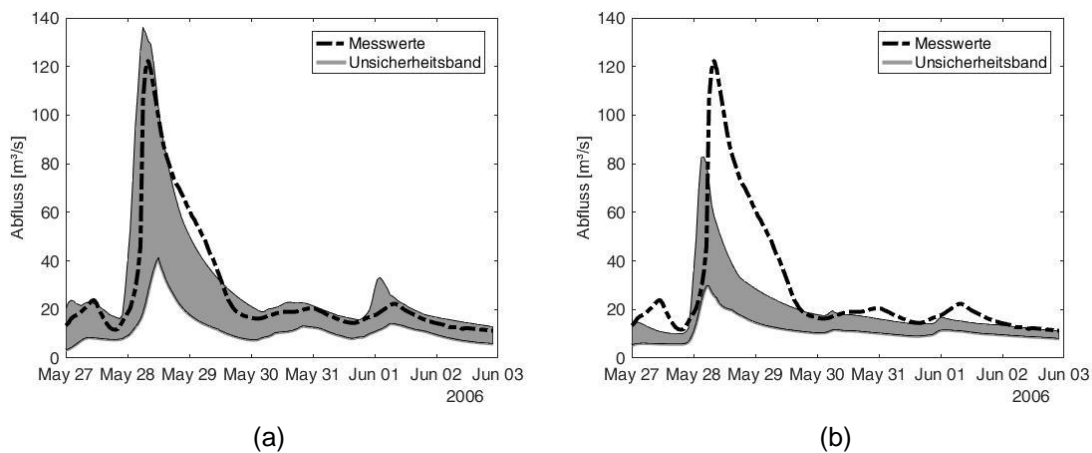
Figure 6-4. Uncertainty bands for the flood event May 2006 for gauges Ködnitz (left) and Kauerndorf (right).

At the gauge Kauerndorf, the measured peak discharge of this flood event is well outside the range of uncertainties. The results of the MCS thus show that the discharge peaks simulated are too low and cannot be based solely on the parameter uncertainty of the model, but that either conceptual model errors or errors of the input data must be the cause. In order to increase the discharge peaks, the correction factor for precipitation KG was adjusted for both sub-catchments and the MCS was repeated. For Ködnitz, the precipitation was increased by a factor of 1.15 and for Kauerndorf by 1.31. Non-behavioural models, an average absolute deviation above the mean of the absolute

deviations, were discarded. From the remaining, approximately 50% of the simulated time series, the 10%, 50% and 90% quantiles were extracted (see Figure 6-5). The effects of the parameter uncertainty of the model estimated in this way on the extension of flooded areas in Kulmbach determined in the hydrodynamic model will be discussed in the next section.

(a)   (b)
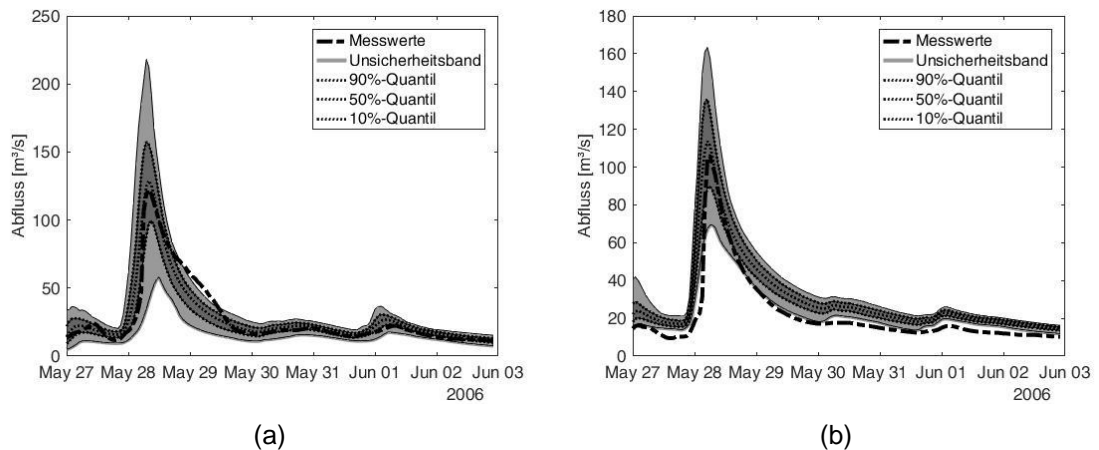
Figure 6-5. Uncertainty bands for the flood event May 2006 after adjusting the precipitation correction factor for the gauges Ködnitz (left) and Kauerndorf (right).

6.4. Uncertainty of dynamic flood maps

The city of Kulmbach has about 26,000 inhabitants and a population density of 280 inhabitants per km². The flood in May 2006 exceeded the 100-year return period discharge (HQ) of 106 m³/s at the White Main near Ködnitz with 123 m³ / s as well as at the Schorgast near Kauerndorf upstream of Kulmbach (see Table 6-1).

Table 6-1. Discharge statistics and simulated peak discharges of the gauges Ködnitz and Kauerndorf.

Gague	MCS 10%-Quantile [m³/s]	MCS average [m³/s]	MCS 90%-Quantile [m³/s]	HQ100 [m³/s]	MQ [m³/s]
White Main gauge Ködnitz	99.5	128.8	157.5	123	4.09
Schorgast gauge Kauerndorf	89.9	113.7	135.8	106	3.66

Kulmbach is currently protected from flooding by a diversion Mühl canal, build in the 1930s, which protects the inner-city by diverting a discharge of 5 m³/s. The recent floods have provoked the city planners to renovate the partly outdated protection infrastructure. By optimizing the dischage profile of the flood basin and increasing the dykes, the city

centre is intended to be protected for a discharge of 100-years in the future (WWA, 2018b).

The 2D hydrodynamic simulation for the event of May 28, 2006, was simulated for 12 hours with 16 hours warm-up phase. As boundary conditions, the discharge hydrographs of the 10%, 50% and 90% quantiles of the MCS simulations of the hydrological model were used (see Figure 6-6).

(a)   (b)
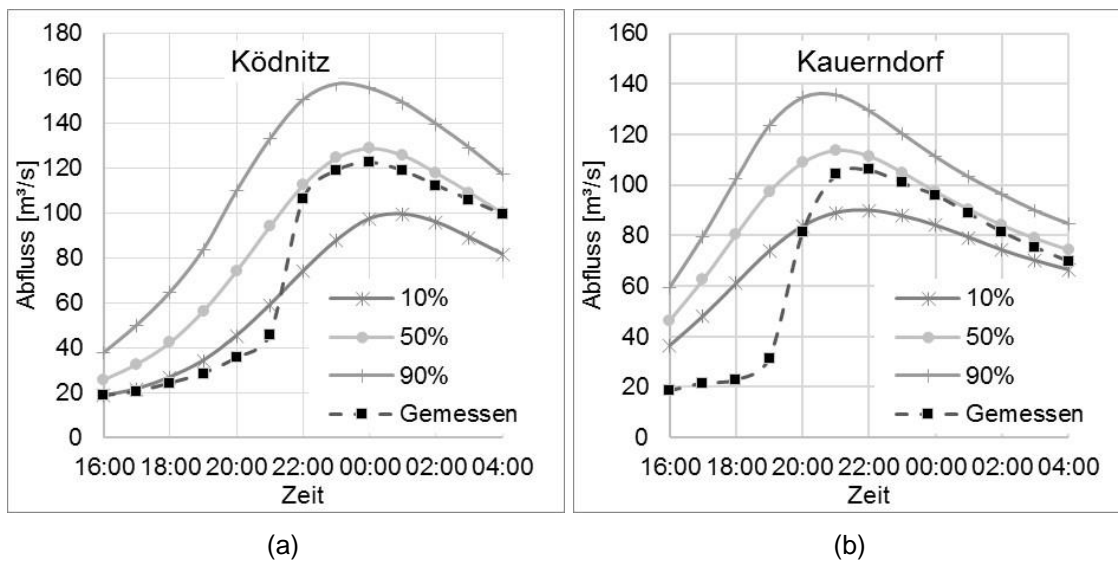
Figure 6-6. Boundary conditions for the hydrodynamic model: discharges at the gauges Ködnitz (left) and Kauerndorf (right) determined with LARSIM 28.05.-29.05.2006.
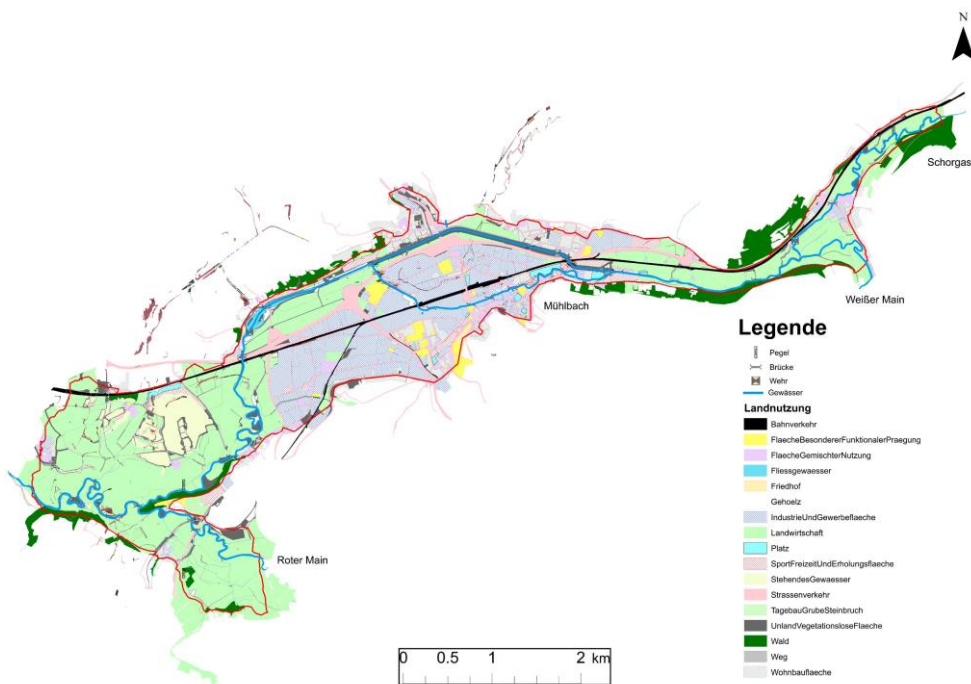
Figure 6-7. Land use map of the city of Kulmbach.

A fine discretization is used for the model domain containing a total of about 300,000 nodes and 600,000 elements. The parameters were adjusted to achieve a stable simulation: the SCF value was changed to 2, the viscosity coefficient to 0.6 and the maximum permissible flow rate to 15 m/s. The minimum water level above which a node is considered wet was defined to be 0.01 m. The most important model parameter, the roughness coefficient, is parameterized in the model as Strickler value (k_{st} [$m^{1/3}$/s]). The values for k_{st} are spatially distributed and are based on a detailed land use map with 17 land use classes (see Figure 6-7).

(a) 28.05.2006 at 19:00

(b) 28.05.2006 at 23:00

(c) 29.05.2006 at 01:00
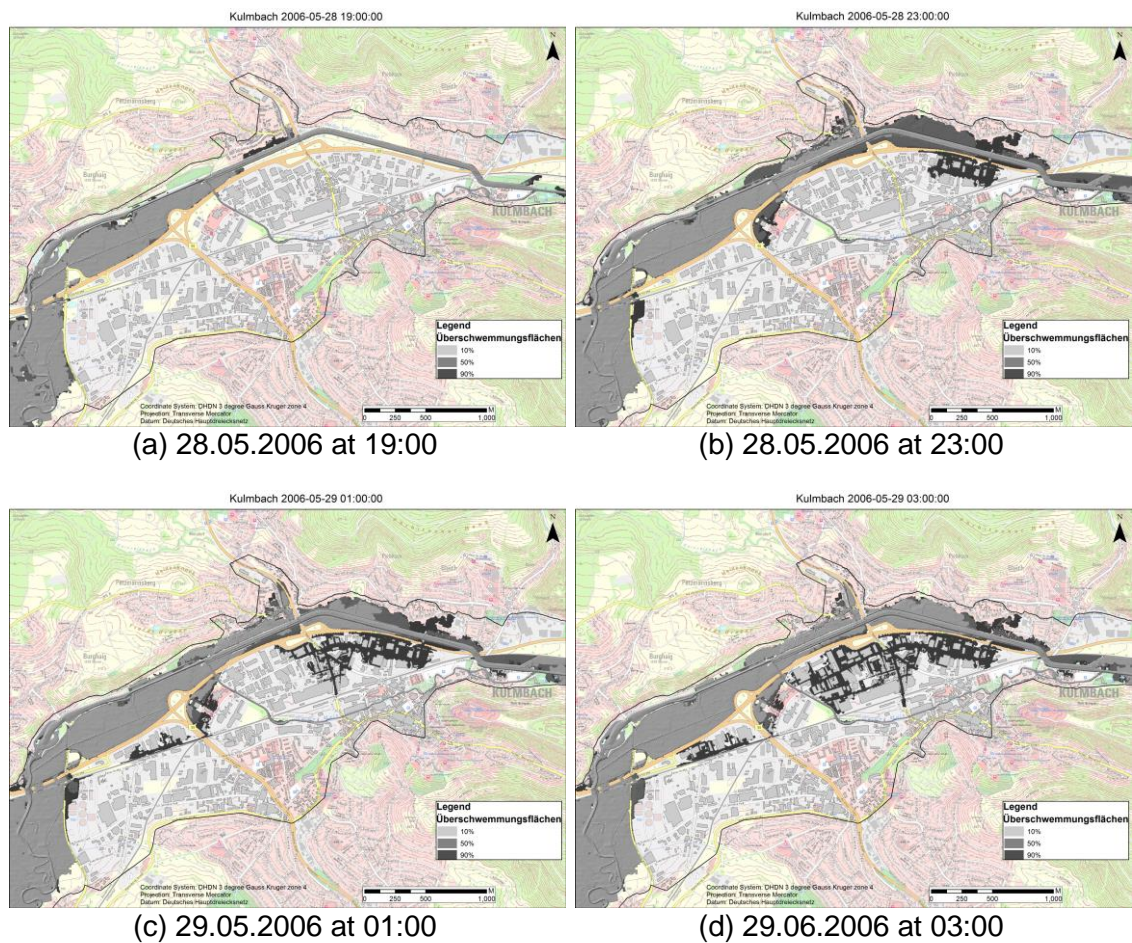
(d) 29.06.2006 at 03:00

Figure 6-8. Flood inundation areas for Kulmbach: a) 28.05.2006 at 19:00, b) 28.05.2006 at 23:00, c) 29.05.2006 at 01:00 and d) 29.06.2006 at 03:00.

The resulting flood maps for four-time steps are shown in Figure 6-8. It can be observed that the floodplains of the 10% and 50% quantiles, which are below the range of the HQ100, are not very different and therefore water remains in the floodplains. The floodplain of the 90% quantile, on the other hand, extends to the city centre, the industrial area and the road B289. This illustrates that the parameter uncertainty of the hydrological model for Kulmbach is a critical factor for the prediction of flood plains. Therefore, the official flood forecasting should not only indicate the uncertainty of the discharges but

also represent the resulting changes in the flooded areas. Depending on the sensitivity of the city, evacuation measures can be prioritised, and early planning should be designed.

6.5. Conclusion and outlook

Every flood forecast is associated with uncertainties. In principle, the uncertainties increase when rainfall predicted due to the (small) size of the catchment area has to be included. The FloodEvac project takes into account the overall uncertainty of precipitation prediction, hydrological and hydrodynamic modelling.

This article investigates the influence of the parameter uncertainty of the LARSIM water balance model, which is operationally used in the Flood Forecasting Center in Bavaria. For the city of Kulmbach, there are significant differences in the floodplains for the event of May 2006, based on the uncertainty quantiles 10%, 50% and 90%. This information is very important for civil protection since different vulnerabilities in terms of flood damage can be covered in time and space by differentiated protection and evacuation measures.

The aim of the FloodEvac project is to provide dynamic flood maps with 1-hour temporal resolution using High Performing Computing (HPC). For example, evacuation routes can be planned well in advance and the corresponding measures can be implemented. However, HPC calculators are currently not able to generate flooding areas including uncertainty bands in a short time. Therefore, in FloodEvac, the solution is to carry out the 2D hydrodynamic simulations in advance for many flood scenarios and to store them every hour. In the event of a flood, those maps are then displayed and optionally interpolated, which correspond most closely to the previously simulated (scenario) hydrographs. As a result, hourly flood prediction maps can also be provided with standard desktops.

Chapter

7. Communication of uncertainties

Hazard maps with differentiated exceedance probability for flood impact assessment[5]

In operational flood risk management, a single best-model is used to assess the impact of flooding, which might misrepresent uncertainties in the modelling process. We have used quantified uncertainties in flood forecasting to generate flood hazards maps that were combined based on exceedance probability scenarios. The purpose is to differentiate the impact of flooding depending on the building use. The aim of the study is thus to develop a novel methodology that uses a multi-model combination of flood forecasting models to generate flood hazard maps with differentiated exceedance probability. These maps take into account uncertainties steaming from the rainfall-runoff generation process and could be used by decision-makers for a variety of purposes in which the building use plays a significant role, e.g. flood impact assessment, spatial planning, early warning and emergency planning.

---

[5] Bhola, P. K., Leandro, J., and Disse, M.: Hazard maps with differentiated exceedance probability for flood impact assessment, Nat. Hazards Earth Syst. Sci. Discuss., https://doi.org/10.5194/nhess-2019-158, in review, 2019

7.1. Introduction

Floods are one of the most destructive natural hazards and lead to severe social and economic impacts (European Union, 2007; Alfieri et al., 2016). The number of people exposed to recent flooding occurred in many Central European countries highlights the importance of assessing flood hazards. During the extensive June 2013 floods in Germany, for example, more than 80,000 people in eight federal states had to be evacuated (Thieken et al., 2016). The vulnerability of settlements calls for an improved flood forecasting, which includes underlying uncertainties and impacts.

In this study, we present a novel methodology that uses a multi-model combination of two-dimensional (2D) hydrodynamic (HD) models to assess the impact of flooding based on water depth hazards. These hazards can be evaluated for key urban features, such as buildings, roads, bridges and green spaces (Leandro et al., 2016). This study focusses in particular on buildings. Furthermore, the hazard maps serve a variety of purposes, e.g. flood impact assessment, spatial planning, early warning and emergency planning (Hammond et al., 2013) for target users. For this paper, the users consist of a group of decision-makers, such as the Bavarian Water Authorities and disaster relief organizations in Germany, the Federal Agency for Technical Relief or the German Red Cross.

In deterministic flood forecasting, the predictions of forecasting models, precipitation forecasts, hydrological models and HD models, are used to generate flood hazard maps. These maps form the basis of flood risk management and are utilised to assess the impact of floods (Schanze, 2006; Hagemeier-Klose and Wagner, 2009). Although advances are continually being made in real-time forecasting, they are still inherently uncertain (Meyer et al., 2009; Bates et. al., 2014; Beven et al., 2018). The decision-making process based on uncertain predictions can have a huge economic impact and possibly lead to life and death situations (Leedal et al., 2010). Thus, a thorough assessment is required of the extent to which uncertainties affects the predictions of flood hazards. In addition, forecasting predictions that inform policy or risk management decisions should include major sources of uncertainty and communicate them coherently (Todini, 2017).

Researchers have addressed various sources of uncertainties in flood modelling, such as precipitation measurements, spatial interpolation of the precipitation, model parameter, model structure (Nester et al., 2012; Leandro et al., 2013), discharge data, measured discharge and uncertainty estimation techniques (Dotto et al., 2012). Although

uncertainties arising from precipitation and HD models are significant, the generation of discharges using a hydrological model is considered as one of the most uncertain steps in flood forecasting (Di Baldassarre and Montanari, 2009). Substantial research has been dedicated to the field of discharge forecasting and reducing uncertainties by using methods, such as Generalized Likelihood Uncertainty Estimation (Beven and Binley, 2014), Global Sensitivity Analyses (Pappenberger et al., 2008) and the Shuffled Complex Evolution Metropolis Algorithm (Dotto et al., 2012). To find the appropriate method, Pappenberger et al. (2006) have provided a decision tree that helps users select a suitable method for a given solution. Furthermore, in a recent study Boelee et al. (2018) reviewed uncertainty quantification methods to provide practitioners with an overview of ensemble modelling techniques. An overview of existing ensemble forecasts in operational use can be found in Cloke and Pappenberger (2009) and Todini (2017). Most notably, in the federal states of Rhineland-Palatinate (Bartels et al., 2017) and Bavaria (Laurent et al., 2010) discharge ensembles is generated using the COSMO-DE-EPS precipitation ensemble as input to a distributed hydrological model LARSIM (Large Area Runoff Simulation Model). These and similar developments offer a potential framework for quantifying uncertainties. A challenging issue in natural hazards, however, remains the effective communication of the quantified uncertainties to decision-makers (Doyle et al., 2019). Researchers have questioned how uncertainties should be communicated to reduce the risk of wrong or inappropriate decisions (Bruen et al., 2010; Todini, 2017).

In operational flood forecasting, hazard maps are provided in the form of exceedance probability scenarios and generally, only one scenario is considered for emergency planning. Normally, a 50% exceedance probability scenario (or median) is expected to be close to the deterministic *best-model* approach (Di Baldassarre et al., 2010). In other examples (Beven et al., 2014; Beven et al., 2015; Disse et al., 2018), model results of various exceedance probabilities are provided on separate or combined maps. Kolen et al. (2019) stated that there is a need for new methodologies that employ a multi-model combination approach by including several scenarios for improving decision making. A multi-model combination is based on the results of several models and creates a more robust forecasting system with a better representation of uncertainties (Kauffeldt et al., 2016). Although the multi-model approach has been used widely in the field of discharge forecasting (Shamseldin et al., 1997; See and Openshaw, 2000; Oudin et al., 2006; Weigel et al., 2008), the approach is not commonly used in the field of real-time flood hazard forecasting. The high-computational time required by the HD models restricts the use of such an approach in real-time forecasting. However, the use of a simple model structure and/or high-performance computing makes it possible to simulate HD models

in real-time; thus, making it feasible to use multi-model combination approaches. Zarzar et al. (2018) have used a multi-model ensemble framework consisting of hydro-metrological and hydraulic models to visualise flood inundation uncertainties. To the best of our knowledge, this combination approach has yet not been used to assess the impact of flooding.

We develop a methodology for obtaining a multi-model combination as an effective alternative to traditional *best-model* approach for producing detailed hazard maps, which are termed as *building hazard maps*. This term can be defined as a map that highlights buildings that are affected by or are vulnerable to flooding with differentiated exceedance probabilities of flood inundation extents as a function of the building use. The maps help prevent serious damage to buildings and aid in evacuation planning in the case of flooding. The methodology is applied for the flood event of January 2011 in the city of Kulmbach, Germany.

7.2. Methodology
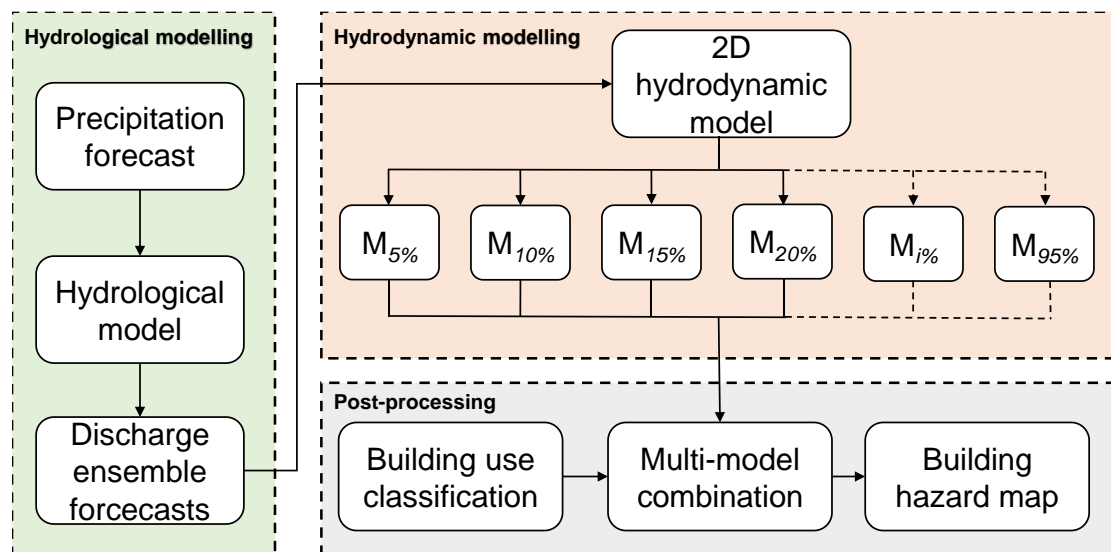
Figure 7-1. Schematic view of the methodology used to generate building hazard maps. The major components consist of the operational hydrological ensemble forecasts (Beg et al., 2018), the hydrodynamic model and post-processing that includes the multi-model ensemble combination. $M_{x\%}$ denotes the HD model results generated using x% confidence interval discharge.

The framework to generate building hazard maps in real-time (as shown in Figure 7-1) consists of three components: (1) Hydrological modelling – discharge ensemble forecasts were produced using forecasted precipitation; (2) HD modelling – the water depths were simulated using a pre-calibrated 2D HD model; (3) Post-processing of the model results – a multi-model combination was used to produce flood hazard maps

based on a classification of buildings. The framework was tested for the flood event of January 2011 in the city of Kulmbach, Germany. The first two components of the framework were developed in previous studies (Beg et al., 2018; Bhola et al., 2018a, Bhola et al., 2018b). The particular focus of this study is on the development of the framework in the post-processing component. For the sake of clarity, each component is described in detail in chronological order.

7.2.1. Hydrological modelling

7.2.1.1. Hydrological model - LARSIM

The conceptual hydrological model LARSIM (Large Area Runoff Simulation Model) was used to study the hydrology of the model area and to generate discharge forecasts. In the model, the hydrological processes are simulated in a series of subarea elements connected by flood routing elements in a pre-determined sequence. LARSIM simulates the hydrologic processes for one element for a defined period and passes the resulting output hydrographs information to the next element (Figure 7-2). The model structure can be both grid-based or based on hydrologic sub-catchments. The model uses a soil module with storage capacities in considering infiltration, evapotranspiration and runoff generation. The discharge generation consists of three components: runoff generation, runoff concentration and river component. In addition to simulating hydrological processes, LARSIM is most suitable in operational flood forecasting (Demuth and Rademacher, 2016). It deals with the gaps in hydrometeorological input data and allows for the correction/manipulation of numeric weather forecasts (e.g. external forcing parameters). Furthermore, the model automatizes processes for the assimilation of hydrological data, which is crucial in flood forecasting (Luce et al., 2006; Haag and Bremicker, 2013).

For this study, a pre-setup model for the study area was provided by the Bavarian Environment Agency and this model is operationally used in the Flood Forecasting Centre for the river Main (Laurent et al., 2010). The model uses a grid-based structure with a resolution of 1 km^2 and a temporal resolution of 1 hour. This LARSIM model considers a soil module with storage capacities in considering the water balance, which consists of three parts: upper, middle and lower soil storages that contribute to the discharge components, modelled as a linear storage system. The model includes 34 parameters that allow the modelling of different processes, such as direct discharge, interflow and groundwater flow. A complete description of calibration parameters is not the scope of this study and has been elaborated on by Ludwig and Bremicker (2006) or Haag et al. (2016). Nevertheless, Table 2-1 presents is provided for a comprehensive

description of important parameters along with eight most sensitive parameters identified in Beg et al. (2018), which were considered in generating the discharge ensemble forecasts.
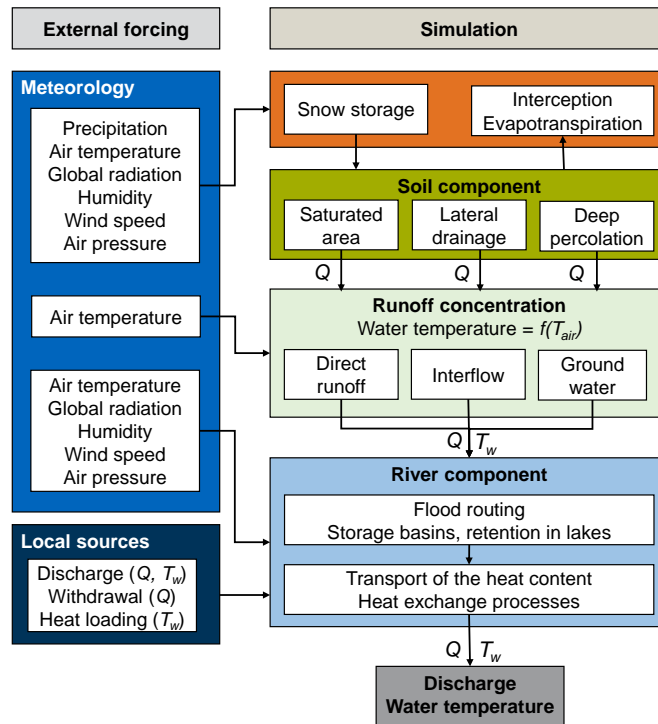
Figure 7-2. LARSIM water balance model. Source based on Ludwig and Bremicker (2006).

7.2.1.2. Discharge ensemble forecasts

The winter flood event of January 2011 was hindcasted to test the framework. The event was one of the largest in terms of its magnitude and corresponds to a discharge of 100-year return period at gauge Kauerndorf (river Schorgast) and 10-year return period at gauge Ködnitz (river White Main). Intense rainfall and snow melting in the Fichtel mountains caused floods in several rivers of Upper Franconia. Within five days, two peak discharges were recorded. The first one occurred on 9th January 2011, and the second peak measured five days later (on 14th January 2011) caused even higher discharges and water levels. The maximum discharge of 92.5 m³/s was recorded at gauge Kauerndorf and 75.3 m³/s at gauge Ködnitz (Table 7-3).

To automatize the generation of forecasts, a tool *FloodEvac* was developed in MATLAB[®] R2018a (Disse et al., 2018). The tool considers model input and model parameter uncertainty in simulating flood scenario combinations. The tool generates rainfall spatial distributions using sequential conditional geospatial simulations and model parameter uncertainty using Monte-Carlo sampling. The uncertainties in the discharge hydrographs

were quantified in Beg et al. (2018) using this FloodEvac tool. In their study, the forecast was performed using 50 ensemble members. Parameter uncertainty module was used to generate 50 different parameter sets (for eight sensitive parameters). In addition, geostatistical simulation for rainfall was implemented using two different R-packages, namely *gstat* and *RandomFields*. The rainfall data was available at hourly interval at 50 gauges in the catchment. Each forecast was simulated for 61 hours: 49 hours of observed hourly rainfall and 12 hours of forecast rainfall data. To hindcast the event of January 2011, 10 different raster dataset of rainfall uncertainty were generated for the catchment. The 50 parameter sets were combined with the 10 rainfall uncertainty cases, linking one rainfall scenario with every 5-parameter sets in a sequential order, thus, making 50 sets of hydrological models for the Upper Main catchment. These 50 models were then simulated, and the results of discharge ensembles were stored.

(a) Ködnitz   (b) Kauerndorf
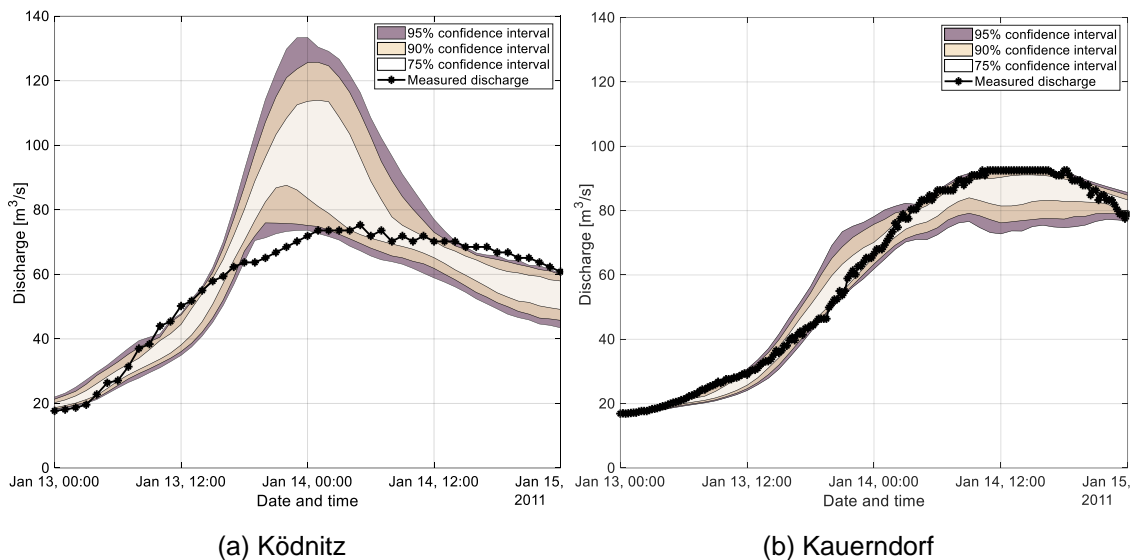
Figure 7-3. Hindcasted flood event of January 2011: measured discharge hydrograph along with 95%, 90% and 75% confidence interval discharges for gauges a) Ködnitz and b) Kauerndorf (Data from Beg et al., 2018).

Figure 7-3 shows the confidence intervals of 75%, 90% and 95% for the January 2011 flood event at two gauging stations upstream of the city, Ködnitz and Kauerndorf. Uncertainty bands are much wider at gauge Ködnitz (Figure 7-3a) than at gauge Kauerndorf, which suggests that the model parameters are more sensitive in the catchment of White Main than Schorgast. In addition, the peak of the measured discharge at gauge Ködnitz was well over-predicted, which suggests that the uncertainty of the discharges is higher in the catchment of White Main than Schorgast. While the peak of the measured discharge at Kauerndorf is very well predicted, the one at the gauge Ködnitz is over-predicted. Nevertheless, it can be seen from Figure 7-3 that ensemble of these 50 members could effectively bracket the observed discharge data.

7.2.2. **Hydrodynamic modelling**

HEC-RAS was used as the 2D HD model to quantify uncertainties in flood inundation. It is a non-commercial hydrodynamic model developed by the U.S. Army Corps of Engineers and has been used widely for various flood inundation applications (Moya Quiroga et al., 2016; Patel et al., 2017). The implicit method allows for larger computational time steps compared to an explicit method. HEC-RAS solves either 2D Saint Venant or 2D diffusion-wave equations. The latter allows faster calculation and has greater stability due to its complex numerical schemes (Martins et al., 2017). Due to these advantages and suitability for use in real-time inundation forecast (Henonin et al., 2013), we have used the diffusive-wave model that was previously set-up, calibrated and validated in Bhola et al. (2018a) and Bhola et al. (2018b). For the diffusive-wave approximation, it is assumed that the inertial terms are less than the gravity, friction, and pressure terms. Flow movement is driven by barotropic pressure gradient balanced by bottom friction (Brunner, 2016). The equations of mass and momentum conservation are as follows:

$$\frac{\partial H}{\partial t} + \frac{\partial (hu)}{\partial x} + \frac{\partial (hv)}{\partial y} + q = 0 \qquad (1)$$

$$g\frac{\partial H}{\partial x} + c_f u = 0 \qquad (2)$$

$$g\frac{\partial H}{\partial y} + c_f v = 0 \qquad (3)$$

$$c_f = \frac{g|V|}{M^2 R^{4/3}} \qquad (4)$$

Where H is the surface elevation (m); h is the water depth (m); u and v are the velocity components in the x- and y- direction respectively (ms^{-1}); q is a source/sink term; g is the gravitational acceleration (ms^{-2}); cf is the bottom friction coefficient (s^{-1}); R is the hydraulic radius (m); |V| is the magnitude of the velocity vector (ms^{-1}); and M is the inverse of the Manning's n (m$^{(1/3)}$s^{-1}).

Table 4-2 and Table 4-3 summarise the model properties, such as the model size and mesh size, and model roughness in the domain. The model parameter consists of roughness coefficient Manning's M for five land use classes. Sensitivity analysis of the model was performed using one thousand uniformly distributed model parameter sets for the flood event of 2011.

Although uncertainties arise in the HD modelling, we have considered discharges in hydrological modelling as the sole source of uncertainties in this paper as we have assumed them to be more significant. Various HD simulations were conducted based on confidence intervals of the discharges (Figure 7-3) as upstream boundary conditions at river gauges Ködnitz and Kauerndorf.

7.2.3. Post-processing

7.2.3.1 Building use classification

In this study, we have considered only buildings as urban features to access the flood impact and in preparation of flood hazard maps. Building damage potential is required for a variety of flood mitigation planning activities including flood damage assessment, multi-hazard analyses and emergency measures (Shultz, 2017).

The shape and use of the buildings were provided by the Bavarian Ministry of the Interior, for Building and Transport (Figure 7-4). They were classified into four classes based on their function following the recommendation of the German standard for risk management in urban areas in the case of flash floods (Krieger et al., 2017). According to this standard, building use is one of the important criteria for assessing the damage potential of a building. In this study, four damage potential classes for each building use were taken into consideration as presented in Table 7-1.

The damage potential varies from *low* to *very high* based on the building use, for example, residential buildings with a basement, industries and schools need special protection and thus were rated with a correspondingly high damage potential (class III). In addition, nursery, hospitals as well as low-lying facilities, such as traffic underpasses, driveways to underground garages and other entrances require greater protection and are thus categorised as having the highest damage potential (class IV). Residential buildings and retail businesses were classified as having moderate damage potential (class II), and gardens and parks relatively low damage potential (class I). Figure 7-4 shows the city centre, where buildings were classified according to Table 7-1. It can be seen that most of the buildings belong to class III as the area is industrial. There are a total of 2695 buildings in Figure 7-4 of which 1, 20, 958 and 1716 buildings were classified in classes I, II, III and IV respectively.

Table 7-1. Building use classification based on the guidelines of Krieger et al. (2017)

Class	Building use	Damage potential
I	Garden buildings Parks / green areas	low
II	Residential building without a basement Retail / small business	moderate
III	Residential building with basement (inhabited) Industry / Trade School / College	high
IV	Nursery / hospital / nursing home / emergency services Energy / telecommunications Underground car park Metro access / Subways	very high
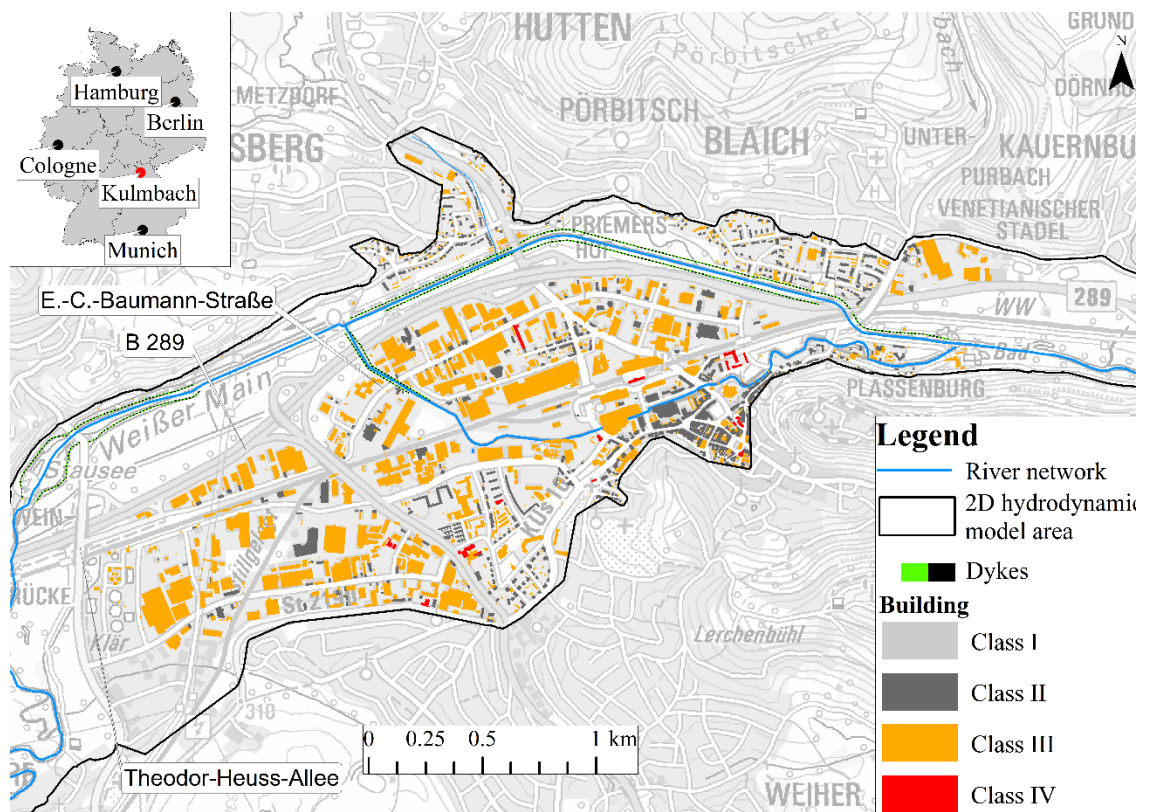
Figure 7-4. City of Kulmbach and building use classification. (Data source: Bavarian Ministry of the Interior, for Building and Transport and Water Management Authority Hof).

7.2.3.2 Hazards classification

In this study, hazard classification was based on the recommendations given in the German standard for risk management in urban flood prevention (Krieger et al., 2017). The classification was based on the estimated water depths of the 2D HD model. Table 7-2 shows the four categories of flooding hazards, which consider water flow in urban areas and vary from *low* to *very high*. It should be noted that in individual cases, the risk

may also arise at lower water depths (<0.10 m) for buildings, such as underground parking and metro stations, which are classified as the building class IV in the previous section.

Table 7-2. Hazard classification used in this study based on water depths. Classification source Krieger et al. (2017)

Hazard class	Flooding hazard	Water depth [m]
1	low	< 0.10 m
2	moderate	0.10 – 0.30 m
3	high	0.30 – 0.50 m
4	very high	> 0.50 m

7.2.3.3 Multi-model combination

The multi-model combination of the 2D HD model results was based on considerations of evacuation planning and gives priority to buildings with higher damage potential. In order to prioritise, it is important to differentiate the impact of water depths on building classes. A certain water depth might have a different impact on a building with higher damage potential. For example, there is more threat for a low water depth in underground metro access that the same water depth to a residential building. Therefore, buildings classified to higher damage potential class relates to model results of a higher confidence interval. Each building class corresponds to a certain discharge confidence interval and the resulting damage potential assessment can be visualised and presented as a building hazard map.
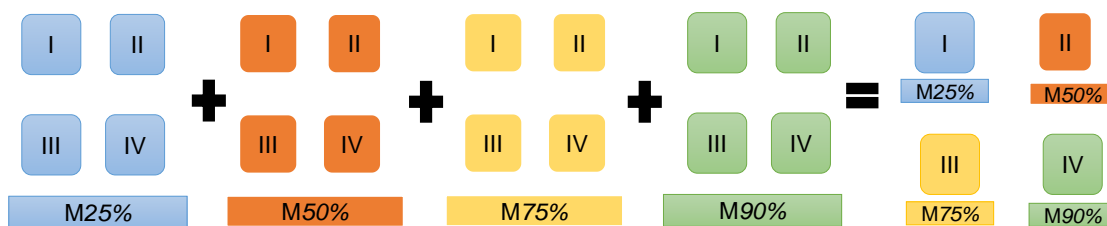
Figure 7-5. An example of a multi-model combination in which the four building classes I, II, III and IV are assigned to the 2D HD model results of 25%, 50%, 75% and 90% respectively.

Figure 7-5 shows an example of a multi-model combination in which the four building classes were assigned four different confidence intervals. The simulation results (water depth in this case) obtained from the HD model with 25%, 50%, 75% and 90% confidence interval discharges were assigned to the building classes I, II, III and IV respectively. The novelty of the multi-model combination approach is that the flood inundation uncertainty is coupled with the building use. As such evacuation planning or

investment planning can take the information of uncertainties in the water depths into consideration.

7.3. Results

In this section, we present the results of five confidence intervals and the performance of the multi-model combination. To assess the methodology, the flood event of January 2011 was used to quantify uncertainties in discharge hydrographs. The forecasts corresponding to 10%, 25%, 50%, 75% and 90% confidence intervals were further used as input boundary conditions to the 2D HD model and water depths were stored. Furthermore, the flood inundation maps and building hazards were then classified.

7.3.1. Flood inundation maps and building hazards

The number of affected buildings in each hazard class for all five HD models are presented in Figure 7-6. As the discharge exceedance probability increases, the number of affected buildings in each hazard class increases. The maximum flood inundation of the five models is presented in Figure 7-7. The figures present both the inundation extent and building hazards based on the classification discussed in section 7.2.3.2.
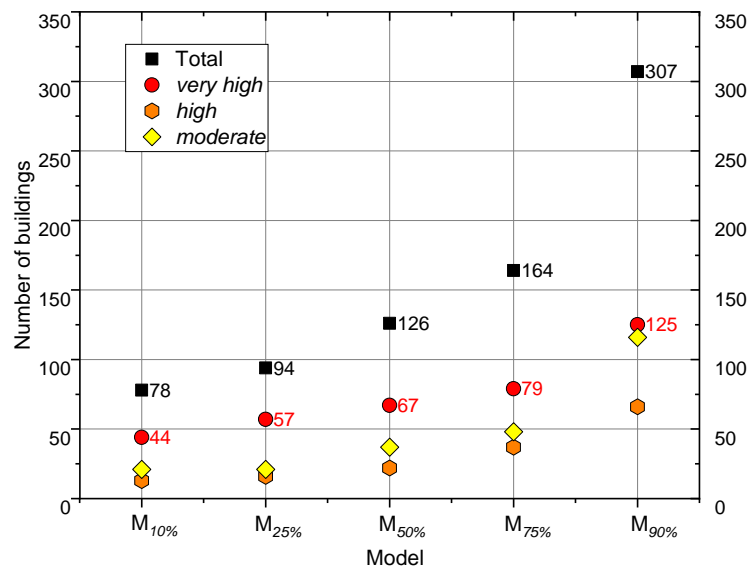
Figure 7-6. Number of affected buildings in each hazard class for 2D HD model results using five confidence interval discharges.

Post-event binary information of the flood extent was collected from newspaper articles and press releases published by the Bavarian Water Authority. The information shows that the dykes were at their full capacity and most of the floodplains and traffic routes were flooded, but no serious damage was reported (Hof, 2011). The streets Theodor-

Heuss-Allee and E.-C.-Baumann-Straße were flooded and some flooding was observed on motorway B289 (see Figure 7-4 for locations).

7.3.2. Multi-model combination

Three combination scenarios based on *high*, *average* and *low* exceedance probability approach were designed for this study and are presented in Table 7-3. The main objective of the combination is to differentiate the impact of water depths on building classes. Therefore, to design the combinations, a high confidence interval was assigned to the buildings with a high damage potential class. The hazard maps for the three scenarios are shown in Figure 7-8.

Table 7-3. Multi-model combination scenarios based on exceedance probability.

Scenario	Exceedance probability	Building class			
		I	II	III	IV
I	High	$M_{10\%}$	$M_{10\%}$	$M_{25\%}$	$M_{50\%}$
II	Average	$M_{10\%}$	$M_{25\%}$	$M_{50\%}$	$M_{75\%}$
III	Low	$M_{25\%}$	$M_{50\%}$	$M_{75\%}$	$M_{90\%}$
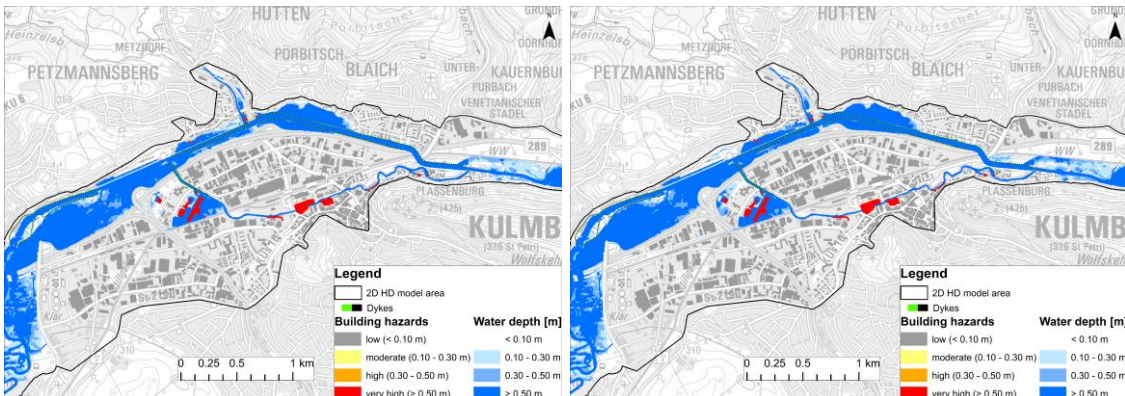
(a) $M_{10\%}$

(b) $M_{25\%}$
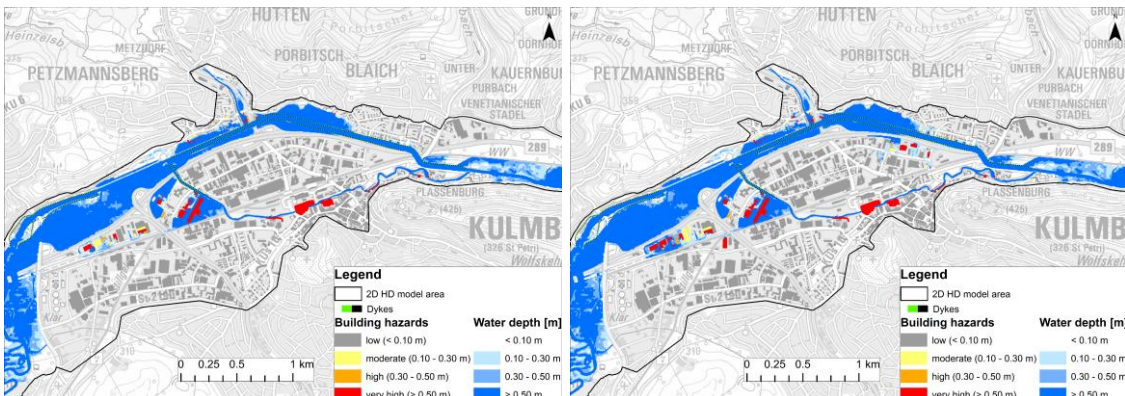
(c) $M_{50\%}$

(d) $M_{75\%}$
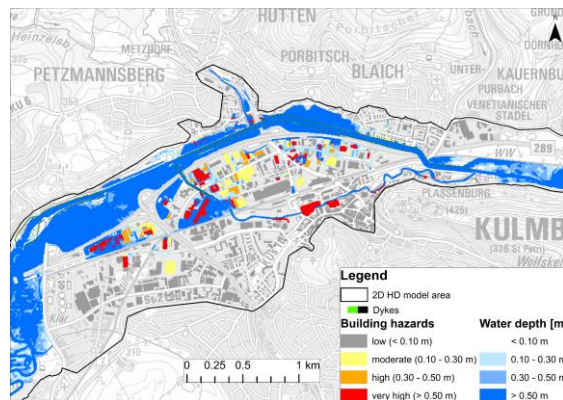
(e) M$_{90\%}$

Figure 7-7. Flood inundation and building hazard maps for five confidence intervals discharge hydrographs.
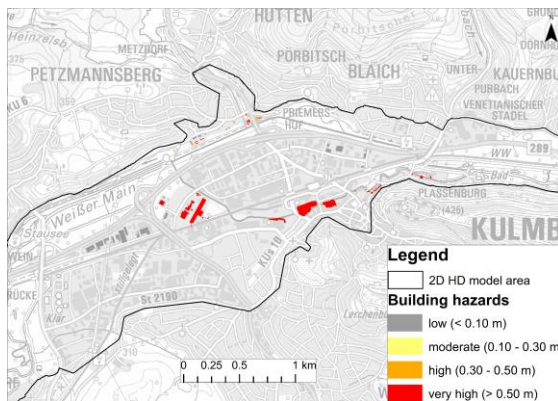
(a) Scenario I
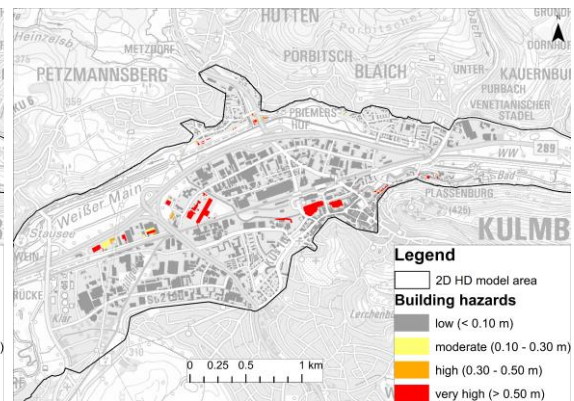
(b) Scenario II
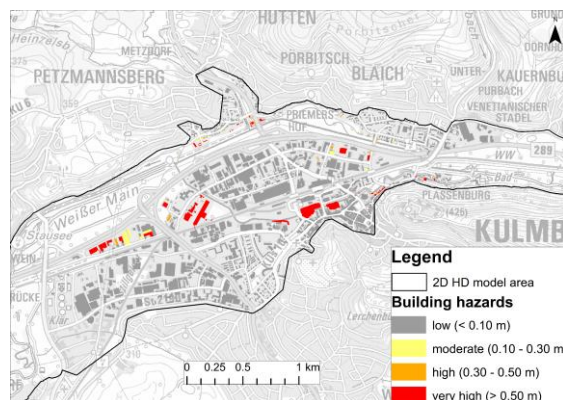
(c) Scenario III

Figure 7-8. Building hazard maps for the three scenarios, the numbers of affected buildings are 84, 107 and 142 respectively. Hazard classification is based on Krieger et al. (2017).

7.4.   Discussion

Prior work in hydrology has demonstrated the effectiveness of multi-model combinations in improving flood forecasts as compared to the *best-model* approach (Weigel et al.,

2008). However, these methodologies were previously limited to discharge ensemble forecasts and were not researched for hazard maps. In this study, we extend the use of multi-model combinations to produce flood hazard maps for buildings depending on their use.

First, the five simulation results are presented in Figure 7-7 as inundation and building hazard maps. It should be noted that few buildings show *very high* hazards due to their proximity to the Mühl canal (Figure 7-7a). Even though there was no over-topping of water from the canal, the buildings near the canal were assigned the highest hazard, starting with a discharge of $M_{10\%}$. Up to a discharge of $M_{50\%}$, no inundation in the city centre was observed as the dykes were not breached. It can be observed in Figure 7-6 that the increment in the number of affected buildings is gradual, especially the buildings belonging to *very high* hazard class. As the peak discharge increases in $M_{75\%}$, the dykes at the B289 road were breached and water entered in the city centre and more buildings were affected. Most damages were observed in $M_{90\%}$ with 307 affected buildings, out of which 125 buildings show *very high* hazard, an increment of 46 from $M_{75\%}$. The affected buildings were located in the city centre (Figure 7-7e), mainly in industrial and commercial areas. Similarly, the streets Theodor-Heuss-Allee and E.-C.-Baumann-Straße were inundated starting from a discharge of $M_{50\%}$.

In operational use, the mean of the discharge ensemble or $M_{50\%}$ would normally have been used as the *best-model*, which according to Figure 7-7c, is in agreement with the post-event information. However, this match might not always be representative, especially in the case of an event of different or higher magnitude, as discussed in Di Baldassarre et al. (2010). They argued that visualising flood hazards as a probability is a more accurate representation as compared to a single *best-model*, which might misrepresent the uncertainty in the modelling process.

With the objective of visualising uncertainties, three scenarios based on exceedance probability were used to combine HD model results and are presented in Figure 7-8. In scenarios I and II, 84 and 107 buildings were affected, which shows that the impact of high and average exceedance probability scenarios was less as compared to $M_{50\%}$ in which a total of 126 buildings were affected, out of which 67 buildings were classified in very *high hazard* class.

Further, as the majority of the buildings were classified in class II and III, the resulting map of a *low* exceedance probability (scenario III) corresponds closely with $M_{50\%}$ and $M_{75\%}$, with 142 affected buildings. In scenario II, 63 buildings were classified in the *very*

high hazard class, which increased to 71 in scenario III. Similarly, 22 buildings belonged to both *moderate* and *high* hazard classes, and shifting to scenario III, the number increased to 33 and 38 in the *moderate* and *high* classes respectively.

(a) Multi-model combination

(b) Building use classification

(c) M$_{50\%}$

(d) Multi-model combination
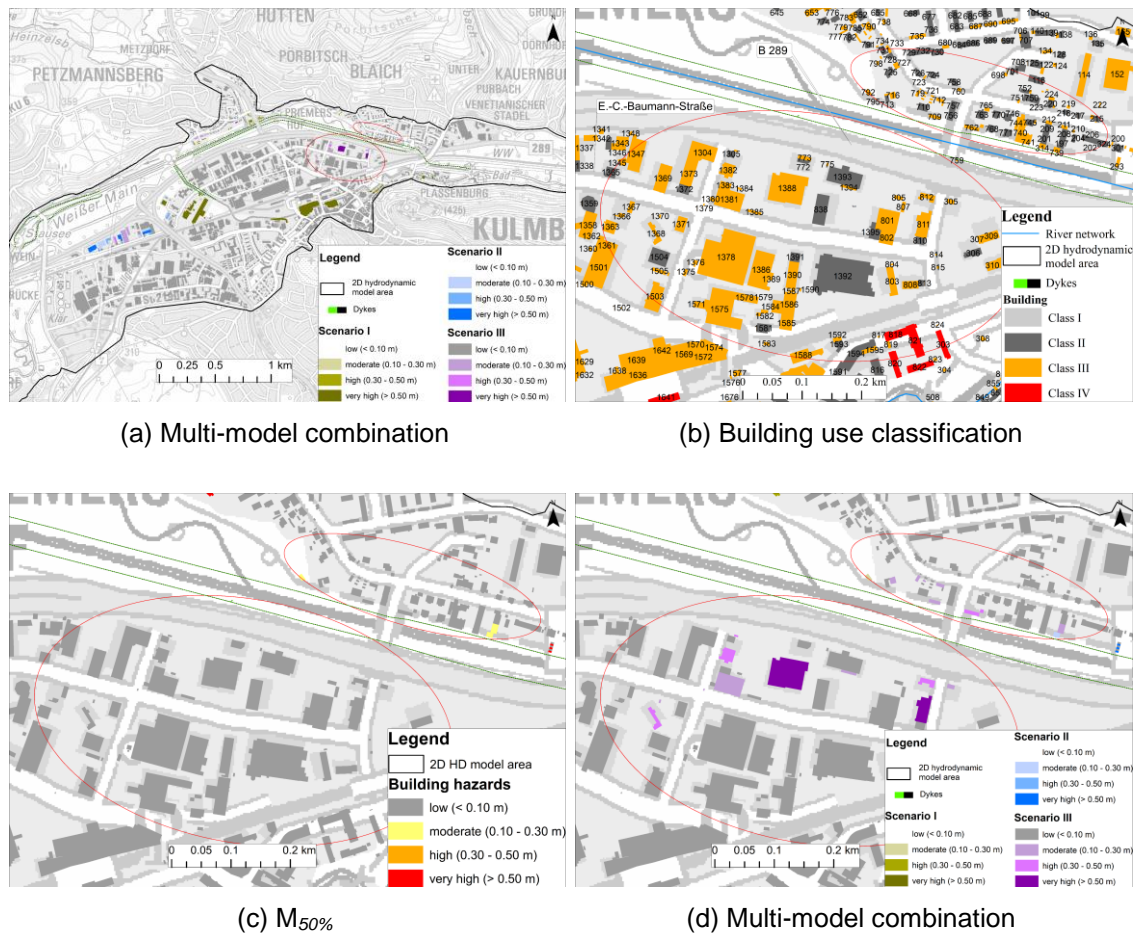
Figure 7-9. Comparison of building hazard maps between *best-model* (M$_{50\%}$) vs. multi-model approach

In Figure 7-9, a comparison is presented between the *best-model* (M$_{50\%}$) and the multi-model approach. The figure presents building hazards resulting from the combination of exceedance probability scenarios and locates 16 buildings that are affected as compared to M$_{50\%}$. The buildings that belong to class III (Figure 7-9b) were assigned the results of M$_{75\%}$, and show a *very high* hazard. Figure 7-9d shows that an adjacent building belonging to class II (ID 1393) was not flooded. This demonstrates that the methodology was implemented accurately and prioritised measures such as flood impact assessment, spatial planning, early warning and emergency planning, according to the damage potential of a building. The prioritisation is important in order to focus on a combination of various evacuation strategies to prevent damage and save lives (Kolen et al., 2010). Hence, decision-makers must be made aware of the impact associated with a lower

probability to improve their planning strategies (Pappenberger and Beven, 2006; Uusitalo et al., 2015).

A potential drawback of the combination is that the hazard classification may shift from *low* to *very high* in two adjacent buildings belonging to different classes. This might confuse evacuation planners by presenting inconsistent information. To tackle this issue, more information and specific guidelines should be provided to them on how to use the maps. In addition, continuous flood inundation maps are hard to obtain, especially at the boundaries of two combinations. There might be a step rise in the water depths while shifting from the results of one model to another. To address this issue, future research should be conducted to provide consistency in interpolation and in combining models (see Zazar et al., 2018). In addition, in order to avoid the confusion, these maps could be forecasted for a regular interval of 3-4 hours.

Overall, the methodology is independent of the choice of models, i.e. hydrological and HD, and is transferable to other study areas. In order to use the methodology in real-time, the run-time of the flood forecasting modelling should be below the flow travel time, which can be ensured by either using a simple model structure (Leandro et al., 2014) and/or high-performance computing (Kuchar et al., 2015). In the absence of such infrastructures or a very large catchment size, HD models can be replaced with alternatives, such as terrain-based models (Zheng et al., 2018) and satellite images (Voigt et al., 2007). In addition, a database of pre-recorded inundation scenarios as shown in Bhola et al. (2018a) can expand the application of this methodology.

Molinari et al. (2014) have stated that a comprehensive uncertainty assessment improves emergency responses by assessing the potential consequences of flood events. Therefore, the target users in the study area would benefit from hazard maps that would enable them to prioritise and coordinate evacuation planning. In addition, the maps should further serve as a tool for flood risk assessment. Furthermore, the methodology can be used for flood mitigation and flood forecast planning in the form of emergency management training, where forecasted hazard scenarios can be presented to the training groups. In addition, by visualising inundation scenarios, potential damage can be estimated for forecasting events.

7.5. Conclusions

In summary, we have presented a new methodology for flood impact assessment using a multi-model combination in the form of *building hazard maps*. These maps inherently

communicate the underlying uncertainties in forecasting models and are ready-to-use for decision-makers in the field of flood risk management. The entire forecasting framework consists of three stages: (i) generation of discharge ensemble forecasts, (ii) 2D HD simulations using the generated forecasts and (iii) hazard maps using multi-model combinations. The framework was applied to the city of Kulmbach and three multi-model combination scenarios were designed based on exceedance probability. The model results of $M_{50\%}$ show a good match with binary information collected after the flood event. The *low* exceedance probability scenario corresponds closely with $M_{50\%}$ and $M_{75\%}$. We expect this multi-model combination to improve the current visualisation techniques in operational flood risk management and evacuation planning.

In this study, we have considered only buildings as a feature; additional urban features, such as bridges (Gebbeken et al., 2016) and roads (Goerigk et al., 2018), should be included in future to extend the methodology. Furthermore, other sources of uncertainty, such as HD model parameters, model structures and measured data should also be incorporated for a comprehensive assessment. In addition, the economic, social and hazardous effects of carrying out an evacuation in the case of false alarm must be considered. Hence, a validation of the combination is crucial to build trust in its prediction in real-time. Further research investigating multi-model combinations and validation in other study areas may be beneficial. A more extensive study on the validation of the combination may be required, possibly by using measuring gauges, post-event survey (as conducted in Thieken et al., 2005), satellite images (as in Triglav-Čekada and Radovan, 2013), and crowd-sourced data (Bhola et al., 2018b).

In future, damage potential classification can further be improved by including additional criteria, such as population density in urban areas. Furthermore, in assessing the damage potential of commercial enterprises, substances or machinery containing elements that are hazardous to water can be included (Krieger et al., 2017). In addition, analysing additional model outputs, such as flow velocity, flood duration and contamination of flood water, should improve the existing forecasting framework by incorporating flood risk assessments.

Chapter

8. Discussion, conclusion and outlook

This dissertation was divided into four key research topics (see also Chapter 1): (i) inundation forecasts validation, (ii) real-time flood inundation forecasting, (iii) uncertainty quantification, and (iv) communication of uncertainties. For each research objective hypotheses were proposed and tested in a series of methodologies (see Chapters 3-7). In this chapter, a summary of the main findings in each chapter is presented and based on the findings a framework is proposed for flood inundation forecasting.

8.1. Inundation forecasts validation

As has been mentioned in Introduction, reliable sources of validation data in urban areas are scarce. Hence, new genres of data sources, such as images and videos from smartphones and CCTV cameras are increasingly used to assess the impact of flooding in urban areas. In Chapter 3, a new methodology was presented that uses this validation data in a flood forecasting framework to improve forecasting and to establish a communication from crowd-source back to the inundation forecasts.

The generation of valuable validation data, such as water levels, flood extent and water quality from the images has been implemented by experts in the field of computer vision (as in Jaehyoung and Hernsoo, 2010; Hies et al., 2012; Narayanan et al., 2014). However, they were previously limited to hindcasting the flood events. Therefore, the focus of Chapter 3, as well as the gap in research, was to discuss how additional validation data can be used in a flood forecasting framework. In the chapter, by applying the hypothesis that the *equifinal model parameters can be used in combination with the validation data*, a framework was designed based on the concept of equifinality in HD model parameters (roughness). The equifinal models not only demonstrated that the multiple model parameter set can give equally good results but also discouraged the use of *best-model* approaches traditionally used in flood inundation forecasting. To test the framework, six equifinal model parameters were identified from a set of 1000 model parameter sets. The optimal model selection (one out of six) for flood forecasting was based on the least error using computer vision at available sites.

Furthermore, another hypothesis tested in Chapter 3 was whether the *accuracy of flood inundation forecasting can be improved using additional validation data* generated with the help of recent advances in technology. This concern, in particular, the segmentation of post-event images with the assistance of a computer vision technique. The results show that with the use of validation data, the number of false alarms, as well as the equifinality in model parameters, can be reduced significantly. The major advantage of

this methodology is its fast run-time and easy applicability in other study areas. In addition, it allows incorporating the information from observations as the flood evolves.

8.2. Real-time flood inundation forecasting

In Chapter 4, the research questions were addressed by developing a framework for real-time flood forecasting based on a pre-recorded database. The framework overcomes the high computational time required by 2D HD models to provide dynamic inundation maps. The framework was validated using four extreme historical hydrological events. A total of 180 convective and advective scenarios were simulated. The forecast duration was 12 hours and a new set of inundation maps was selected every three hours using real-time discharge forecasts as an input.

The hypothesis that the *pre-recorded database of flood maps provides accurate flood inundation maps* was successfully validated in the results. It was concluded that the methodology works for both convective and advective events with a threshold error of 0.25 m in water depths.

A major advantage of the forecasting framework is its fast run-time and its easy application to other study areas, regardless of their size. This methodology can be applied to virtually any catchment size. The 2D HD model run-times are not a limitation since all simulations are prepared beforehand. In addition, the framework is independent of the choice of models. A simpler model structure (diffusive-wave) was used in this case but the framework can easily adapt a full dynamic-wave model since there is no limitation on the computational time.

Major challenges in the operational application of these systems are, in particular: the recompilation of the database in the case of major land use changes, an exhaustive database to cover all possible scenarios, the validation of the query to select the optimal scenario and real-time validation of the forecast. A limitation of this framework was that it could not predict multiple peak events. The outlook of Chapter 4, therefore, stated that additional discharge scenarios based on historical data should be included to strengthen the proposed framework.

As discussed in Chapter 4, the discharge database was enhanced with the objective to simulate multi-peak events and the historical genesis of a flood. Figure 8-1 presents the two discharge hydrographs databases for the gauge Ködnitz and Kauerndorf. Figures 8-1a-b show the synthetic databases as described in Chapter 4 and Figures 8-1c-d present

the updated database based on historical events. To generate the database, all historical flood events recorded between 1978 and 2018 were selected. The selected hydrographs contain a wide variety of shapes and peaks (multi-peak) and durations. Furthermore, the hydrographs were normalised and rescaled to $HQ_{extreme}$ for each gauge. By combining both databases the final number of scenarios was increased from 180 to 360, which made it possible to forecast a wide range of scenarios that include multi-peak events and shapes with historical discharge genesis.
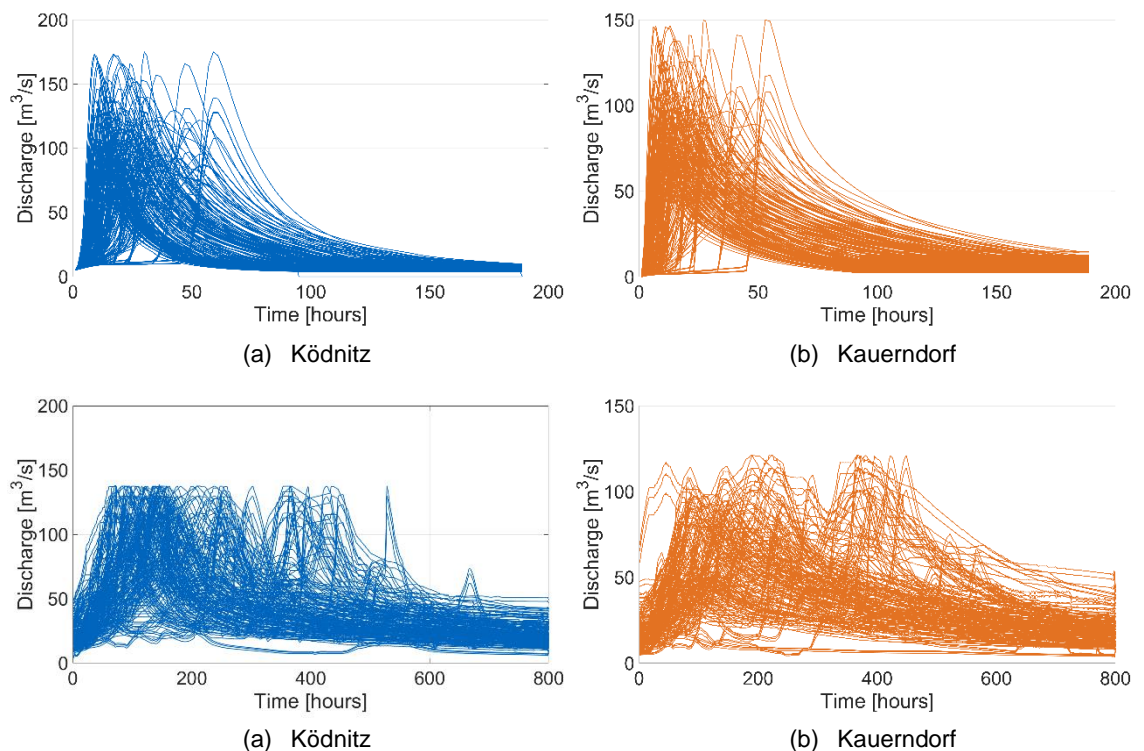
Figure 8-1. Discharge database based on synthetic and historical events. (a-b) Synthetic database and (b-c) Historical event-based database.

In addition, an outlook of Chapter 4 was to extend the method to forecast urban pluvial flooding by including rainfall as an additional input in the query. This component to enhance the existing framework to both fluvial and pluvial flooding has been further developed in Saeed (2019) but was not included in this dissertation. The research was focused on integrating rainfall forecasts as additional input along with the discharge forecasts in order to forecast flood inundation maps for both fluvial and pluvial flooding.

In summary, end-users can use this framework for flood mitigation and flood forecast planning strategies well in advance by visualising inundation scenarios for different magnitudes of floods and associated potential damages for various quantiles of discharge hydrographs.

8.3. Uncertainty quantification

8.3.1. Model parameter

Even though HD models are physically deterministic, they contain numerous uncertainties in model outputs. Hence HD model parameter (roughness) uncertainties were quantified in Chapter 5 and a reduced posterior of model roughness was identified based on measured water levels. The hypothesis tested in Chapter 5 was whether *the measured water levels can be used to reduce uncertainty bounds.* The results showed that the maximum uncertainty in roughness generated an uncertainty bound in the water level of 1.26 m (90% confidence interval) and by constraining roughness, the bounds were reduced as much as 0.92 m.
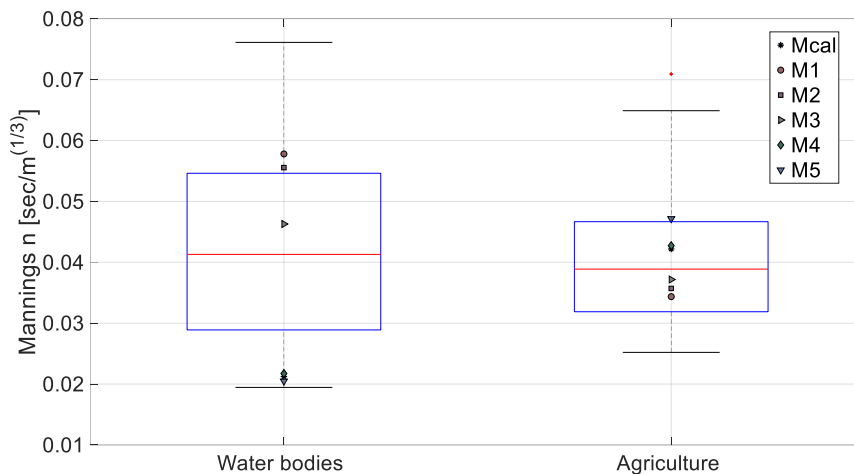
Figure 8-2. Box plot of the posterior Manning's n for land uses water bodies and agriculture along with equifinal model parameters identified in Chapter 3.

One of the main purposes of the uncertainty quantification in model parameters was to find the equifinal model parameter space. In Chapter 3, six equifinal models were identified, which were in the ranges of the posterior model parameters in Chapter 5. Figure 8-2 presents a box plot of reduced posterior parameter ranges and six equifinal model parameters for two sensitive land uses, water bodies and agriculture. Even though different objective functions were used in the chapters, all six agriculture (or flood plains) Manning's n lie within the reduced parameter ranges (25-75%). In the main channel or water bodies, the equifinal parameters lie in the full range. Furthermore, the uncertainty analysis presented in Chapter 5 provides not only a better understanding of the model roughness used in HD models, but also raises awareness of major sources of uncertainties in models. These ranges researched for Manning's n in Chapter 5 can represent a good starting point (prior distribution) for other studies, especially for cities located in the Upper Main catchment.

8.3.2. Model input

In Chapter 6, uncertainties in the hydrological model LARSIM, which is an input to the HD models were first quantified and then the uncertainties were propagated to 2D HD model (Hydro_AS-2D) outputs. Many authors have concluded that this source of uncertainty is one of the most significant ones and needs to be quantified for a forecasting application. Hence, the hypothesis tested in the chapter was whether *the impact of the extent of flooding is significant* if we consider uncertainties in discharges.

Flood inundation maps at an hourly interval were proposed to access the impact of flooding and the uncertainties were visualized using a combined exceedance probability map consisting of HD model results using the discharges of 10%, 50%, and 90% confidence interval. The model results of the inundation extent show that while the floodplains of the 10% and 50% quantiles (below HQ100) were similar, the 90% quantile extends to the city centre over the flood protection measures. This illustrates that the parameter uncertainty of the hydrological model for Kulmbach is a critical factor for the prediction of floodplains and that the official flood inundation forecasting should incorporate the uncertainty of the discharges in decision-making.

Furthermore, a drawback of the methodology used was that the resulting uncertainty ranges were found to be too wide, especially for gauge Ködnitz. To tackle this issue, additional work in discharge forecasting was published or submitted as a non-first author in Beg et al. (2018), Beg et al. (2019) and Leandro et al. (2019), but not included in this dissertation. The research published in these papers focused on reducing uncertainties in real-time discharge forecasting using novel methods namely *Discharge intervals*, *Rising and receding* and *Slope interval.*

8.4. Communication of uncertainties

With the objective to improve current visualisation methods in operational flood risk management, a novel methodology for flood impact assessment using a multi-model combination in the form of building hazard maps was presented in Chapter 7. The hazard maps inherently communicate the underlying uncertainties in forecasting models and are ready-to-use for decision-makers in the field of flood risk management.

The quantified uncertainties in discharge forecasting are used as boundary conditions in the 2D HD model. Various HD simulations were conducted based on confidence intervals of the discharge forecasts. The methodology combines HD model results to

assess the impact of flooding based on flood hazards. These hazards are evaluated for buildings as the urban feature.

In the simulations results, the best-model or the median confidence interval (M50%) shows a good match with the binary information collected after the flood event. However, this model might not always be representative, especially in the case of an event of different or higher magnitude. To address this gap, three multi-model combination scenarios were designed based on differentiated exceedance probabilities, which prioritise buildings based on their damage potential. This prioritisation is important in order to differentiate the impact of flooding on building use, such as residential, industrial, hospitals and subways.

In this chapter, the hypotheses were tested whether *the multi-model combination of 2D HD models approach can communicate uncertainties to decision-makers* and whether *the multi-model based approach can outperform a single best-model approach in flood inundation forecasting*. The results demonstrate that the methodology prioritises measures, such as flood impact assessment, spatial planning, early warning and emergency planning, according to the damage potential of a building. This prioritisation is important to focus on a combination of various evacuation strategies to prevent damage and to save lives. Hence, decision-makers must be made aware of the impact associated with a lower probability flooding scenario to improve their planning strategies. Furthermore, the major advantage of the proposed methodology is that it is independent of the choice of models, i.e. hydrological and HD models, and is transferable to other study areas. It is concluded that the multi-model combination presented will improve current visualisation techniques in operational flood risk management and evacuation planning.

8.5. Framework for flood inundation forecasting including uncertainties

As stated in the review in Introduction, almost none of the flood management agencies perform real-time flood inundation mapping due to the fact that the unsteady HD models are data-rich and computationally too expensive to run in real-time. To address this gap, a framework is proposed based on the methodologies developed in this dissertation. The framework of real-time flood forecasting is presented in Figure 8-3. It consists of five components:

(i)   Pre-processing: the appropriate HD model (dimensionality and structure) is selected based on the purpose and scale of the modelling

(ii)   Hydrological modelling: discharge ensemble forecasts are simulated using a hydrological model. If the peak discharge is greater than a 1-year return period (RP), the coupled hydrological-HD forecasts are activated, and discharges are forwarded to the next component

(iii)   Uncertainty analysis: HD models are set up and equifinal model parameters are identified. The uncertainties in discharge forecasting are propagated in the HD model outputs

(iv)   Real-time flood forecasting: based on the model run-time and availability of HPC system, the appropriate forecasting method (online or offline) is selected and flood inundation maps are provided to end-users

(v)   Post-processing: if validation data is available, the optimal map is selected. If this is not the case, then a multi-model combination is used to generate hazard maps, which are provided to end-users. The end-users consist of decision-makers in flood forecasting agencies, disaster relief organizations and experts in the field of flood risk.
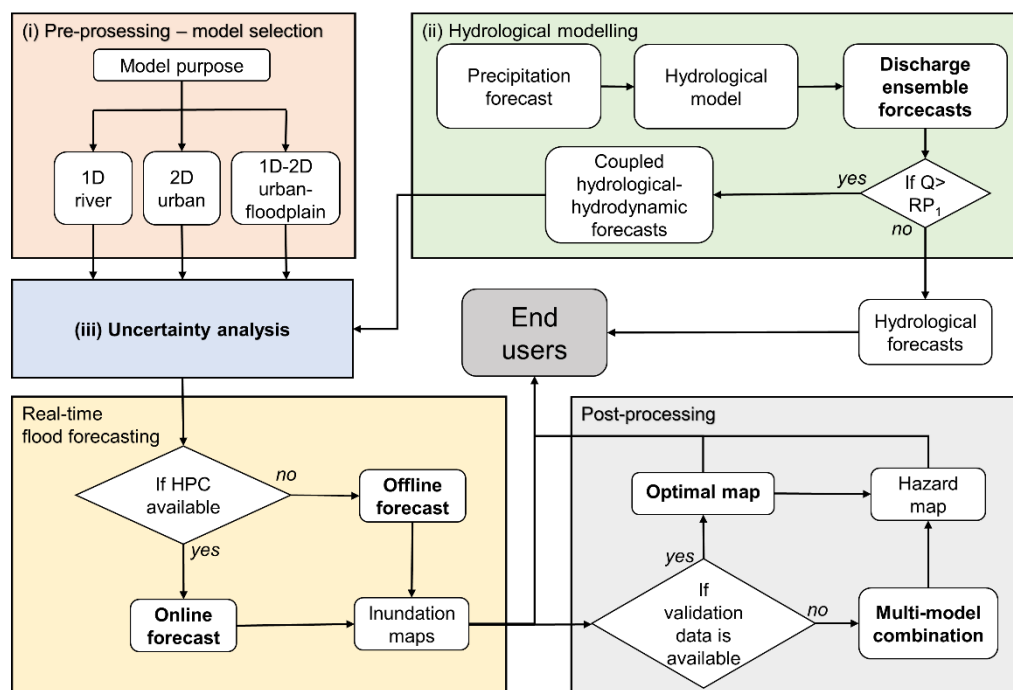
Figure 8-3. Framework for dynamic flood inundation and hazard forecasting in real-time including underlying uncertainties in forecasting models. The components presented as chapters are highlighted in bold. RP$_1$ denotes one-year return period.

The major advantage of the framework is that it is independent of the choice of the forecasting models – hydrological or HD. Thus, making it suitable to use in other study areas. In addition, it can be used both in offline or online mode depending on the run-time of the models and the use of HPC systems. The design of a framework is purely technical, but its implementation needs to be non-technical. The non-technical aspects include planning evacuation measures, ensure early warning, communication systems, and post-event management (Jain et al., 2018). The effectiveness of such a framework largely depends on these non-technical aspects. It is important that both technical and non-technical aspects are integrated for an improved flood forecasting.

The framework components can either be applied on a regional scale or can be ideally integrated into existing flood forecasting framework, such as EFAS, NOAA, FIMAN (Alfieri et al., 2014; Demargne et al., 2014; FIMAN, 2016; Emerton et al., 2016; Jain et al., 2016). The maps then can be used in real-time by the end-users to serve a variety of purposes, e.g. flood impact assessment, spatial planning, early warning and emergency planning.

8.6. Conclusion and outlook

In summary, existing flood forecasting frameworks are in urgent need of enhancement. Previously, research focused mainly on discharge forecasting, but this dissertation stressed the importance of integrating flood inundation, particularly the hydrodynamic component in a flood forecasting framework. Future work should focus on enhancing methodologies to reduce errors in pre-simulated HD scenario systems and to include radar rainfall as an additional input in the query in order to extend the application to forecast urban pluvial flooding. In future, development of HPC forecasting models should be in focus, especially with ever-increasing computational performance in the field of multi-core CPU- and GPU-based systems. These models would enable the simulations of HD models in real-time.

In addition, the significance of both the quantification and communication of uncertainties in flood forecasting has been established in this dissertation. For a comprehensive assessment, other sources of uncertainty, such as discharge measurement error or flood frequency estimations, digital elevation map and measured water level, should also be incorporated and combined. Novel methodologies need to be developed in this regard and should be included in a forecasting framework.

Furthermore, validation data generated using recent advances in technology, such as satellite images, crowd-source data and CCTV footage must be assimilated. This calls for interdisciplinary research approaches including the fields of computer vision and image processing to generate accurate data and in the field of flood risk to develop new methodologies in order to incorporate these data sources to improve the accuracy of forecasting in urban areas. Future work should be focused on automatizing the data extraction process and on image enhancement techniques to deal with the issue of poor lighting conditions in an image, particularly during a storm event. Furthermore, assimilation of validation data should be explored using gauging stations and images recorded from a well-distributed network of CCTV cameras in urban areas. In addition to the developments in validation data, improving the rainfall estimation in urban areas should also be in focus. Recent developments in low-cost sensors, such as NETATMO network (NETATMO, 2019), would substantially improve the quality of input data used for forecasting.

While these challenges need to be addressed in future projects/studies, I conclude this dissertation with the developed framework to forecast dynamic inundation and hazard maps for end-users in real-time. The maps include uncertainties in the modelling process, which can be communicated coherently to end-users. These maps can substantially improve emergency responses by assessing potential consequences of forecasted events and by providing information to the end-users of early warning systems, which allows them to prioritise and coordinate evacuation planning.

9. References

Adams, T. E., and Pagano, T. C.: Flood Forecasting: A Global Perspective, in: Flood Forecasting, edited by: Adams, T. E., and Pagano, T. C., Academic Press, Boston, xxiii-xlix, 2016.

Alfieri, L., Salamon, P., Bianchi, A., Neal, J., Bates, P., and Feyen, L.: Advances in pan-European flood hazard mapping, Hydrol. Process., 28, 4067-4077, 10.1002/hyp.9947, 2014.

Alfieri, L., Feyen, L., Salamon, P., Thielen, J., Bianchi, A., Dottori, F., and Burek, P.: Modelling the socio-economic impact of river floods in Europe, Nat. Hazards Earth Syst. Sci., 16, 1401-1411, 10.5194/nhess-16-1401-2016, 2016.

Arcement, G. J., and Schneider, V. R.: Guide for selecting Manning's roughness coefficients for natural channels and flood plains, 1989.

Arnbjerg-Nielsen, K., Langeveld, J., and Marsalek, J.: Urban drainage research and planning. Quo vadis?, in: Global Trends & Challenges in Water Science, Research and Management, IWA Publishing, 133-135, 2016.

Aronica, G., Hankin, B., and Beven, K.: Uncertainty and equifinality in calibrating distributed roughness coefficients in a flood propagation model with limited data, Adv. Water Resour., 22, 349-365, http://dx.doi.org/10.1016/S0309-1708(98)00017-7, 1998.

Bach, P. M., Rauch, W., Mikkelsen, P. S., McCarthy, D. T., and Deletic, A.: A critical review of integrated urban water modelling – Urban drainage and beyond, Environ. Modell. Softw., 54, 88-107, 10.1016/j.envsoft.2013.12.018, 2014.

Bales, J. D., and Wagner, C. R.: Sources of uncertainty in flood inundation maps, J. Flood Risk. Manag., 2, 139-147, 10.1111/j.1753-318X.2009.01029.x, 2009.

Bartels, J., Bliefernicht, J., Seidel, J., Bárdossy, A., Kunstmann, H., Johst, M., and Demuth, N.: Bewertung von Ensemble-Abflussvorhersagen für die operationelle Hochwasserwarnung, Hydrol. Wasserbewirtsch., 61, 297-310, 10.5675/HyWa_2017,5_1 2017.

Bates, P. D., and De Roo, A. P. J.: A simple raster-based model for flood inundation simulation, J. Hydrol., 236, 54-77, https://doi.org/10.1016/S0022-1694(00)00278-X, 2000.

Bates, P. D.: Integrating remote sensing data with flood inundation models: how far have we got?, Hydrol. Process., 26, 2515-2521, 10.1002/hyp.9374, 2012.

Bates, P. D., Pappenberger, F., and Romanowicz, R. J.: Uncertainty in flood inundation modelling, in: Applied Uncertainty Analysis for Flood Risk Management, edited by: Beven, K., and Hall, J., Imperial College Press, London, UK, 232-269, 2014.

Bauwerke: http://www.wpm-ingenieure.de/include.php?path=sib_bauwerke&pid=21&subid=35, access: 16.03.2018, 2016.

Beg, M. N. A., Leandro, J., Bhola, P. K., Konnerth, I., Amin, K., Koeck, F., Carvalho, R. F., and Disse, M.: Flood forecasting with uncertainty using a fully automated flood model chain: A case study for the city of Kulmbach, 13th International Conference on Hydroinformatics (HIC 2018), Palermo, Italy, 1-5 July 2018, 2018.

Beg, M. N. A., Leandro, J., Bhola, P. K., Konnerth, I., Willems, W., Carvalho, R. F., and Disse, M.: Discharge interval method for uncertain flood forecasts using a flood model chain: city of Kulmbach, J. Hydroinform., https://doi.org/10.2166/hydro.2019.131, 2019.

Bermúdez, M., Neal, J. C., Bates, P. D., Coxon, G., Freer, J. E., Cea, L., and Puertas, J.: Quantifying local rainfall dynamics and uncertain boundary conditions into a nested regional-local flood modeling system, Water Resour. Res., 53, 2770-2785, 10.1002/2016wr019903, 2017.

Bermúdez, M., Ntegeka, V., Wolfs, V., and Willems, P.: Development and comparison of two fast surrogate models for urban pluvial flood simulations, Water Res. Manag., 32, 2801-2015, 10.1007/s11269-018-1959-8, 2018.

References

Beven, K., and Binley, A.: The future of distributed models: Model calibration and uncertainty prediction, Hydrol. Process., 6, 279-298, 10.1002/hyp.3360060305, 1992.

Beven, K.: A manifesto for the equifinality thesis, J. Hydrol., 320, 18-36, https://doi.org/10.1016/j.jhydrol.2005.07.007, 2006.

Beven, K., and Binley, A.: GLUE: 20 years on, Hydrol. Process., 28, 5897-5918, 10.1002/hyp.10082, 2014.

Beven, K., Leedal, D., and McCarthy, S.: Framework for assessing uncertainty in fluvial flood risk mapping, CIRIA, London, UK, 58 pp., 2014.

Beven, K., Lamb, R., Leedal, D., and Hunter, N.: Communicating uncertainty in flood inundation mapping: A case study, Intl. J. River Basin Management, 13, 285-295, 10.1080/15715124.2014.917318, 2015.

Beven, K. J., Almeida, S., Aspinall, W. P., Bates, P. D., Blazkova, S., Borgomeo, E., Freer, J., Goda, K., Hall, J. W., Phillips, J. C., Simpson, M., Smith, P. J., Stephenson, D. B., Wagener, T., Watson, M., and Wilkins, K. L.: Epistemic uncertainties and natural hazard risk assessment – Part 1: A review of different natural hazard areas, Nat. Hazards Earth Syst. Sci., 18, 2741-2768, 10.5194/nhess-18-2741-2018, 2018.

Bhatt, C. M., Rao, G. S., Diwakar, P. G., and Dadhwal, V. K.: Development of flood inundation extent libraries over a range of potential flood levels: a practical framework for quick flood response, Geomatics Nat. Hazards Risk, 8, 384-401, https://doi.org/10.1080/19475705.2016.1220025, 2017.

Bhola, P. K., Disse, M., Kammereck, B., and Haas, S.: Uncertainty quantification in the flood inundation modelling, applying the GLUE methodology, 12th International Conference on Hydroinformatics (HIC 2016): Smart Water for the Future, Incheon, South Korea, 21-26 August 2016, 2016.

Bhola, P. K., Leandro, J., and Disse, M.: Framework for offline flood inundation forecasts for two-dimensional hydrodynamic models, Geosciences, 8, 346, 10.3390/geosciences8090346, 2018a.

Bhola, P. K., Nair, B. B., Leandro, J., Rao, S. N., and Disse, M.: Flood inundation forecasts using validation data generated with the assistance of computer vision, J. Hydroinform., 21, 240-256, 10.2166/hydro.2018.044, 2018b.

Bhola, P. K., Ginting, B. M., Leandro, J., Mundani, R.-P., and Disse, M.: Model parameter uncertainty of a 2D hydrodynamic model for the assessment of disaster resilience, EnviroInfo, Garching, Garching, Germany, 5-7 September 2018, 2018c.

Bhola, P. K., Leandro, J., Videkhina, I., and Disse, M.: Dynamic risk mapping in fluvial flood application using a two-dimensional hydrodynamic model incorporating the model parameter uncertainties, International Conference on "Natural Hazards and Risks in a Changing World", Potsdam. Germany, 2018d.

Bhola, P. K., Leandro, J., Konnerth, I., Amin, K., and Disse, M.: Dynamic flood inundation forecast for the city of Kulmbach using offline two-dimensional hydrodynamic models, 13th International Conference on Hydroinformatics (HIC 2018), Palermo, Italy, 1-5 July 2018, 2018e.

Bhola, P. K., Leandro, J., and Disse, M.: Reducing uncertainty bounds of two-dimensional hydrodynamic model output by constraining model roughness, Nat. Hazards Earth Syst. Sci., 2019, 1-17, https://doi.org/10.5194/nhess-2018-369, 2019a.

Bhola, P. K., Leandro, J., and Disse, M.: Hazard maps with differentiated exceedance probability for flood impact assessment, Nat. Hazards Earth Syst. Sci. Discuss., https://doi.org/10.5194/nhess-2019-158, in review, 2019b.

Boelee, L., Lumbroso, D. M., Samuels, P. G., and Cloke, H. L.: Estimation of uncertainty in flood forecasts—A comparison of methods, J. Flood Risk. Manag., 0, e12516, 10.1111/jfr3.12516, 2018.

Bruen, M., Krahe, P., Zappa, M., Olsson, J., Vehvilainen, B., Kok, K., and Daamen, K.: Visualizing flood forecasting uncertainty: some current European EPS platforms—COST731 working group 3, Atmos. Sci. Lett., 11, 92-99, 10.1002/asl.258, 2010.

Brunner, G. W., United, S., Army, Corps of, E., Institute for Water, R., and Hydrologic Engineering, C.: HEC-RAS river analysis system: Hydraulic reference manual Version 5.0, US Army Corps of Engineers, Institute for Water Resources, Hydrologic Engineering Center, Davis, CA, 2016.

Buahin, C. A., Sangwan, N., Fagan, C., Maidment, D. R., Horsburgh, J. S., Nelson, E. J., Merwade, V., and Rae, C.: Probabilistic Flood Inundation Forecasting Using Rating Curve Libraries, JAWRA Journal of the American Water Resources Association, 53, 300-315, 10.1111/1752-1688.12500, 2017.

Butts, M. B., Payne, J. T., Kristensen, M., and Madsen, H.: An evaluation of the impact of model structure on hydrological modelling uncertainty for streamflow simulation, J. Hydrol., 298, 242-266, https://doi.org/10.1016/j.jhydrol.2004.03.042, 2004.

Chang, L.-C., Amin, M. Z. M., Yang, S.-N., and Chang, F.-J.: Building ANN-Based Regional Multi-Step-Ahead Flood Inundation Forecast Models, Water, 10, 1283, 2018a.

Chang, L.-C., Chang, F.-J., Yang, S.-N., Kao, I.-F., Ku, Y.-Y., Kuo, C.-L., and Amin, I. M. Z. b. M.: Building an Intelligent Hydroinformatics Integration Platform for Regional Flood Inundation Warning Systems, Water, 11, 9, 2018b.

Chen, A. S., Hsu, M. H., Chen, T. S., and Chang, T. J.: An integrated inundation model for highly developed urban areas, Water Sci. Technol., 51, 221-229, 10.2166/wst.2005.0051, 2005.

Chen, A. S., Hsu, M.-H., Teng, W.-H., Huang, C.-J., Yeh, S.-H., and Lien, W.-Y.: Establishing the database of inundation potential in Taiwan, Nat. Haz., 37, 107-132, 10.1007/s11069-005-4659-7, 2006.

Chow, V. T.: Development of uniform flow and its formulas, in: Open-channel hydraulics, McGraw-Hill Book Company, USA, 1959.

Cloke, H. L., and Pappenberger, F.: Ensemble flood forecasting: A review, J. Hydrol., 375, 613-626, 10.1016/j.jhydrol.2009.06.005, 2009.

Coccia, G., and Todini, E.: Recent developments in predictive uncertainty assessment based on the model conditional processor approach, Hydrol. Earth Syst. Sci., 15, 3253-3274, 10.5194/hess-15-3253-2011, 2011.

Dapeng, Y., Jie, Y., and Min, L.: Validating city-scale surface water flood modelling using crowd-sourced data, Environ. Res. Lett., 11, 124011, 2016.

Demargne, J., Wu, L., Regonda, S. K., Brown, J. D., Lee, H., He, M., Seo, D.-J., Hartman, R., Herr, H. D., Fresch, M., Schaake, J., and Zhu, Y.: The Science of NOAA's Operational Hydrologic Ensemble Forecast Service, Bulletin of the American Meteorological Society, 95, 79-98, 10.1175/bams-d-12-00081.1, 2014.

Demuth, N., and Rademacher, S.: Chapter 5 - Flood Forecasting in Germany — Challenges of a Federal Structure and Transboundary Cooperation, in: Flood Forecasting, edited by: Adams, T. E., and Pagano, T. C., Academic Press, Boston, 125-151, 2016.

DHI: MIKE 21 Flow Model & MIKE 21 Flood Screening Tool - Hydrodynamic Module Scientific Documentation, 2017.

Di Baldassarre, G., and Montanari, A.: Uncertainty in river discharge observations: a quantitative analysis, Hydrol. Earth Syst. Sci., 13, 913-921, 10.5194/hess-13-913-2009, 2009.

Di Baldassarre, G., Schumann, G., and Bates, P.: Near real time satellite imagery to support and verify timely flood modelling, Hydrol. Process., 23, 799-803, 10.1002/hyp.7229, 2009.

Di Baldassarre, G., Schumann, G., Bates, P. D., Freer, J. E., and Beven, K. J.: Flood-plain mapping: A critical discussion of deterministic and probabilistic approaches, Hydrolog. Sci. J., 55, 364-376, 10.1080/02626661003683389, 2010.

Dietrich, J., Schumann, A. H., Redetzky, M., Walther, J., Denhard, M., Wang, Y., Pfützner, B., and Büttner, U.: Assessing uncertainties in flood forecasts for decision making: prototype of an operational flood management system integrating ensemble predictions, Nat. Hazards Earth Syst. Sci., 9, 1529-1540, 10.5194/nhess-9-1529-2009, 2009.

Disse, M., Konnerth, I., Bhola, P. K., and Leandro, J.: Unsicherheitsabschätzung für die Berechnung von dynamischen Überschwemmungskarten – Fallstudie Kulmbach, in: Vorsorgender und nachsorgender Hochwasserschutz: Ausgewählte Beiträge aus der Fachzeitschrift WasserWirtschaft Band 2, edited by: Heimerl, S., Springer Fachmedien Wiesbaden, Wiesbaden, 350-357, 2018.

Djordjević, S., Vojinović, Z., Dawson, R., and Savić, D. A.: Uncertainties in flood modelling in urban areas, in: Applied Uncertainty Analysis for Flood Risk Management, edited by: Beven, K., and Hall, J., 297-334, 2014.

Dotto, C. B. S., Mannina, G., Kleidorfer, M., Vezzaro, L., Henrichs, M., McCarthy, D. T., Freni, G., Rauch, W., and Deletic, A.: Comparison of different uncertainty techniques in urban stormwater quantity and quality modelling, Water Res., 46, 2545-2558, 10.1016/j.watres.2012.02.009, 2012.

Dottori, F., Kalas, M., Salamon, P., Bianchi, A., Alfieri, L., and Feyen, L.: An operational procedure for rapid flood risk assessment in Europe, Nat. Hazards Earth Syst. Sci., 17, 1111-1126, 10.5194/nhess-17-1111-2017, 2017.

Doyle, E. E. H., Johnston, D. M., Smith, R., and Paton, D.: Communicating model uncertainty for natural hazards: A qualitative systematic thematic review, Int. J. Disast. Risk Re., 33, 449-476, 10.1016/j.ijdrr.2018.10.023, 2019.

Einfalt, T., Arnbjerg-Nielsen, K., Golz, C., Jensen, N.-E., Quirmbach, M., Vaes, G., and Vieux, B.: Towards a roadmap for use of radar rainfall data in urban drainage, J. Hydrol., 299, 186-202, https://doi.org/10.1016/j.jhydrol.2004.08.004, 2004.

Emerton, R. E., Stephens, E. M., Pappenberger, F., Pagano, T. C., Weerts, A. H., Wood, A. W., Salamon, P., Brown, J. D., Hjerdt, N., Donnelly, C., Baugh, C. A., and Cloke, H. L.: Continental and global scale flood forecasting systems, Wiley Interdisciplinary Reviews: Water, 3, 391-418, 10.1002/wat2.1137, 2016.

European Union: Directive 2007/60/EC of the European Parliament and of the Council of 23 October 2007 on the assessment and management of flood risks, 2007.

Faig, W., and Kahmen, H.: Differential levelling, in: Surveying, edited by: Kahmen, H., and Faig, W., De Gruyter, Berlin, Germany, 321–386, 2012.

FIMAN: NC FLOOD INUNDATION MAPPING AND ALERT NETWORK (FIMAN) - North Carolina Emergency Management's Rain, Stream, Weather and Flooding Risk Information Website: https://fiman.nc.gov/About.aspx, access: 27.03.2019, 2016.

FloodArea: ArcGIS-Erweiterung zur Berechnung von Überschwemmungsbereichen - ANWENDERHANDBUCH Version 10.3, geomer GmbH, 2017.

Früh-Müller, A., Wegmann, M., and Koellner, T.: Flood exposure and settlement expansion since pre-industrial times in 1850 until 2011 in north Bavaria, Germany, Regional Environmental Change, 15, 183-193, 10.1007/s10113-014-0633-9, 2015.

Gebbeken, N., Videkhina, I., Pfeiffer, E., Garsch, M., and Rüdiger, L.: Risikobewertung und Schutz von baulichen Infrastrukturen bei Hochwassergefahr, Bautechnik, 93, 199-213, 10.1002/bate.201600003, 2016.

Geetha, M., Manoj, M., Sarika, A. S., Mohan, M., and Rao, S. N.: Detection and estimation of the extent of flood from crowd sourced images, 2017 International Conference on Communication and Signal Processing (ICCSP), 2017, 0603-0608,

Gerlinger, K., Bremicker, M., and Haag, I.: Echtzeit-Vorhersagen des Abflusses mit dem Wasserhaushaltsmodell LARSIM am Beispiel des Neckargebiets, in: Klima, Wasser, Flussgebietsmanagement im Lichte der Flut, Forum für Hydrologie und Wasserbewirtschaftung, 2003, 163-166,

Germann, U., Berenguer, M., Sempere-Torres, D., and Zappa, M.: REAL—Ensemble radar precipitation estimation for hydrology in a mountainous region, Q. J. Roy. Meteor. Soc., 135, 445-456, 10.1002/qj.375, 2009.

Ginting, B. M., Bhola, P. K., Ertl, C., Mundani, R.-P., Disse, M., and Rank, E.: Hybrid-parallel simulations and visualisations of real flood and tsunami events using unstructured meshes on high-performance cluster systems, SimHydro 2019, Sophia Antipolis, France, 12-14 June 2019, 2019.

Ginting, B. M., and Mundani, R.-P.: Parallel Flood Simulations for Wet–Dry Problems Using Dynamic Load Balancing Concept, Journal of Computing in Civil Engineering, 33, 04019013, doi:10.1061/(ASCE)CP.1943-5487.0000823, 2019.

GKD, Gewässerkundlicher Dienst Bayern: https://www.gkd.bayern.de, access: 27.03.2019, 2019.

Goerigk, M., Hamacher, H. W., and Kinscherff, A.: Ranking robustness and its application to evacuation planning, Eur. J. Oper. Res., 264, 837-846, 10.1016/j.ejor.2016.05.037, 2018.

Golding, B. W.: Quantitative precipitation forecasting in the UK, J. Hydrol., 239, 286-305, https://doi.org/10.1016/S0022-1694(00)00354-1, 2000.

Gopalakrishnan, U., N, R., Rangan, P. V., and Hariharan, B.: Re-orchestration of remote teaching environment in eLearning, Proceedings of the 18th International Conference on Enterprise Information Systems, Rome, Italy, 2016.

Haag, I., and Bremicker, M.: Möglichkeiten und Grenzen der Schneesimulation mit dem Hochwasservorhersagemodell LARSIM, Forum für Hydrologie und Wasserbewirtschaftung, 33, 47-58, 2013.

Haag, I., Johst, M., Sieber, A., and Bremicker, M.: Guideline for the calibration of LARSIM water balance models for operational application in flood forecasting, LARSIM Entwicklergemeinschaft – Hochwasserzentralen LUBW, BLfU, LfU RP, HLNUG, BAFU, 2016.

Hagemeier-Klose, M., and Wagner, K.: Evaluation of flood hazard maps in print and web mapping services as information tools in flood risk communication, Nat. Hazards Earth Syst. Sci., 9, 563-574, 10.5194/nhess-9-563-2009, 2009.

Hall, J., and Solomatine, D.: A framework for uncertainty analysis in flood risk management decisions, Intl. J. River Basin Management, 6, 85-98, 10.1080/15715124.2008.9635339, 2008.

Hall, J. W., Tarantola, S., Bates, P. D., and Horritt, M. S.: Distributed sensitivity analysis of flood inundation model calibration, J. Hydraul. Eng., 131, 117-126, doi:10.1061/(ASCE)0733-9429(2005)131:2(117), 2005.

Hammond, M. J., Chen, A. S., Djordjevi, S., Butler, D., and Mark, O.: Urban flood impact assessment: A state-of-the-art review, Urban Water J., 12, 14-29, 10.1080/1573062X.2013.857421, 2013.

Henonin, J., Russo, B., Mark, O., and Gourbesville, P.: Real-time urban flood forecasting and modelling – a state of the art, J. Hydroinform., 15, 717-736, 10.2166/hydro.2013.132, 2013.

Hervouet, J.-M.: A high resolution 2D dam-break model using parallelization, Hydrol. Process., 14, 2211-2230, 10.1002/1099-1085(200009)14:13<2211::Aid-hyp24>3.0.Co;2-8, 2000.

Hies, T., B. Parasuraman, S., Wang, Y., Duester, R., Eikaas, H., and M. Tan, K.: Enhanced water-level detection by image processing, 10th International Conference on Hydroinformatics (HIC 2012): Understanding changing climate and environment and finding solutions, Hamburg, Germany, 14-18 July 2012, 2012.

HND, Hochwassernachrichtendienst Bayern: https://www.hnd.bayern.de/, access: 27.03.2019, 2019.

Horritt, M. S., and Bates, P. D.: Evaluation of 1D and 2D numerical models for predicting river flood inundation, J. Hydrol., 268, 87-99, http://dx.doi.org/10.1016/S0022-1694(02)00121-X, 2002.

HOPLA Main: Hochwasserrisikomanagement-Plan Einzugsgebiet bayerischer Main: https://www.hopla-main.de/, access: 27.03.2019, 2016.

Hu, X., and Song, L.: Hydrodynamic modeling of flash flood in mountain watersheds based on high-performance GPU computing, Nat. Haz., 91, 567-586, 10.1007/s11069-017-3141-7, 2018.

Hunter, N. M., Bates, P. D., Horritt, M. S., and Wilson, M. D.: Simple spatially-distributed models for predicting flood inundation: A review, Geomorphology, 90, 208-225, https://doi.org/10.1016/j.geomorph.2006.10.021, 2007.

Jaehyoung, Y. U., and Hernsoo, H.: Remote detection and monitoring of a water level using narrow band channel, J. Inf. Sci. Eng., 26, 71-82, 2010.

Jain, S. K., Mani, P., Jain, S. K., Prakash, P., Singh, V. P., Tullos, D., Kumar, S., Agarwal, S. P., and Dimri, A. P.: A Brief review of flood forecasting techniques and their applications, Intl. J. River Basin Management, 16, 329-344, 10.1080/15715124.2017.1411920, 2018.

Jung, Y., and Merwade, V.: Uncertainty quantification in flood inundation mapping using generalized likelihood uncertainty estimate and sensitivity analysis, J. Hydrol. Eng., 17, 507-520, 10.1061/(asce)he.1943-5584.0000476, 2012.

References

Kampf, S., Strobl, B., Hammond, J., Anenberg, A., Etter, S., Martin, C., Puntenney-Desmond, K., Seibert, J., and van Meerveld, I.: Testing the waters: Mobile apps for crowdsourced streamflow data, Eos, 99, 10.1029/2018EO096355, 2018.

Kauffeldt, A., Wetterhall, F., Pappenberger, F., Salamon, P., and Thielen, J.: Technical review of large-scale hydrological models for implementation in operational flood forecasting schemes on continental level, Environ. Modell. Softw., 75, 68-76, 10.1016/j.envsoft.2015.09.009, 2016.

Kolen, B., Kutschera, G., and Helsloot, I.: A comparison between the netherlands and germany of evacuation in case of extreme flooding, 2019.

Komma, J., Reszler, C., Blöschl, G., and Haiden, T.: Ensemble prediction of floods – catchment non-linearity and forecast probabilities, Nat. Hazards Earth Syst. Sci., 7, 431-444, 10.5194/nhess-7-431-2007, 2007.

Krause, P. B., D. P.; Bäse, F.: Comparison of different efficiency criteria for hydrological model assessment, Adv. Geosci., 5, 89-97, https://doi.org/10.5194/adgeo-5-89-2005, 2005.

Krieger, K., Schmitt, T. G., and Illgen, M.: Risikomanagement in der kommunalen überflutungsvorsorge nach DWA-Merkblatt M 119. In: GWF Wasser Abwasser, 6, 2017.

Kuchar, S., Golasowski, M., Vavrik, R., Podhoranyi, M., Sir, B., and Martinovic, J.: Using high performance computing for online flood monitoring and prediction, Int. J. Env. Chem. Ecolog. Geolog. Geophy. Eng., 101, 432 - 437, 10.5281/zenodo.1100428, 2015.

Kutija, V., Bertsch, R., Glenis, V., Alderson, D., Parkin, G., Walsh, C., Robinson, J., and Kilsby, C.: Model validation using crowd-sourced data from a large pluvial flood, 11th International Conference on Hydroinformatics (HIC 2014): Informatics and the Environment: Data and Model Integration in a Heterogeneous Hydro World, New York, 2014,

Laurent, S., Hangen-Brodersen, C., Ehret, U., Meyer, I., Moritz, K., Vogelbacher, A., and Holle, F.-K.: Forecast uncertainties in the operational flood forecasting of the Bavarian Danube catchment, in: Hydrological Processes of the Danube River Basin, edited by: Brilly, M., Springer, Dordrecht, Netherlands, 367-387, 2010.

Leandro, J., Djordjević, S., Chen, A. S., Savić, D. A., and Stanić, M.: Calibration of a 1D/1D urban flood model using 1D/2D model results in the absence of field data, Water Sci. Technol., 64, 1016-1024, 10.2166/wst.2011.467, 2011.

Leandro, J., Leitão, J. P., and de Lima, J. L. M. P.: Quantifying the uncertainty in the Soil Conservation Service flood hydrographs: a case study in the Azores Islands, J. Flood Risk. Manag., 6, 279-288, 10.1111/jfr3.12010, 2013.

Leandro, J., Chen, A. S., and Schumann, A.: A 2D parallel diffusive wave model for floodplain inundation with variable time step (P-DWave), J. Hydrol., 517, 250-259, 10.1016/j.jhydrol.2014.05.020, 2014.

Leandro, J., Schumann, A., and Pfister, A.: A step towards considering the spatial heterogeneity of urban key features in urban hydrology flood modelling, J. Hydrol., 535, 356-365, 10.1016/j.jhydrol.2016.01.060, 2016.

Leandro, J., Konnerth, I., Bhola, P. K., Amin, K., Köck, F., and Disse, M.: FloodEvac Interface zur Hochwassersimulation mit integrierten Unsicherheitsabschätzungen, FloodEvac interface for flood simulation with integrated uncertainty assessments, Tag der Hydrologie, Trier, 23-24 March 2017, 2017.

Leandro, J., Gander, A., Beg, M. N. A., Bhola, P. K., Konnerth, I., Willems, W., Carvalho, R. F., and Disse, M.: Forecasting upper and lower uncertainty bands of river flood discharges with high predictive skill, J. Hydrol., https://doi.org/10.1016/j.jhydrol.2019.06.052, 2019.

Leedal, D., Neal, J., Beven, K., Young, P., and Bates, P.: Visualization approaches for communicating real-time flood forecasting level and inundation information, J. Flood Risk. Manag., 3, 140-150, 10.1111/j.1753-318X.2010.01063.x, 2010.

Liu, Z., Merwade, V., and Jafarzadegan, K.: Investigating the role of model structure and surface roughness in generating flood inundation extents using one- and two-dimensional hydraulic models, J. Flood Risk. Manag., 12, e12347, 10.1111/jfr3.12347, 2019.

Lowry, C. S., and Fienen, M. N.: Crowdhydrology: Crowdsourcing hydrologic data and engaging citizen scientists, Ground Water, 51, 151-156, 2013.

LRZ: Overview of the Cluster Configuration: https://www.lrz.de/services/compute/linux-cluster/overview/, access: 27.03.2019, 2019.

Luce, A., Haag, I., and Bremicker, M.: Daily discharge forecasting with operational water-balance models in Baden-Württemberg, Hydrol. Wasserbewirtsch., 50, 58-66, 2006.

Ludwig, K., and Bremicker, M.: The water balance model LARSIM : Design, content and applications, Inst. für Hydrologie der Univ., Freiburg i. Br., 2006.

Ly, S., Charles, C., and Degré, A.: Different methods for spatial interpolation of rainfall data for operational hydrology and hydrological modeling at watershed scale: a review, 2013.

Maini, R., and Aggarwal, H.: A comprehensive review of image enhancement techniques, Journal of Computing, 2, 8-13, 2010.

Mair, A., and Fares, A.: Comparison of Rainfall Interpolation Methods in a Mountainous Region of a Tropical Island, J. Hydrol. Eng., 16, 371-383, doi:10.1061/(ASCE)HE.1943-5584.0000330, 2011.

Maksimovic, C., and Prndanovic, D.: Modelling of Urban Flooding—Breakthrough or Recycling of Outdated Concepts, Specialty Symposium on Urban Drainage Modeling at the World Water and Environmental Resources Congress 2001, Orlando, Florida, United States, 2001, 1-9,

Maniak, U.: Niederschlag-Abfluss-Modelle für Hochwasserabläufe, in: Hydrologie und Wasserwirtschaft: Eine Einführung für Ingenieure, Springer Berlin Heidelberg, Berlin, Heidelberg, 261-360, 2010.

Mantoglou, A., and Wilson, J. L.: The Turning Bands Method for simulation of random fields using line generation by a spectral method, Water Resour. Res., 18, 1379-1394, 10.1029/WR018i005p01379, 1982.

Mark, O., Weesakul, S., Apirumanekul, C., Aroonnet, S. B., and Djordjević, S.: Potential and limitations of 1D modelling of urban flooding, J. Hydrol., 299, 284-299, https://doi.org/10.1016/j.jhydrol.2004.08.014, 2004.

Martins, R., Leandro, J., Chen, A. S., and Djordjević, S.: A comparison of three dual drainage models: shallow water vs local inertial vs diffusive wave, J. Hydroinform., 19, 331-348, 10.2166/hydro.2017.075, 2017.

Matott, L. S., Babendreier, J. E., and Purucker, S. T.: Evaluating uncertainty in integrated environmental models: A review of concepts and tools, Water Resour. Res., 45, doi:10.1029/2008WR007301, 2009.

McDougall, K.: An assessment of the contribution of volunteered geographic information during recent natural disasters, in: Spatially enabling government, industry and citizens: research and development perspectives, Needham, MA, United States, 201-214, 2012.

Merwade, V., Olivera, F., Arabi, M., and Edleman, S.: Uncertainty in flood inundation mapping: Current issues and future directions, J. Hydrol. Eng., 13, 608-620, doi:10.1061/(ASCE)1084-0699(2008)13:7(608), 2008.

Meyer, V., Scheuer, S., and Haase, D.: A multicriteria approach for flood risk mapping exemplified at the Mulde river, Germany, Nat. Haz., 48, 17-39, 10.1007/s11069-008-9244-4, 2009.

Molinari, D., Ballio, F., Handmer, J., and Menoni, S.: On the modeling of significance for flood damage assessment, Int. J. Disast. Risk Re., 10, 381-391, 10.1016/j.ijdrr.2014.10.009, 2014.

Moriasi, D., Arnold, J., Van Liew, M., Bingner, R., Harmel, R. D., and Veith, T.: Model evaluation guidelines for systematic quantification of accuracy in watershed simulations, Trans. ASABE, 50, 885–900, 10.13031/2013.23153, 2007.

Moya Quiroga, V., Kure, S., Udo, K., and Mano, A.: Application of 2D numerical simulation for the analysis of the February 2014 Bolivian Amazonia flood: Application of the new HEC-RAS version 5, RIBAGUA - Revista Iberoamericana del Agua, 3, 25-33, https://doi.org/10.1016/j.riba.2015.12.001, 2016.

Munich Re: Natural catastrophes 2016 – Analyses, assessments, positions. In: TOPICS GEO, Munich, 2017.

Murphy, A. T., Gouldby, B., Cole, S. J., Moore, R. J., and Kendall, H.: Real-time flood inundation forecasting and mapping for key railway infrastructure: a UK case study, E3S Web Conf., 7, 18020, 2016.

Musall, M., Oberle, P., and Nestmann, F.: Hydraulic modelling, in: Flood Risk Assessment and Management: How to Specify Hydrological Loads, Their Consequences and Uncertainties, edited by: Schumann, A. H., Springer Netherlands, Dordrecht, 187-209, 2011.

Nair, B., and Rao, S.: Flood monitoring using computer vision, The 15th ACM International Conference on Mobile Systems, Applications, and Services (ACM Moises 2017), New York, 2017.

Narayanan, R., Lekshmy, V. M., Rao, S., and Sasidhar, K.: A novel approach to urban flood monitoring using computer vision, 5th International Conference on Computing, Communications and Networking Technologies (ICCCNT), 2014, 1-7,

Neal, J., Fewtrell, T., and Trigg, M.: Parallelisation of storage cell flood models using OpenMP, Environ. Modell. Softw., 24, 872-877, https://doi.org/10.1016/j.envsoft.2008.12.004, 2009.

Néelz, S., Pender, G., Agency, G. B. E., Great Britain. Department for Environment, F., and Affairs, R.: Desktop review of 2D hydraulic modelling packages, Environment Agency, 2009.

Nester, T., Komma, J., Viglione, A., and Blöschl, G.: Flood forecast errors and ensemble spread—A case study, Water Resour. Res., 48, 10.1029/2011wr011649, 2012.

NETATMO, Der Regenmesser: https://www.netatmo.com/de-de/weather/weatherstation/accessories#raingauge, access: 28.04.2019, 2019.

Nujić, M.: HYDRO_AS-2D – 2D-Strömungsmodell für die wasserwirtschaftliche Praxis. Benutzer-handbuch, Version 4.2.1, Hydrotec Ingenieurgesellschaft für Wasser und Umwelt mbH, 2006.

Oberle, P., and Merkel, U.: Urban flood management – Simulation tools for decision makers, in: Advances in urban flood management, edited by: Ashley, R., Garvin, S., Pasche, E., Vassilopoulos, A., and Zevenbergen, C., Taylor & Francis, Leiden, The Netherlands, 2007.

Oubennaceur, K., Chokmani, K., Nastev, M., Tanguy, M., and Raymond, S.: Uncertainty analysis of a two-dimensional hydraulic model, Water, 10, 272, 2018.

Oudin, L., Andréassian, V., Mathevet, T., Perrin, C., and Michel, C.: Dynamic averaging of rainfall-runoff model simulations from complementary model parameterizations, Water Resour. Res., 42, 10.1029/2005wr004636, 2006.

Pakosch, S.: Development of a fuzzy rule based expert system for flood forecasts within the meso-scale Upper Main basin, PhD, Institut für Wasserwesen Wasserwirtschaft und Ressourcenschutz, Universitätsbibliothek der Universität der Bundeswehr, Neubiberg, 2011.

Pappenberger, F., Beven, K., Horritt, M., and Blazkova, S.: Uncertainty in the calibration of effective roughness parameters in HEC-RAS using inundation and downstream level observations, J. Hydrol., 302, 46-69, 10.1016/j.jhydrol.2004.06.036, 2005.

Pappenberger, F., and Beven, K. J.: Ignorance is bliss: Or seven reasons not to use uncertainty analysis, Water Resour. Res., 42, 10.1029/2005WR004820, 2006.

Pappenberger, F., Harvey, H., Beven, K., Hall, J., and Meadowcroft, I.: Decision tree for choosing an uncertainty analysis methodology: a wiki experiment http://www.floodrisknet.org.uk/methods http://www.floodrisk.net, Hydrol. Process., 20, 3793-3798, 10.1002/hyp.6541, 2006a.

Pappenberger, F., Matgen, P., Beven, K. J., Henry, J.-B., Pfister, L., and Fraipont, P.: Influence of uncertain boundary conditions and model structure on flood inundation predictions, Adv. Water Resour., 29, 1430-1449, http://dx.doi.org/10.1016/j.advwatres.2005.11.012, 2006b.

Pappenberger, F., Beven, K. J., Ratto, M., and Matgen, P.: Multi-method global sensitivity analysis of flood inundation models, Adv. Water Resour., 31, 1-14, 10.1016/j.advwatres.2007.04.009, 2008.

Park, Y.-Y., Buizza, R., and Leutbecher, M.: TIGGE: Preliminary results on comparing and combining ensembles, Q. J. Roy. Meteor. Soc., 134, 2029-2050, 10.1002/qj.334, 2008.

Patel, D. P., Ramirez, J. A., Srivastava, P. K., Bray, M., and Han, D.: Assessment of flood inundation mapping of Surat city by coupled 1D/2D hydrodynamic modeling: a case application of the new HEC-RAS 5, Nat. Haz., 89, 93-130, 10.1007/s11069-017-2956-6, 2017.

Patro, S., Chatterjee, C., Mohanty, S., Singh, R., and Raghuwanshi, N. S.: Flood inundation modeling using MIKE FLOOD and remote sensing data, Journal of the Indian Society of Remote Sensing, 37, 107-118, 10.1007/s12524-009-0002-1, 2009.

Pflugbeil, T., Broich, K., and Disse, M.: Hydrodynamic simulation of the flash flood events in Baiersdorf and Simbach (Bavaria) - A model comparison, EGU General Assembly 2019, Vienna, Austria, 2019,

Poser, K., and Dransch, D.: Volunteered geographic information for disaster management with application to rapid flood damage estimation, Geomatica, 64, 89—98, 2010.

Raymond, M., Peyron, N., Bahl, M., Martin, A., and F. Alfonsi, F.: Un Outil Innovant Pour la Gestion en Temps Réel Descrues Rrbaines, Novatech 6th Conference of Sustainable Techniques and Strategies in Urban Water Management, Lyon, France, 2007, 793-800,

Razavi, S., Tolson, B. A., and Burn, D. H.: Review of surrogate modeling in water resources, Water Resour. Res., 48, 10.1029/2011wr011527, 2012.

René, J.-R., Djordjević, S., Butler, D., Madsen, H., and Mark, O.: Assessing the potential for real-time urban flood forecasting based on a worldwide survey on data availability, Urban Water J., 11, 573-583, 10.1080/1573062X.2013.795237, 2014.

Romanowicz, R., and Beven, K.: Estimation of flood inundation probabilities as conditioned on event inundation maps, Water Resour. Res., 39, doi:10.1029/2001WR001056, 2003.

Roth, C.: Quality management for discharge measurements in Bavaria, IOP Conf. Ser.: Earth Environ. Sci., 2008, 012014.

Saeed, M..: Prediction of peak flood inundation using a two-dimensional hydrodynamic model: River and flash floods, Case Study: Kulmbach city, Master Thesis, TU Munich, 2019.

Saksena, S., and Merwade, V.: Incorporating the effect of DEM resolution and accuracy for improved flood inundation mapping, J. Hydrol., 530, 180-194, https://doi.org/10.1016/j.jhydrol.2015.09.069, 2015.

Sayers, P., Yuanyuan, L., Galloway, G., Penning-Rowsell, E., Fuxin, S., Kang, W., Yiwei, C., and Quesne, T. L.: Flood risks management : a strategic approach, Asian Development Bank, Paris, UNESCO, 2013.

Schanze, J.: A hybrid multi-model approach to river level forecasting, in: Flood Risk Management: Hazards, Vulnerability and Mitigation Measures, edited by: Schanze, J., Zeman, E., and Marsalek, J., Flood Risk Management: Hazards, Vulnerability and Mitigation Measures, Springer Netherlands, Dordrecht, 1-20, 2006.

Schumann, A. H., Wang, Y., and Dietrich, J.: Framing uncertainties in flood forecasting with ensembles, in: Flood Risk Assessment and Management: How to Specify Hydrological Loads, Their Consequences and Uncertainties, edited by: Schumann, A. H., Springer Netherlands, Dordrecht, 53-76, 2011.

See, L., and Openshaw, S.: A hybrid multi-model approach to river level forecasting, Hydrolog. Sci. J., 45, 523-536, 10.1080/02626660009492354, 2000.

Sellin, R, Bryant, T.B., and Loveless, J.H.: An improved method for roughening floodplains on physical river models, J. Hydra. Res., 41:1, 3-14, DOI: 10.1080/00221680309499924, 2003.

Shamseldin, A. Y., O'Connor, K. M., and Liang, G. C.: Methods for combining the outputs of different rainfall–runoff models, J. Hydrol., 197, 203-229, 10.1016/S0022-1694(96)03259-3, 1997.

Shultz, S.: The extent and nature of potential flood damage to commercial property structures in the midwestern United States, J. Contemp. Water Res. Educ., 161, 81-91, 10.1111/j.1936-704X.2017.3253.x, 2017.

Skublics, D. A.: Grossräumige Hochwassermodellierung im Einzugsgebiet der bayerischen Donau: Retention, Rückhalt, Ausbreitung (Large-scale flood modeling in the catchment area of the Bavarian Danube: retention, backwater, widening), PhD, Chair of Hydraulic and Water Resources Engineering, Technical University of Munich, Munich, Germany, 2014.

References

Smith, L., Liang, Q., James, P., and Lin, W.: Assessing the utility of social media as a data source for flood risk management using a real-time modelling framework, J. Flood Risk. Manag., 10, 370-380, 10.1111/jfr3.12154, 2017.

Teng, J., Jakeman, A. J., Vaze, J., Croke, B. F. W., Dutta, D., and Kim, S.: Flood inundation modelling: A review of methods, recent advances and uncertainty analysis, Environ. Modell. Softw., 90, 201-216, https://doi.org/10.1016/j.envsoft.2017.01.006, 2017.

Thieken, A. H., Müller, M., Kreibich, H., and Merz, B.: Flood damage and influencing factors: New insights from the August 2002 flood in Germany, Water Resour. Res., 41, 10.1029/2005wr004177, 2005.

Thieken, A. H., Bessel, T., Kienzler, S., Kreibich, H., Müller, M., Pisi, S., and Schröter, K.: The flood of June 2013 in Germany: how much do we know about its impacts?, Nat. Hazards Earth Syst. Sci., 16, 1519-1540, 10.5194/nhess-16-1519-2016, 2016a.

Thieken, A. H., Kienzler, S., Kreibich, H., Kuhlicke, C., Kunz, M., Mühr, B., Müller, M., Otto, A., Petrow, T., Pisi, S., and Schröter, K.: Review of the flood risk management system in Germany after the major flood in 2013, Ecol. Soc., 21, 10.5751/ES-08547-210251, 2016b.

Thorndahl, S., Einfalt, T., Willems, P., Nielsen, J. E., ten Veldhuis, M. C., Arnbjerg-Nielsen, K., Rasmussen, M. R., and Molnar, P.: Weather radar rainfall data in urban hydrology, Hydrol. Earth Syst. Sci., 21, 1359-1380, 10.5194/hess-21-1359-2017, 2017.

Timbadiya, P., Patel, P., and Porey, P.: A 1D–2D Coupled Hydrodynamic Model for River Flood Prediction in a Coastal Urban Floodplain, J. Hydrol. Eng., 20, 05014017, 10.1061/(ASCE)HE.1943-5584.0001029, 2014.

Todini, E.: Flood forecasting and decision making in the new millennium. Where are we?, Water Res. Manag., 31, 3111-3129, 10.1007/s11269-017-1693-7, 2017.

Triglav-Čekada, M., and Radovan, D.: Using volunteered geographical information to map the November 2012 floods in Slovenia, Nat. Hazards Earth Syst. Sci., 13, 2753-2762, 10.5194/nhess-13-2753-2013, 2013.

TVO, Hochwasserschutz Kulmbach: Neugestaltung der Flutmulde (Flood protection Kulmbach: redesign of the flood basin): https://www.tvo.de/hochwasserschautz-kulmbach-neugestaltung-der-flutmulde-142915/, access: 16.03.2018, 2015.

Tyralla, C., and Schumann, A. H.: Incorporating structural uncertainty of hydrological models in likelihood functions via an ensemble range approach, Hydrolog. Sci. J., 61, 1679-1690, 10.1080/02626667.2016.1164314, 2016.

Uusitalo, L., Lehikoinen, A., Helle, I., and Myrberg, K.: An overview of methods to evaluate uncertainty of deterministic models in decision support, Environ. Modell. Softw., 63, 24-31, 10.1016/j.envsoft.2014.09.017, 2015.

Verworn, H.-R.: Praxisrelevante Extremwerte des Niederschlags, Institut für Wasserwirtschaft, Hydrologie und Landwirtschaftlichen Wasserbau, Magdenburg, Germany, 173–185, 2005.

Vogel, R. M., and Arumugam, S.: Foreword, in: Flood Forecasting, edited by: Adams, T. E., and Pagano, T. C., Academic Press, Boston, xvii-xx, 2016.

Voigt, S., Kemper, T., Riedlinger, T., Kiefl, R., Scholte, K., and Mehl, H.: Satellite image analysis for disaster and crisis-management support, IEEE T. Geosci. Remote., 45, 1520-1528, 10.1109/TGRS.2007.895830, 2007.

Wagener, T., and Gupta, H. V.: Model identification for hydrological forecasting under uncertainty, Stoch. Env. Res. Risk A., 19, 378-387, 10.1007/s00477-005-0006-5, 2005.

Wang, Y., Chen, A., Fu, G., Djordjević, S., Zhang, C., and Savic, D.: An integrated framework for high-resolution urban flood modelling considering multiple information sources and urban features, Environ. Modell. Softw., 107, 85-95, 10.1016/j.envsoft.2018.06.010, 2018.

Warmink, J. J., Janssen, J. A. E. B., Booij, M. J., and Krol, M. S.: Identification and classification of uncertainties in the application of environmental models, Environ. Modell. Softw., 25, 1518-1527, https://doi.org/10.1016/j.envsoft.2010.04.011, 2010.

Weigel, A. P., Liniger, M. A., and Appenzeller, C.: Can multi-model combination really enhance the prediction skill of probabilistic ensemble forecasts?, Q. J. Roy. Meteor. Soc., 134, 241-260, 10.1002/qj.210, 2008.

Werner, M., Blazkova, S., and Petr, J.: Spatially distributed observations in constraining inundation modelling uncertainties, Hydrol. Process., 19, 3081-3096, 10.1002/hyp.5833, 2005a.

Werner, M. G. F., Hunter, N. M., and Bates, P. D.: Identifiability of distributed floodplain roughness values in flood extent estimation, J. Hydrol., 314, 139-157, https://doi.org/10.1016/j.jhydrol.2005.03.012, 2005b.

Wolf, Hochwasser-Großeinsatz in Kulmbach (Floods in Kulmbach): https://fotothurnau.wordpress.com/2011/01/15/hochwasser-groseinsatz-in-kulmbach/, access: 20.03.2018, 2011.

WWA: Gebiet des Mains: https://www.wwa-ho.bayern.de/hochwasser/hochwasserereignisse/januar2011/main/index.htm, access: 27.03.2019, 2011.

WWA: Hochwasserschutz Kulmbach: https://www.wwa-ho.bayern.de/hochwasser/hochwasserschutzprojekte/kulmbach/index.htm, access: 27.03.2019, 2018a.

WWA, Hochwasserschutz Kulmbach, Weißer Main - Flutmulde: https://www.wwa-ho.bayern.de/hochwasser/hochwasserschutzprojekte/kulmbach_flutmulde/index.htm, access: 27.03.2019, 2018b.

Xing, Y., Liang, Q., Wang, G., Ming, X., and Xia, X.: City-scale hydrodynamic modelling of urban flash floods: the issues of scale and resolution, Nat. Haz., 10.1007/s11069-018-3553-z, 2018.

Yörük, A.: Unsicherheiten bei der hydrodynamischen Modellierung von Überschwemmungsgebieten, PhD, Institut für Wasserwesen Siedlungswasserwirtschaft und Abfalltechnik, Universitätsbibliothek der Universität der Bundeswehr, Neubiberg, 2009.

Zappa, M., Jaun, S., Germann, U., Walser, A., and Fundel, F.: Superposition of three sources of uncertainties in operational flood forecasting chains, Atmospheric Research, 100, 246-262, https://doi.org/10.1016/j.atmosres.2010.12.005, 2011.

Zarzar, C. M., Hosseiny, H., Siddique, R., Gomez, M., Smith, V., Mejia, A., and Dyer, J.: A hydraulic multimodel ensemble framework for visualizing flood inundation uncertainty, J. Am. Water Resour. As., 54, 807-819, 10.1111/1752-1688.12656, 2018.

Zhai, L., Dong, S., and Ma, H.: Recent methods and applications on image edge detection, 2008 International Workshop on Education Technology and Training & 2008 International Workshop on Geoscience and Remote Sensing, 2008, 332-335,

Zhang, J., Li, Y., Huang, G., Chen, X., and Bao, A.: Assessment of parameter uncertainty in hydrological model using a Markov-Chain-Monte-Carlo-based multilevel-factorial-analysis method, J. Hydrol., 538, 471-486, https://doi.org/10.1016/j.jhydrol.2016.04.044, 2016.

Zhang, S., Yuan, R., Wu, Y., and Yi, Y.: Parallel computation of a dam-break flow model using OpenACC applications, J. Hydraul. Eng., 143, 04016070, doi:10.1061/(ASCE)HY.1943-7900.0001225, 2017.

Zheng, X., Tarboton, D. G., Maidment, D. R., Liu, Y. Y., and Passalacqua, P.: River channel geometry and rating curve estimation using height above the nearest drainage, J. Am. Water Resour. As., 54, 785-806, 10.1111/1752-1688.12661, 2018.

Chair of Hydrology and River Basin Management
TUM Department of Civil, Geo and Environmental Engineering
Technical University of Munich

TUM

Curriculum Vitae

Punit Bhola was born in Varanasi and studied Civil Engineering in India. He moved to Europe to pursue his masters in Environmental Engineering thanks to the EuroAquae consortium and funding from BMBF. He completed his doctoral research in the field of flood risk management from the Chair of Hydrology and River Basin Management in the Technical University of Munich.

He specializes in Environmental Engineering with a focus on modelling of hydro-metrological hazards. He has been a part of several environmental research projects primarily focused on probabilistic and deterministic modelling of inland, flash, coastal and groundwater floods. Apart from research, he loves playing tennis, hiking in the Alps and travelling.

EDUCATION

09/2015 – 07/2019	**Dr.-Ing., Environmental Engineering** Technical University of Munich, Germany
10/2010 – 09/2012	**M. Sc., Hydro-Informatics and Water Management (EUROAQUAE)** A joint masters from Brandenburg University of Technology, Germany; University of Nice Sophia Antipolis, France & Newcastle University, UK
07/2006 – 05/2010	**B.Tech., Civil Engineering** National Institute of Technology, Rourkela, India

RESEARCH EXPERIENCE

04/2014 – 06/2019	**Research Assistant** Chair of Hydrology and River Basin Management, Technical University of Munich, Germany
02/2013 – 01/2014	**Research Assistant** Department of Water Resources & Environment DHI-WASY GmbH, Berlin, Germany
03/2012 – 12/2012	**Research Internship** Department of Water Resources & Environment DHI-WASY GmbH, Berlin, Germany
07/2011 – 09/2011	**Internship** Ingenieurgesellschaft Prof. Dr. Sieker MBH, Berlin, Germany

AWARDS

06/2018	Summer school: Imperial College – TU Munich Global Fellows Program in London on "Cities of the future"
10/2010 – 12/2012	BMBF scholarship programme for M.Sc. "International Postgraduate Studies in Water Technologies – IPSWaT"